

THE FEASIBILITY OF USING SUPERCRITICAL CARBON DIOXIDE
AS A COOLANT FOR THE CANDU REACTOR

by

Samsun Kwok Sun / TOM

B.A.Sc., The University of British Columbia, 1975

A THESIS SUBMITTED IN PARTIAL FULFILLMENT OF
THE REQUIREMENTS FOR THE DEGREE OF
MASTER OF APPLIED SCIENCE

in

THE FACULTY OF GRADUATE STUDIES
Department of Mechanical Engineering

We accept this thesis as conforming
to the required standard

THE UNIVERSITY OF BRITISH COLUMBIA

January, 1978



Samsun Kwok Sun TOM; 1978

In presenting this thesis in partial fulfilment of the requirements for an advanced degree at the University of British Columbia, I agree that the Library shall make it freely available for reference and study.

I further agree that permission for extensive copying of this thesis for scholarly purposes may be granted by the Head of my Department or by his representatives. It is understood that copying or publication of this thesis for financial gain shall not be allowed without my written permission.

Department of Mechanical Engineering

The University of British Columbia
2075 Wesbrook Place
Vancouver, Canada
V6T 1W5

Date 1 January 1978

ABSTRACT

This study indicates the technical feasibility of using supercritical carbon dioxide as a coolant for a CANDU-type reactor. A new concept of supercritical cooling loop is proposed in this study. The reactor is cooled by a single phase coolant, which is pumped at a high density liquid-like state. The supercritical-fluid-cooled reactor has the advantage of avoiding dryout as in gas-cooled reactors, and the advantage of low coolant-circulation power as for liquid-cooled reactors.

As a result of eliminating dryout, the maximum operating temperature of the fuel sheath can be increased to 1021°F (550°C) for existing Canadian fuel bundles. Accordingly, the coolant temperature in the case study of this work was calculated to be 855°F. This high temperature coolant can produce steam at a temperature and pressure comparable to that of conventional fossil-fuel plants. However, since the exit coolant temperature from the steam generator may be as low as 280°F, a portion of the supercritical carbon dioxide coolant is used to produce low-pressure steam.

A new dual-reheat cycle is proposed to reduce the high degree of irreversibility in the steam generation process. In the new dual-reheat cycle, the coolant heats the low and high pressure feeds in a parallel manner instead of alternative heating as in dual-pressure cycles. The ideal overall plant efficiency of the new proposed dual-reheat cycle is 33.02%, which is comparable to that of the Pickering generating station.

TABLE OF CONTENTS

	Page
ABSTRACT	ii
TABLE OF CONTENTS	iii
LIST OF TABLE	v
LIST OF FIGURES	vi
NOMENCLATURE	ix
ACKNOWLEDGEMENTS	xii
 1. INTRODUCTION	 1
2. CRITERIA FOR SELECTING ALTERNATE COOLANTS (FOR CANDU-TYPE REACTORS)	 5
2.1 General	5
2.2 Overall Cost and Performance Criteria	6
2.3 Nuclear Properties	7
2.4 Chemical Properties	9
3. HEAT TRANSFER TO A LIQUID COOLANT AND MAXIMUM FUEL SHEATH OPERATING TEMPERATURE	 11
3.1 Dryout in Coolant Channels	11
3.2 Maximum Operating Sheath Temperature	13
4. PROPOSED SUPERCRITICAL CO ₂ COOLING LOOP FOR CANDU REACTORS	16
4.1 Use of the Supercritical Cycle in Reactor Power Generation	16
4.2 Supercritical CO ₂ Cooling Loop	18
5. HEAT TRANSFER TO SUPERCRITICAL CO ₂ COOLANT	21
5.1 Heat Transfer to Supercritical Fluids in Pipes	21
5.1.1 Peculiarities of Heat Transfer to Supercritical Fluids	 21

	Page
5.1.2 Previous Studies of Heat Transfer to Supercritical Fluids	26
5.2 Engineering Calculation of Heat Transfer to Supercritical Fluids	31
5.2.1 Choice of Correlations	31
5.2.2 Examination of Chosen Correlation	34
5.3 Heat Transfer to Single Phase Fluids in Fuel Bundles	39
5.4 Heat Transfer to Supercritical CO ₂ in Fuel Bundle	42
5.4.1 Specifications and Assumptions	42
5.4.2 Fuel Bundle Geometry and Subchannel Analysis	46
5.4.3 Predicted Heat Transfer to Supercritical Carbon Dioxide in 32-element Fuel Bundles	50
6. POSSIBLE STEAM CYCLES	54
6.1 General	54
6.2 Steam Cycle for the Supercritical Carbon Dioxide Cooled CANDU Reactor Plant	56
7. RESULTS AND DISCUSSION	59
7.1 Typical Heat Transfer in Bundles	59
7.2 Typical Steam Cycles	61
8. SUMMARY AND CONCLUSIONS	63
REFERENCES	117
APPENDIX I. Computing Procedure	124
APPENDIX II. Typical Calculation of Ideal Overall Efficiency	137

LIST OF TABLE

	Page
TABLE 1	8

LIST OF FIGURES

	Page
FIGURE 1. Thermo-hydraulic Features of PHW CANDU Reactor Power Plant	66
FIGURE 2. Typical Property Variations in Near-critical Carbon Dioxide	67
FIGURE 3. Process Path of Supercritical Cooling Loop on P-V Diagram	68
FIGURE 4. PHW CANDU Reactor Arrangement	69
FIGURE 5. Fuel Bundle	70
FIGURE 6. Thermal Hydraulic Regions in a Boiling Channel	71
FIGURE 7. Boiling Regions	72
FIGURE 8. Subchannel Temperature Rises in a 28-element Bundle Versus Reactor Channel Length (from [12])	73
FIGURE 9. High Sheath Temperature Operation vs. Time for Various Zirconium Alloy Fuel Elements (from [13])	74
FIGURE 10. Proposed Supercritical CO ₂ Cooling Loop	75
FIGURE 11. Heat Transfer Regions: I - Liquids, II - Subcritical Gases, III - Two-Phase, IV - Above-Critical Fluids, V - Near-Critical Fluids (from [18])	76
FIGURE 12. List of Equations	77
FIGURE 13. Routine for Calculating Wall Temperature	79
FIGURE 14. Computer Program Flow Chart for Calculating Heat Transfer to Supercritical Flow in Heated Pipes	80
FIGURE 15. Prediction of Heat Transfer to Supercritical Flow, Experimental Results from [61]	81
FIGURE 16. Prediction of Heat Transfer to Supercritical Flow, Experimental Results from [49]	82
FIGURE 17. Prediction of Heat Transfer to Supercritical Flow, Experimental Results from [55]	83
FIGURE 18. Prediction of Heat Transfer to Supercritical Flow, Experimental Results from [42]	84
FIGURE 19. Equivalent Annulus Models for Rod-Bundles	85

	Page
FIGURE 20. Lumped Parameter Model for Rod-Bundles (from [71])	86
FIGURE 21. Thermal Entrance Following a Grid Type Spacer (from [73])	87
FIGURE 22. Comparison of Heat Transfer Data in a Uniformly Heated Seven-Rod Bundle ($Pr = 0.7$) with Wire-Wrap Spacers (from [74])	88
FIGURE 23. Comparison of Friction Factors for Seven-Rod Bundle with Wire-Wrap Spacers ($l/d = 12, 24, 36, \infty$) in a Scalloped Liner ($p/d = 1.237$) (from [74])	89
FIGURE 24. Temperature Profiles in Coolant Channel with Difference Fuel Bundle Orientation	90
FIGURE 25. Effect of Ratio of Pitch to Rod Diameter on Nusselt Number and Friction Factor (from [78])	91
FIGURE 26. Cross Section of Fuel and Coolant Tube (from [12])	92
FIGURE 27. Channel for Boiling Reactor (from [79])	93
FIGURE 28. Tube-in-Shell Fuel Element (from [79])	93
FIGURE 29. Maximum Operating Temperature Versus Inlet Coolant Temperature	94
FIGURE 30. Pressure Drop Versus Inlet Coolant Temperature	95
FIGURE 31. Selection of Minimum Equivalent Hydraulic Diameter	96
FIGURE 32. Cross Section of 32-Element Fuel Bundle	97
FIGURE 33. Radial Neutron Flux Distribution in Fuel Bundle	98
FIGURE 34. Subchannel Coolant Temperature Rise in 32-Element Fuel Bundles Versus Reactor Channel Length	99
FIGURE 35. Subchannel Sheath Temperature Rise in 32-Element Fuel Bundles Versus Reactor Channel Length	100
FIGURE 36. Pressure Drop Along Reactor Channel Length	101
FIGURE 37. Single Pressure Steam Generation	102
FIGURE 38. Dual-Pressure 600.0/70.3 (psia) Steam Generation	103
FIGURE 39. Turbine Circuit Heat Balance of Single Pressure Cycle	104
FIGURE 40. Turbine Circuit Heat Balance of Dual-Pressure 600/70.3 (psia) Cycle	105

	Page
FIGURE 41. Dual-Pressure 1200.0/70.3 (psia) Steam Generation	106
FIGURE 42. Turbine Circuit Heat Balance of Dual-Pressure 1200.0/70.3 (psia) Cycle	107
FIGURE 43. Dual-Reheat 1200.0/70.3 (psia) Steam Generation	108
FIGURE 44. Turbine Circuit Heat Balance of Dual-Reheat 1200/70.3 (psia) Cycle	109
FIGURE 45. Results of Heat Transfer to Supercritical CO ₂ Coolant in 32-Element Fuel Bundles	110
FIGURE 46. Overall Performance of Supercritical Carbon Dioxide Coolant	111
FIGURE 47. Overall Dimensions of 32-Element Fuel Bundle	112
FIGURE 48. Summary of Steam Conditions of Thermal Cycles	113
FIGURE 49. Overall Performance of Thermal Cycles	114
FIGURE 50. Turbo-Generator Heat Balance (from [12])	115
FIGURE 51. Expansion Line of CANDU Reactor Turbine Stages (from [82])	116

NOMENCLATURE^{*}

A	experimental constant
b	experimental constant
C _p	specific heat at constant pressure
$\overline{C_p}$	integrated specific heat, equation (13)
CWP	unheated wetted perimeter
c	experimental constant
D	equivalent hydraulic diameter, equation (25)
d	diameter
eff	efficiency
\overline{F}	integrated fluid property
F(T)	fluid property as a function of temperature
f	normalized neutron flux
f(x/d)	correction factor, equation (24)
Gr	Grashof number
h	enthalpy
K	thermal conductivity
k	constant, 0.51504
M	mass flow rate
m	experimental constant
Nu	Nusselt number
n	experimental constant
P	pressure
P _c	critical pressure
Pr	Prandtl number

^{*} Dimensional quantities are evaluated in both S.I. and British units.

\overline{Pr}	integrated Prandtl number, equation (15)
p	pitch distance
Q	heat flux
q	linear heat rate
Re	Reynolds number
T	temperature
\overline{T}	integrated temperature, equation (21b)
T_c	critical temperature
$T(x)$	temperature as a function of distance
TWP	total wetted perimeter
u	velocity
W	work
x	distance from channel inlet
y	distance
Z	dimensionless parameter, equation (5)

Subscripts

b	bulk
in	inlet
m	pseudo-critical temperature
min	minimum
o	constant property
out	outlet
w	wall or sheath
z	dimensionless parameter
1	location 1
2	location 2

Greek Symbols

τ	shear stress
μ	viscosity
ρ	density
ϵ_m	momentum eddy diffusivity
ϵ_h	thermal eddy diffusivity
ξ	friction factor
ℓ	length
$\overline{\rho u}$	average product of ρu
$\tilde{\rho}$	integrated density
Δ	differential change
\sum	summation
ϕ	constant, 0.25744

Critical Values of Carbon Dioxide

p_c	critical pressure, 73.82 bars or 1071.3 psia
T_c	critical temperature, 31.04°C or 87.9°F

ACKNOWLEDGEMENTS

I would like to express my sincere thanks and appreciation to my supervisor, Dr. E.G. Hauptmann for his help and guidance throughout the project. Additional thanks are due to Dr. P.G. Hill for invaluable comments on phases of the research.

I would also like to express my deep gratitude to my parents for encouraging me throughout the academic years.

This work was sponsored by the National Research Council of Canada.

1. INTRODUCTION

It has become evident that the world's limited oil and gas resources will have to be supplemented by nuclear energy for electrical power generation. Nuclear power plants have already operated successfully for many years, and most public utilities are counting heavily on nuclear power to meet the bulk of electrical demands in the next century.

Power reactors can be classified according to types of coolant, moderator, and fuel. The most popular types are the pressurized water and boiling water reactors, which use enriched uranium as fuel and ordinary water as both coolant and moderator. Of special interest to Canada is the CANDU (CANadian Deuterium Uranium) system, which uses natural uranium as fuel and heavy water (deuterium oxide) as coolant and moderator. Figure 1 shows the main thermo-hydraulic features of a PHW (Pressurized Heavy Water cooled) CANDU reactor power plant.

The CANDU system is a successful design in terms of fuel economy and safety. Nevertheless, it still has several weaknesses. One of these is that the pressurized heavy water coolant cannot be raised to a temperature high enough to generate steam at a pressure and temperature comparable to that of conventional fossil-fuel stations. As a result, the practical overall plant efficiency of the CANDU system is relatively low (29.7%).

Atomic Energy of Canada Limited (AECL) is pursuing many routes toward increasing the efficiency of the existing CANDU system. One such route is looking for alternate coolants to heavy water^[1].

In the development of the CANDU system, a prototype reactor using ordinary water instead of heavy water has been operating at Gentilly,

Quebec since 1971^[2]. A research reactor at Whiteshell, Manitoba has been operating since 1966, and is cooled by terphenyl, an organic liquid that boils at a temperature above 700°F at atmospheric pressure^[2]. However, in both boiling and pressurized water reactors, operation at higher power levels may result in blanketing of the heat transfer surface with a layer of vapor. Such blanketing of the surface by vapor may result in "dryout" of the coolant with the possibility of fuel sheath failure. Thus, to avoid accidental rupture of the fuel sheath, its maximum temperature must be only slightly higher than the saturation temperature of the coolant used. Because the temperatures of both coolant and fuel sheath are constrained, the overall plant efficiency is limited.

To obviate dryout and obtain higher coolant temperatures, the reactor can be cooled by gaseous coolants. Because gaseous coolants do not change phase throughout the operating temperature range, dryout due to phase change of coolant cannot occur. The fuel sheath can operate at its maximum temperature (based on metallurgical considerations), which is usually much higher than the saturation temperature of most coolants. Compared with liquid coolants, however, gaseous coolants are characterized by low specific heat at constant pressure, low heat transfer coefficients, and low specific volume. For this reason, gas cooled reactors have large flow passages through the reactor, and require higher pumping power for coolant circulation^[3].

To retain the advantages and overcome the disadvantages of gaseous coolants, reactors may be cooled with "supercritical" coolants. These are fluids compressed above their critical pressure, and as a result always exist as a single phase. For a given pressure of a supercritical fluid, there is a temperature at which the maximum specific heat occurs, known as the pseudo-

critical or transposed critical temperature. The thermophysical properties of supercritical fluids change drastically across the pseudo-critical temperature. Figure 2 shows the thermal conductivity, viscosity, and density of supercritical CO_2 at 1100 psia. Above the pseudo-critical temperature, the properties of a supercritical fluid are somewhat like a normal gas. The thermal conductivity or dynamic viscosity is not greatly affected by changes in temperature, and the density is low. In this region, the fluid is termed "vapor-like". Below the pseudo-critical temperature, the fluid is termed "liquid-like", since it has properties very much like a liquid. The thermal conductivity and dynamic viscosity decrease with increasing temperature as in ordinary liquids, and the density is high. Therefore, a supercritical cooling loop which has its process path as shown in Figure 3 can be arranged so that the liquid is pumped while in a liquid-like state, thereby greatly reducing pumping power.

The purpose of the present work is to investigate not only the possibility of using supercritical carbon dioxide (CO_2) as a coolant, but also the application of a supercritical cooling loop to the CANDU system. The major part of this work involves an analytical study of heat transport in the coolant channels and the thermodynamics of the CANDU reactor power station when supercritical CO_2 is used as a coolant. Carbon dioxide was selected because of its availability at low cost, its inertness in contact with fuel and reactor materials, and its stability at relative high temperature. In addition, its low critical pressure makes application of a supercritical cooling loop particularly suitable to the CANDU reactor. In this investigation, the basic design of the CANDU reactor was assumed to be unchanged when supercritical CO_2 was used as a coolant. However, the operating temperature of the fuel sheath was taken to be the maximum

allowable temperature (1021°F or 550°C).

In the initial part of this study, standard single and dual reactor steam cycles were analysed when using supercritical CO₂ as a coolant. The results indicated the overall plant efficiencies would be lower than the current CANDU ideal plant efficiency of 33.94%. As a result, a new dual-reheat reactor steam cycle is proposed. In this new cycle, supercritical CO₂ generates high pressure steam at 1200 psia, 815°F and low pressure steam at 70.3 psia, 567°F simultaneously for high and low pressure turbines respectively. The expanded steam from the high pressure turbines is mixed with low pressure feed water to be evaporated in the steam generator before expansion through the low pressure turbines. This new steam cycle has a comparable ideal overall plant efficiency of 33.02%. This indicates the possibility of increasing of the overall plant efficiency of CANDU reactor power stations, if the performance of supercritical CO₂ coolant was optimized in this preliminary study.

This study also points out other possible advantages of using supercritical CO₂ as a coolant for the CANDU system:

1. lower coolant capital and upkeep costs;
2. compatibility with uranium carbide fuel having high uranium content and high thermal conductivity;
3. increased safety due to elimination of possible dryout.

2. CRITERIA FOR SELECTING ALTERNATE COOLANTS (FOR CANDU-TYPE REACTORS)

2.1 General

Choosing the coolant is a major consideration in the design of nuclear reactors. It strongly affects the performance of reactors, and eventually the cost of power generation. In selecting a good coolant for power reactors, several criteria must be considered:

1. overall cost and performance:
 - a) low capital and upkeep costs,
 - b) availability;
2. nuclear properties of coolant:
 - a) low neutron absorption cross-section,
 - b) good radiation-stability,
 - c) low induced-radioactivity;
3. chemical properties of coolant:
 - a) stable at high temperature,
 - b) compatible with fuel and reactor materials;
4. heat transport and fluid properties of coolant:
 - a) low pumping power,
 - b) high density,
 - c) high heat capacity,
 - d) high heat conductivity,
 - e) high saturation temperature (liquid coolant).

Past studies have not identified a coolant which can adequately

meet all the above criteria. Supercritical CO_2 is no exception. For example, at high temperature it has poor heat transfer characteristics. However, when used in a supercritical cooling loop, the designer can still achieve good overall heat exchange by increasing the flow rate. The resulting high pressure losses do not result in excessive pumping power since the coolant is pumped in a liquid-like state.

The economics of using supercritical CO_2 as a coolant for the CANDU system will be discussed in this chapter. Nuclear and chemical properties of the coolant are also discussed, while heat transport criteria are left to a later chapter.

2.2 Overall Cost and Performance Criteria

One of the major direct costs of a CANDU reactor power generation station is the capital and upkeep costs of the coolant. For example, the total cost of building a 2 x 600 MWe CANDU-PHW (for Pressurized Heavy Water cooled) reactor power generation plant was about 300 million dollars in 1972^[4]. The heavy water cost alone was 65 million dollars, with 37.4% of the heavy water used as coolant. The coolant upkeep cost of the Pickering station was as high as 35% of the fueling cost^[2]. Because of the relatively low cost of CO_2 , the cost of power generation would be significantly reduced if CO_2 were used as a substitute for heavy water in CANDU reactors.

The capital and upkeep costs of a coolant depend on the initial inventory and rate of leakage of the coolant. The evaluation of the costs of using supercritical CO_2 as a coolant for the CANDU system and the comparison with heavy water can only be made after a detailed study for a particular design of power generating plant, which was beyond the scope of this

study.

2.3 Nuclear Properties

If supercritical CO_2 is used as a coolant, it must have good nuclear properties. Since these properties are usually functions of temperature but not pressure, supercritical CO_2 has similar microscopic nuclear properties to gaseous CO_2 . Experience with British and French designed reactors has shown that gaseous CO_2 is a good coolant in terms of nuclear properties.

The most important requirement of a coolant from a nuclear point of view is that it has low neutron absorption. The rate of neutron absorption is a function of the macroscopic absorption cross-section, which is proportional to the product of the density and the microscopic absorption cross-section of the coolant molecules. Under present CANDU reactor operating conditions of 570°F and 1450 psia, the macroscopic absorption cross-section of heavy water is $2.7095 \times 10^{-5} \text{ cm}^2/\text{cm}^3$. On the other hand, because of the low density of supercritical CO_2 , its macroscopic cross-section is only $5.9543 \times 10^{-6} \text{ cm}^2/\text{cm}^3$ which is much smaller than heavy water.

The low macroscopic absorption cross-section usually means good radiation stability and low induced-radioactivity, because the coolant has little chance to be broken down or capture nuclear particles and become radioactive. Moreover, most of the possible neutron capture in CO_2 results in further stable nuclides. Therefore, CO_2 is stable in a radioactive environment.

It would be unrealistic to consider coolant-grade CO_2 as a pure

substance. A typical coolant analysis might be 10 p.p.m. H_2O , 3 p.p.m. Ar, 10 p.p.m. H_2 , 17 p.p.m. O_2 , and 94 p.p.m. N_2 ^[5]. The reactions which are important in considering induced radioactivity of impurities are listed in Table 1. Because of the shorter half-lives, the N^{16} and O^{19} nuclides decay quickly. The Ar^{41} which has an intermediate half-life gives a low residual activity in the cooling circuit, but the activity level taken in coolant leakage from the circuit as whole is too small to constitute a hazard.

REACTION	CROSS-SECTION (barns)	HALF-LIFE
$Ar^{40}(n,\gamma)Ar^{41}$	0.53	110 min.
$O^{18}(n,\gamma)O^{19}$	2.2×10^{-4}	29.0 sec.
$O^{16}(n,p)N^{16}$	16.0×10^{-6}	7.5 sec.
$O^{17}(n,\alpha)C^{14}$	0.4	5500 yrs.
$C^{13}(n,\gamma)C^{14}$	0.1	5500 yrs.
$N^{14}(n,p)C^{14}$	1.76	5500 yrs.

TABLE 1.

From a health physics point of view C^{14} is an important long-lived constituent of the coolant when it is released to atmosphere by leakage or during blowdown. The C^{14} is expected from three main sources which are also listed in the Table 1.

Although a proper estimate of radiation level or intensity from C^{14} is beyond the scope of the present study, it is clear that because its long half-life, any amount of C^{14} production in the coolant will require

careful measures to prevent its escape. This is parallel to the requirement of controlling tritium (T^3) discharge while using heavy water as a coolant.

2.4 Chemical Properties

The thermal stability of supercritical CO_2 is quite satisfactory up to the temperature envisaged for most reactor operations. Carbon dioxide tends to dissociate into CO and O_2 as the temperature is increased, but even at $1000^\circ K$ the equilibrium concentration of CO at a pressure as low as 10 atmospheres would be only 3 p.p.m. according to the data of Wagman et al.^[6] Moreover, CO_2 is relatively stable when irradiated so that the concentration of radiolysis products in supercritical CO_2 coolant should be low. This observation is confirmed by Bridge and Narin^[7]. In the presence of impurities (e.g., NO_2) that can react with small equilibrium concentrations of radiolysis products, CO_2 is progressively broken down^[8]. In British and French reactors, which use graphite as a moderator, a further reaction takes place between graphite and the chemically reactive species produced by the irradiation breakdown of CO_2 , resulting in a problem of attrition of graphite. However, dissociation of CO_2 is not a serious problem in CANDU reactors which use heavy water instead of graphite as a moderator.

When a reactor coolant is selected, the choice of reactor fuel is restricted. Today, uranium dioxide (UO_2) is used in CANDU reactors because of its compatibility with heavy water and light water. Uranium dioxide is an excellent fuel with a high melting point and high uranium content, but very low thermal conductivity. Uranium metal and uranium

carbide are also good fuels. They have high melting points, high uranium content and high thermal conductivity, but react vigorously with heavy or light water. For this reason, AECL has been looking for alternate coolants which are compatible with uranium carbide fuel developed by AECL^[9].

Using supercritical CO_2 as a coolant will allow use of uranium metal and uranium carbide as fuels. Although CO_2 reacts with uranium metal and uranium carbide, the rate of reaction is very slow. Measurements of the rate of change of weight of sintered uranium monocarbide specimens in dry CO_2 over the temperature range of $500^\circ\text{--}830^\circ\text{C}$ ($931\text{--}1525^\circ\text{F}$) were made by Atill et al.^[10]. The weight increased only by 120-170 mg/Kg/hr which was about 100 times as fast as the rate of change of weight of uranium metal under the same condition. The low rate of reaction between CO_2 and either uranium metal or uranium carbide allows enough time for defective fuel to be recovered before it becomes a serious problem. Wyatt^[11] has pointed out that when high integrity cans are used, it should be possible to use uranium metal and uranium carbide fuels with CO_2 coolant.

3. HEAT TRANSFER TO A LIQUID COOLANT AND MAXIMUM FUEL SHEATH OPERATING TEMPERATURE

3.1 Dryout in Coolant Channels

AECL has pioneered in-reactor heat transfer testing with experimental and power reactors, and has gained a large amount of operating experience with effects of coolant flow on fuel sheath behavior. Figure 4 shows a PHW CANDU reactor arrangement, and Figure 5 shows the details of the fuel bundle. The coolant flows into the coolant channels and travels within subchannels between fuel rods. The phenomenon of "dryout" has been detected in coolant channels, resulting in sudden and significant increase in fuel sheath temperature. Figure 6 shows variation in sheath or wall temperature in a coolant channel, along with a notation of the types of flow regions believed to be present.

Forced convection boiling in channels is an extremely complex phenomenon, but the main idea can be more easily understood by considering heat transfer from a small heating element submerged in a large stationary pool of liquid (pool boiling). Figure 7 shows the conventional representation of the heat flux q versus the temperature difference ΔT between the heating surface and liquid coolant bulk temperature. This curve can only be obtained if the temperature of the heating surface is carefully controlled. In the region preceeding point "a" on the curve, the heating surface temperature is nearly at or only a few degrees above the liquid temperature. Thus, there is insufficient liquid superheat and no bubble formation. Heat transfer in this region is therefore by liquid natural convection only. As the heating surface temperature is increased, the heat

flux increases and the region "a-b" is reached. A small number of nucleation centers become active, and a few bubbles are formed. These bubbles soon collapse as they move away from the surface. As ΔT is further increased between "b-c", the number of nucleation centers, and consequently the number of bubbles, increases rapidly with ΔT . The bubbles cause considerable agitation and turbulence of the liquid in the boundary layer and consequently a greater increase of the heat flux with ΔT . Region "b-c" is called the "nucleate boiling region". Point "c" is called the point of "departure from the nucleate boiling" (DNB), and the corresponding heat flux is called the "critical heat flux". The value of critical heat flux or the temperature of DNB depends on local coolant conditions. When region "c-d" is reached, the bubbles become so numerous that they begin to coalesce on the heating surface. In this case, a portion of the heating surface gets blanketed with vapor which acts as a heat insulator. This region is called "mixed nucleate-film boiling". In the region "d-e", a continuous blanket of vapor forms over the entire heating surface, and the heat transfer coefficient reaches its lowest value. This region is called "stable film boiling". In the region "e-f", called "film and radiation region", the temperature of the heating surface is so high that thermal radiation from the surface comes into play.

The curve in Figure 7 could not be obtained if the temperature of the heating surface was not closely controlled. In most practical cases, such as heat transfer in reactors, the heat flux is controlled. Referring to Figure 6, a sequence of events similar to that of pool boiling can now be imagined. The liquid enters as a single phase; the vapor bubbles start to form; small bubbles collapse together to form slugs, and a liquid annulus

forms. Finally, the local heat flux becomes critical to the local coolant condition, corresponding to the point "c" of the curve in Figure 7. A further increase in heat flux or increase in vapor quality results in a sudden local temperature jump which corresponds to the jump from "c" to "c'" into the film-radiation region. The heating surface temperature at "c'" may be high enough to exceed the safe operating limit. The complete loss of coolant along with a sudden jump of temperature of the heating surface is called "dryout".

Dryout can occur not only in a boiling channel where phase change takes place, but also at a point in a compressed liquid coolant channel because of increase in local heat flux or local coolant starvation. Dryout is very dangerous in reactor operation, since local temperature increases may soften the fuel elements. They may bend toward the coolant tube and cause poor heat transfer due to local coolant starvation, which further elevates the temperature. This may finally result in fuel sheath failure.

3.2 Maximum Operating Sheath Temperature

Since dryout is a critical design parameter, all coolant channel conditions must be controlled so that a significant margin of safety is available to prevent dryout from occurring during normal operation. In other words, the operating temperature of the fuel sheath must be kept below the critical heat flux temperature, which is approximately equal to the temperature of the reactor coolant.

Figure 8^[12] shows the calculated subchannel temperatures in a 28-element fuel bundle design with a given heat flux shape along the channel and given maximum linear rates for individual subchannels. The

heat flux shape and the maximum linear heat rates are based on data during steady state operation of a CANDU 500 reactor at the Pickering station*.

An inter-subchannel mixing rate was assumed in calculating the temperatures in Figure 8. The calculation agrees well with the measurement, and shows that the maximum local external sheath temperature exceeds the coolant saturation temperature by only about 5°F. Nucleate boiling would actually begin on the sheath surface at a temperature about 10°F above the coolant saturation temperature.

The maximum operating sheath temperature in a CANDU reactor is usually kept much below the maximum withstanding (metallurgical) temperature of the fuel sheath. Zircaloy clad UO_2 fuel elements (like those used in CANDU reactors) can actually operate at an elevated temperature for a certain period without failure. Operating life is assumed inversely proportional to the magnitude of the temperature. Some data from various tests are summarized in Figure 9^[13] which is a semilog plot of time-to-defect versus temperature. It shows that zircaloy clad fuel elements can operate at a temperature below approximately 550°C without defect for a relatively long period.

If supercritical CO_2 were used as a coolant for a CANDU reactor, dryout could not happen since supercritical CO_2 would remain in a single phase throughout the operating temperature range. Therefore, fuel sheath temperature jump would no longer be a cause of worry under normal operating conditions. The saturation temperature of the coolant is no longer a barrier to the upper limit of the maximum fuel sheath temperature, and the operating

* Pickering station is the first commercial CANDU-PHW reactor power generating station, owned and operated by Ontario Hydro.

fuel sheath temperature can be as high as 550°C (1021°F). This implies that the maximum coolant temperature, and thus the efficiency of reactor power generation, can be higher than the corresponding liquid coolant.

4. PROPOSED SUPERCRITICAL CO₂ COOLING LOOP FOR CANDU REACTORS

4.1 Use of the Supercritical Cycle in Reactor Power Generation

Supercritical fluids have gained much attention as coolant media in many applications. Currently, supercritical hydrogen is used as the fuel and coolant in combustion chambers of large rocket engines. Supercritical water is used as a working fluid in fossil-fuel power generating stations, and near-critical helium is used as a coolant in super-conducting applications. Many other applications are being proposed and investigated. Among them is an entirely supercritical turbine power cycle, with a nuclear reactor as a direct heat source (the entirely supercritical turbine power cycle will be referred to as the supercritical cycle in this work).

Although the supercritical cycle with a reactor as a direct heat source has not been previously investigated, both the supercritical cycle and the supercritical fluid cooled reactor have been separately studied. The performance of supercritical cycles has been analysed by many workers^[14,15,16], who pointed out the high efficiency of the cycle. In a case study of a supercritical CO₂ power cycle^[16], the power plant has an overall efficiency as high as 48%. There are many advantages to the cycle: low volume-to-power ratio, no blade erosion in turbines, no cavitation in pumps and single stage turbine and pump operation. The SCOTT-R reactor system^[17], which is cooled by using supercritical light water, is currently under investigation. Reactors cooled by using supercritical fluids have the advantage of avoiding the limitations imposed by boiling heat transfer and also the advantage of high enthalpy rise through the core. As expected, direct application of the coolant as the working fluid

of a supercritical cycle has the combined advantages as discussed above.

The high operating pressure is the basic engineering problem when a supercritical fluid is used not only as the working fluid of the cycle, but also as the coolant of a reactor. The high operating pressure requires thicker structural parts of the system. The increase of reactor material results in an increase of neutron absorption, and hence, the decrease of the reactor neutron economy which directly determines the fueling cost in nuclear power generation. Therefore, the high efficiency of the supercritical cycle with a reactor as a direct heat source can be overshadowed by high fueling costs.

The maximum operating pressure of the supercritical cycle depends on the critical pressure of the fluid used. For example, according to an analysis of the supercritical CO_2 cycle^[14], the ratio of required turbine inlet pressure to pump inlet pressure is equal to two for optimum performance, and pump inlet pressure should be maintained above the critical value. If that is also true for the supercritical water cycle (critical pressure of 3206 psia), the turbine inlet pressure must be approximately equal to 6500 psia. This pressure is too high to be practical in engineering designs.

To solve the problem of high pressure operation, alternative fluids having a low critical pressure must be sought as substitutes for water. However, when the fluid is used not only as a working fluid but also as a coolant, the choice of the fluid is restricted not only by the requirement of low critical pressure but also by coolant characteristics. Carbon dioxide has a low critical pressure ($P_c = 1071.3$ psia) and seems to meet almost all other necessary requirements. Supercritical CO_2 may make use of a supercritical cycle with a reactor as a direct heat source possible in the

future.

4.2 Supercritical CO₂ Cooling Loop

While the direct cycle described in the previous section appears attractive for future use, several major hardware development programs are required before a power plant using the cycle could be built. For example, power turbines which could operate with CO₂ would have to be developed and built. In addition, the present CANDU reactors would have to be modified. In order to be able to use present CANDU reactor technology and conventional steam turbine power generating equipment, an intermediate step of using a supercritical cooling loop is proposed in this work.

A schematic diagram of the proposed loop is shown in Figure 10, along with its process path on a temperature-entropy diagram. The loop contains the following steps:

- (a)-(b). liquid-like supercritical CO₂ is pumped from low pressure to high pressure;
- (b)-(c). high pressure CO₂ gains heat in the recuperator from low pressure CO₂ leaving the steam generator;
- (c)-(d). supercritical CO₂ is heated in the reactor;
- (d)-(e). hot supercritical CO₂ generates steam in the steam generator;
- (e)-(f). low pressure CO₂ from the steam generator gives up heat in the recuperator;

(f)-(a). supercritical CO_2 is further cooled to become a high density liquid-like fluid.

Recuperation is used in the loop to maintain high entry temperature of the coolant into the reactor. High entry temperature results in generation of higher pressure and temperature steam. The temperature of the coolant entering the reactor, i.e., the temperature of the coolant leaving the steam generator, affects the overall efficiency of power generation as will be discussed in a later chapter. Supercritical CO_2 from the recuperator is further cooled below the pseudo-critical temperature in order to reduce pumping power.

Although gas-cooled reactors also have no limitations imposed by boiling heat transfer, the basic design concept of a supercritical CO_2 cooled CANDU reactor is entirely different, due to the drastic changes of thermophysical properties of supercritical CO_2 across the pseudo-critical temperature. In the gas-cooled reactor, because the gaseous coolant is circulated in a low density state, the flow areas are large and the speed of the coolant is low in order to have minimum pressure drop and low pumping power. To cope with the problem of poor heat transfer to the slow moving coolant, fuel elements normally have fins added to their outer surfaces. Hence, the flow area is further increased to deal with the problem of high pressure drop introduced by the fins. Therefore, gaseous coolants are not suitable for use in the CANDU reactor since:

1. large diameter coolant tubes would be required;
2. large amounts of coolant are required in the reactor, increasing the capital and upkeep costs;

3. poor heat transport characteristics of gaseous coolants may limit the coolant temperature.

Because the pumping power would be low using supercritical CO_2 , the designer can afford higher pressure drops from high speed coolant flow in smaller cross-sectional area channels in order to create high heat transfer rates. For this reason, the supercritical CO_2 -cooled reactor does not have the previously discussed problems of gas-cooled reactors, despite the poor thermophysical characteristics of supercritical CO_2 at high temperature. Supercritical CO_2 cooling appears very practical for the CANDU reactor, which uses bundle-cluster or tube-in-shell fuel elements in small diameter coolant tubes.

5. HEAT TRANSFER TO SUPERCRITICAL CO₂ COOLANT

Heat transfer to supercritical fluids in fuel bundles has not been studied as far as the author is aware. However, the separate cases of heat transfer to supercritical fluids in heated pipes and to single phase fluids in fuel bundles are currently under investigation. This chapter will discuss the previous investigations of these cases individually. Finally, based on these separate studies, heat transfer to supercritical CO₂ in fuel bundles is analysed.

5.1 Heat Transfer to Supercritical Fluids in Pipes

5.1.1 Peculiarities of Heat Transfer to Supercritical Fluids

This section discusses the peculiarities of heat transfer to supercritical fluids which must be taken into account in actual design of heat exchanger equipment. These peculiarities strongly affect the performance of a supercritical cooling loop.

Heat transfer problems are classified according to the fluid states as shown in Figure 11^[18]. The five regions are the liquid, gas, two-phase, above-critical, and near-critical regions. Regions I and II refer to single phase liquid and gas in which heat transfer rates can be predicted by the usual forced convection equations. The fluid in region III is a two-phase fluid and heat transfer occurs by boiling. Region IV is the above-critical region where the mechanism for heat transfer is not well understood. Region V is the near-critical region where special heat transfer phenomena still require a great deal of study.

It is very difficult to precisely define the boundaries of the

regions, especially the boundaries which separate the near-critical region from its adjacent regions. There are two important reasons for this: the transition is not abrupt and sharp, and the extent of the influence of the critical region on heat transfer is a function of the process or path by which the fluid approaches the critical point. For example, a hysteresis loop in density near the critical point^[19] could be obtained by first heating and then cooling along an isobar. The supercritical CO₂ cooling loop investigated in this study uses a fluid which passes through the above-critical and near-critical regions.

Interest in the study of heat transfer to supercritical fluids was initiated by the work of Schmidt^[20] in the early 1930's. He pointed out that because the specific heat at constant pressure and the compressibility both grow very large at the critical point, the heat transfer coefficient, which is a function of the Prandtl and Grashof numbers (Pr, Gr), should be very large. For supercritical ammonia, Schmidt^[21] later found an apparent thermal conductivity (the thermal conductivity required of a solid bar of the same dimension as the test chamber to transfer the experimentally observed amount of heat for a given temperature gradient) as large as 4000 times that of pure copper over a narrow temperature range. However, until the mid-1950's, very few investigations into supercritical heat transfer were reported. Because of the increase of applications of heat transfer to supercritical fluids, investigations in this region have been greatly increased in recent years. Although some workers^[22,23,24,25] reported that the heat transfer coefficient was enhanced as proposed previously by Schmidt, many other workers^[26,27,28,29] reported that heat transfer in the near-critical region actually approached a minimum value.

In his survey, Petukov^[30] classified the heat transfer to supercritical fluids into three regimes: normal, reduced, and improved. In the normal heat transfer regime, there is significant variation in physical properties of the supercritical fluid across the flow, but the dependence of Nusselt number (Nu) on Reynolds number (Re) and Pr is approximately the same as in the case of heat transfer to constant property flows. Therefore, relationships which govern the normal heat transfer can usually be derived.

In the reduced heat transfer regime, the heat transfer coefficient and wall temperature do not satisfy the same relationships which govern normal heat transfer in the supercritical region. The heat transfer coefficient depends not only on Re and Pr but also on the heat flux, and is less than the value calculated from the normal heat transfer relationships. The reduced heat transfer condition usually occurs when the mean fluid temperature is less than the pseudo-critical temperature at a particular combination of bulk velocity and heat flux, and the wall temperature is usually, but not necessarily, much greater than the pseudo-critical temperature.

The improved heat transfer regime occurs only at a high heat flux with the bulk temperature less than the pseudo-critical and the wall temperature slightly greater than the pseudo-critical temperature. The heat transfer rate increases with increasing bulk density and velocity, but decreases with increasing bulk temperature. As in the reduced heat transfer regime, the heat transfer coefficient depends on Re, Pr, and also the heat flux.

Hsu^[37] explained the increases and decreases of heat transfer rates by comparison with the boiling mechanisms of a liquid, discussed in Chapter 3. He pointed out that when the temperature difference is small,

the mechanism can be linked to nucleate boiling, a regime of very good heat transfer, thus the maximum. When the temperature difference is large, the mechanism can be compared to film boiling, a regime of poor heat transfer, thus the minimum. Many other workers^[31,32,33] strongly supported this explanation of a pseudo-two-phase fluid. However, when a supercritical fluid is in equilibrium, it must exist as a single phase, which opposes such a pseudo-two-phase fluid hypothesis. Hauptmann^[34] showed that "boiling" does not exist during heat transfer to supercritical fluids, and concluded that all of the unusual results could be explained in single phase terms. Kafengauz^[35] explained the physical nature of the unusual results of heat transfer at supercritical pressure. He suggested boiling could be observed in some experiments because fluctuations in pressure caused bulk pressure to fall below the critical. In his work, a theoretical approach was developed which was verified by experimental data with diisopropyl cyclohexane.

Disregarding the possible existence of boiling, Petukhov^[30] described reduction and improvements in heat transfer to supercritical fluids with a rather clear picture. The onset of the regime with reduced heat transfer is apparently associated with a change in the hydrodynamics of the flow and, in particular, with turbulent transfer processes due to the great variation in thermophysical properties of the medium over the cross section of the flow. For example, Wood^[36] found M-shape velocity profiles during supercritical fluid flow in pipes. This was very different from the U-shape velocity profiles of constant property fluid in pipes. Free convection due to the large density gradient present may also have a significant effect on the nature of the flow. This point is confirmed by the fact that reduced heat transfer occurs only in a heated tube with

ascending flow but not descending flow. In the latter case, normal heat transfer is observed. This is probably because of the more intense mixing due to opposing directions of forced and free convection near the wall.

Petukhov^[30] explained that improvement in heat transfer at high heat flux is also apparently due to the very pronounced changes in thermophysical properties of the medium (mainly density and specific heat at constant pressure) over the cross section of the flow. The density of the medium at the wall is several times less and the specific heat is several times more than in the core of the flow. Fluid which reaches the hot wall from the core, owing to turbulent transport, has a relatively high thermal conductivity and low specific heat. If there are large differences in temperature between the fluid next to the wall and the fluid arriving from the core, the fluid picks up heat very rapidly and expands in an explosive manner. This process must result in more intense mixing of the fluid in the layer next to the wall, and hence, in improved heat transfer. These special features of variable property turbulent heat transfer are not taken into account in existing theories, and therefore, present theories cannot satisfactorily describe the improved heat transfer regime.

Although dryout due to boiling would not be a limitation in the design of a supercritical cooling loop, other limitations due to the peculiarities of heat transfer to supercritical fluids must be taken into account. The reduced heat transfer regime could occur in the recuperator of the proposed supercritical cooling loop, where the coolant is at a temperature near the critical value. However, the reduced heat transfer regime can be avoided by careful design of the heat transfer surface and the fluid velocity, etc., for a given heat flux distribution. On the

other hand, a compact and efficient recuperator can be designed based on knowledge of the improved heat transfer characteristics of supercritical fluids.

5.1.2 Previous Studies of Heat Transfer to Supercritical Fluids

Heat transfer mechanisms in supercritical fluids are not yet well understood. However, many investigations are currently underway in the near-critical region where most of the heat transfer peculiarities take place. Heat transfer in the above-critical region, where variations in thermophysical properties of the fluid across the flow affect heat transfer to a lesser extent, is usually thought of as a special case of the near-critical region. Therefore, the mechanisms of heat transfer in the near-critical region may also apply to the above-critical region.

Theoretical analyses of heat transfer in the supercritical region with allowance for the temperature dependence of thermophysical properties of the fluid were first made by Deissler^[38] and Goldmann^[39]. In these investigations, fluids were assumed to be incompressible, the effect of body forces were negligible, the dissipation of kinetic energy and fluctuation of the thermophysical properties were ignored, and the pressure was assumed to be constant over the cross section of the flow. In some later investigations^[40,41], the effect of fluid inertia and buoyant forces were also taken into account.

Theoretical analyses which are based on the continuity, energy, and Navier-Stokes equations usually employ the Prandtl mixing length concept. The basic idea is to simplify the shear stress term of the Navier-Stokes equation and the heat conduction term of the energy equation. Then

the shear stress and heat flux can be expressed in the simpler forms^[40]:

$$\tau = (\mu + \rho \epsilon_m) \frac{\partial u}{\partial y} , \quad \dots (1)$$

$$q = - (K + \rho C_p \epsilon_h) \frac{\partial T}{\partial y} . \quad \dots (2)$$

Most types of eddy diffusivities can be broken into two categories:

(1) continuous, and (2) multiple-part. In each category, the turbulent momentum transport can be further considered as a function of local thermophysical properties.

Numerical solutions are usually presented as a part of theoretical analyses. However, correlation of predictions and experiments are successful only for the particular experiments used to provide the modified eddy diffusivities. For this reason, theoretical methods are not widely used for designing heat transfer equipment using supercritical fluids.

Experimental studies have been a major part of the research on heat transfer to supercritical fluids. The experimental works can be classified as either free or forced convection. Since free convection is minimal in the supercritical cooling loop of this study, it is not discussed further.

Forced convection experiments can be further divided into two major categories: experiments which attempt to explain the mechanism of heat transfer to supercritical fluids, and conventional heated pipe experiments which are used to determine dimensionless correlations. The second category is directly related to the application of a supercritical CO₂ cooling loop and is the only one discussed here.

Many heated tube experiments have been carried out in England, Japan, U.S.A., and U.S.S.R. All of these experiments were very similar in design and used mainly water and CO_2 as experimental fluids. Hydrogen, oxygen, and Freon^{*} have also been studied by some authors. The results of most of these efforts fall into the range of the near-critical region, where heat transfer differs most from normal heat transfer as governed by single phase fluid correlations.

The earliest form of correlation was in the form of the Dittus-Boelter equation^[42,43,44]:

$$\text{Nu} = A(\text{Re}_z)^b (\text{Pr}_w)^c, \quad \text{..... (3)}$$

where A, b, and c are experimental constants. The Reynolds number Re_z is evaluated at the reference temperature T_z for a given pressure, which is expressed in the form:

$$T_z = T_b + Z(T_w - T_b) \quad \text{..... (4)}$$

The parameter Z is a function of the dimensionless temperature:

$$Z = (T_m - T_b) / (T_w - T_b), \quad \text{..... (5)}$$

and Pr_w is the Prandtl number evaluated at the wall temperature. The subscripts represent the conditions of fluid bulk, wall, and pseudocritical, respectively.

Another early correlation was proposed by Miropolski and Shitsman^[45]. It has a form similar to the Dittus-Boelter equation:

* Freon: dichlorofluor methane (12).

$$Nu = 0.023(Re_b)^{0.8} Pr_{min} , \quad \dots (6)$$

where Pr_{min} is the minimum Prandtl number defined as:

$$Pr_{min} = \begin{cases} Pr_b & ; \quad Pr_b < Pr_w \\ Pr_w & ; \quad Pr_w < Pr_b \end{cases} . \quad \dots (7)$$

This simple modification, however, produces some remarkable results. It correlates some experimental data at the near-critical region with great accuracy^[54].

Correlation factors were later introduced for bulk temperature^[46] and thermophysical property variations^[22,47,48,49,50]. The correlations can be expressed as:

$$Nu = Nu_o (T_b/T_w)^n , \quad \dots (8)$$

$$Nu = Nu_o (\mu_w/\mu_b)^a (K_w/K_b)^b (\rho_w/\rho_b)^c (\overline{Cp}/Cp_b)^d , \quad \dots (9)$$

where a , b , c , d , and n are experimental constants. The Nusselt number Nu_o is evaluated from constant property fluid flow correlations:

$$Nu_o = 0.023(Re_b)^{0.8} (Pr_b)^{0.4} , \quad \dots (10)$$

or by ^[51]:

$$Nu_o = \frac{(\xi_o/8.0) Re_b Pr_b}{12.7[\xi_o/8.0]^{1/2} [(Pr_b)^{2/3} - 1.0] + 1.07} , \quad \dots (11)$$

$$\xi_o = [1.82 \log (Re_b) - 1.64]^{-2.0} \quad \dots (12)$$

The term \overline{Cp} in equation (9) is called the integrated specific heat, defined as:

$$\overline{Cp} = (h_w - h_b) / (T_w - T_b) \quad \dots (13)$$

The integrated specific heat has been proven by experiments to be an efficient term for correlating data. Therefore, Swenson et al. [23] generalized their experimental data for heat transfer by:

$$Nu = 0.00459 (Re_w)^{0.923} (\overline{Pr}_w)^{0.63} (\rho_w / \rho_b)^{0.231} \quad \dots (14)$$

where \overline{Pr}_w is called the integrated Prandtl number and defined as:

$$\overline{Pr}_w = \overline{Cp} (\mu_w / K_w) \quad \dots (15)$$

The concept of using not only integrated specific heat but all physical properties on an integrated average basis was suggested by Hiroharu et al. [52] for supercritical fluids. They suggested the normal correlations for heat transfer to single phase fluids be used as correlations for supercritical fluids. However, the Nusselt number is evaluated at integrated property values which would be expressed as:

$$\overline{F} = \frac{1}{T_w - T_b} \int_{T_b}^{T_w} F(T) dT \quad \dots (16)$$

As with theoretical analyses, most of the experimentally determined correlations must be modified to fit the data of particular experiments.

However, these correlations usually predict heat transfer with greater accuracy than the theoretical analyses, especially in the experimental data range from which the correlations have been derived. Some correlations cover a rather wide range of experimental data, and have sufficient accuracy for engineering designs. Therefore, it is possible to study some applications of heat transfer to supercritical fluids simply by choosing an appropriate correlation.

5.2 Engineering Calculation of Heat Transfer to Supercritical Fluids

5.2.1 Choice of Correlations

The correlation chosen for the supercritical CO₂ cooling loop of this work must be: (1) accurate in correlating heat transfer in the operating range of the proposed supercritical cooling loop, and (2) easy to use in computing programs. In this section, several types of correlation are discussed.

Although reference temperature correlations were the earliest ones developed, there are drawbacks in their use. First, they fail to predict heat transfer coefficients accurately in the temperature range near the pseudo-critical temperature; a small difference of the reference temperature value T_z can cause a large variation in the predicted heat transfer coefficient because of the extremely sharp property variations near the pseudo-critical temperature. Second, this type of correlation is very inconvenient when heat flux is specified and the wall temperature is to be calculated.

In contrast to the reference temperature correlations, the minimum Prandtl number correlations produce accurate results in the near-critical

region. Although these types of correlation were derived from supercritical water heat transfer data, they successfully correlated oxygen data of Powell^[26] and CO₂ data of Bringer and Smith^[43]. However, they failed to predict heat transfer to supercritical hydrogen. More important is the fact that these correlations can account for the maximum heat transfer reported by Powell^[26], as well as Dickson and Welch^[54]. Therefore, the minimum Prandtl number correlations should be considered for use in calculating heat transfer to supercritical CO₂.

The correction factor types of correlation are also popular, although the temperature correction factor is not very accurate. For example, the correlation^[47]:

$$Nu = Nu_o (T_w/T_b)^{-0.27} , \quad \dots (17)$$

adequately predicts heat transfer to supercritical fluids at high temperature but breaks down when the heat flux is increased. This is mainly due to the fact that the dependence of fluid properties on temperature is different in different temperature ranges. Therefore, correction factors must be used on fluid properties which strongly affect the fluid dynamics and heat transfer of the flow. The first correlation with property factors was introduced by Petukhov et al.^[22]:

$$Nu = Nu_o (\mu_b/\mu_w)^{0.11} (K_b/K_w)^{-0.33} (Cp/Cp_b)^{0.35} . \quad \dots (18)$$

The key feature of this correlation is the use of the integrated specific heat \overline{Cp} . This correlation covers a rather wide range of experimental data for water and CO₂. However, it fails to predict heat transfer rates correctly at very high heat flux, possibly because at high temperature

drops (high heat flux) the density difference becomes important. The significance of the density correction factor was pointed out by Kutateladze and Leontev^[48], and also by Swenson et al.^[23].

A correlation modified by a density ratio correction factor was first introduced by Kranshchekov and Protopopov^[49], based on CO₂ data. This correlation was later developed for calculation of heat transfer to supercritical CO₂ at a normalized pressure $(P/P_c) = 1.02 - 5.25$ ^[50] as:

$$Nu = Nu_o (\overline{C_p}/C_{p_b})^n (\rho_w/\rho_b)^m, \quad \dots (19)$$

where: $m = 0.35 - 0.5(P/P_c)$, and $n = 0.4$

at $T_w/T_m \leq 1.0$ or $T_b/T_m \geq 1.2$,

and, $n = n_1 = 0.22 + 0.18 (T_w/T_m)$

at $1.0 \leq T_w/T_m \leq 2.5$,

and, $n = n_1 + (5n_1 - 2)(1 - T_b/T_m)$

at $1.0 \leq T_b/T_m \leq 1.2$.

The correlation was later tested by Kransnoshchekov et al.^[55] with data from heat transfer to supercritical CO₂ at temperature differences up to 805°C. Experimental data agreed with this correlation within an accuracy of $\pm 15\%$. Petukhov et al.^[56] also tested this correlation with their experimental data, and gained satisfactory agreement. This correlation was further used to calculate local heat transfer rates to supercritical CO₂ in annular channels with internal heating by Glushcheznko and Gandzyuk^[57], and in a rectangular channel heated from one side by Protopopov^[58]. Despite the fact that the correlation (19) was derived from heat transfer data for a circular heated tube, in both the previous cases the calculated

wall temperatures agreed well within the experimental data range of $T_b > T_m$ and $T_b < T_m$. Heat transfer rates were most unpredictable at $T_b = T_m$ with heat transfer coefficients about 30-50% too low.

An integrated Prandtl number correlation has been developed for studying heat transfer to supercritical water coolant in reactors^[59]. However, this type of correlation was based on supercritical water data and gave poor results when used to predict heat transfer to supercritical CO_2 ^[23].

Hiroharu et al.^[52] confirmed experimentally the accuracy of the types of correlation using all properties as integrated properties. However, all their experiments were carried out with low temperature differences (low heat flux), and the correlations have not been tested by other authors. This suggests that these types of correlations have no guarantee of accuracy for predicting heat transfer rates at high temperature differences.

The above discussion shows that the minimum Prandtl number and integrated specific heat types of correlations are preferable for calculation of heat transfer for the supercritical CO_2 cooling loop of this work. The correlation given in equation (19) was finally chosen instead of the minimum Prandtl number correlation because not only does it meet all requirements pointed out at the beginning of this section, but because it has been widely tested with experimental heat transfer data for supercritical CO_2 .

5.2.2 Examination of Chosen Correlation

When the correlation given by equation (19) was first developed,

it was based on the data range: $1.01 \leq P/P_c \leq 1.33$; $0.6 \leq T_b/T_m \leq 1.2$; $0.6 \leq T_w/T_m \leq 2.6$; $2 \times 10^4 \leq Re_b \leq 8 \times 10^5$; $0.85 \leq Pr_b \leq 55.0$; $0.09 \leq \rho_w/\rho_b \leq 1.0$; $0.02 \leq \overline{Cp}/Cp \leq 4.0$; $2.3 \times 10^4 \leq q_w \leq 2.6 \times 10^6 \text{ W/cm}^2$; and $l/d \geq 15.0$. This correlation predicted heat transfer coefficients in a heated circular pipe within the accuracy of $\pm 15.0\%$. Later, this correlation was further developed to cover data up to $P/P_c = 5.25$. It was particularly interesting that this correlation predicted the pronounced peak of wall temperatures in experiments within the suggested accuracy up to the data range of $Re_b = (0.6 - 1.2) \times 10^6$ and $T_w/T_m \leq 3.6$.

In equation (19), Nu_0 is calculated from equation (11). This formula was developed by Petukhov and Kirillov^[51] from a theoretical analysis of fully developed heat transfer to a single phase, constant property flow in a circular, heated pipe. This formula predicts heat transfer coefficients for constant property fluids within the accuracy of $\pm 10.0\%$ for the range: $0.5 \leq Pr_b \leq 2000.0$ and $1.0 \times 10^4 \leq Re_b \leq 5.0 \times 10^6$. It must be noted that in contrast to the conventionally used formula with constant exponents for Re_b and Pr_b , this formula more accurately corresponds to the dependence of heat transfer on Re_b and Pr_b . This is particularly apparent in the case of $Re_b \geq 1.0 \times 10^5$ and $Pr_b \geq 10.0$.

In the regions more remote from the critical state, the properties of a supercritical fluid become approximately constant over a relatively wide range of temperature and the correlation in equation (19) reduces to equation (11). Petukhov et al.^[22] showed that the formula in equation (11) also agrees with experimental data in the near critical region under the condition of small variation of properties over the cross section; i.e., at small temperature drops. Thus, the correlation is a very general

expression for heat transfer in the near-critical region as well as in regions remote from the critical state.

In order to calculate the temperature distribution along a heated channel, the pressure distribution of the supercritical fluid along the channel must be known since the thermophysical properties which determine heat transfer are a function of both temperature and pressure. Many works are devoted to the investigation of heat transfer at supercritical pressure. However, studies of flow and pressure drop are scant.

Tarsova and Leontez^[61] developed one of the first engineering correlations for the calculation of friction coefficients. Later, Kuraeva and Protopopov^[62] further developed this correlation by including the effects of possible free convection. The improved correlation was based on the data of Kranoshchekov et al.^[49]. This correlation can be put into the following form:

$$\begin{aligned} \xi &= \xi_s = \xi_o (\bar{\mu}_w / \tilde{\mu}_b)^{0.22} \quad \text{for} \quad Gr/Re_b^2 \leq 5 \times 10^{-4}, \\ \xi &= \xi_s 2.15 (Gr/Re_b^2)^{0.1} \quad \text{for} \quad 5 \times 10^{-4} < Gr/Re_b^2 \leq 3 \times 10^{-1}, \end{aligned}$$

.... (20)

where ξ_o is calculated from equation (12). The viscosity $\tilde{\mu}_b$ is evaluated at the temperature \tilde{T}_b which corresponds to the average pressure and integrated density:

$$\tilde{\rho} = \left[\frac{1}{\Delta \ell} \int_0^{\Delta \ell} \frac{dx}{\rho(x)} \right]^{-1}, \quad \dots (21a)$$

and the viscosity $\bar{\mu}_w$ is evaluated at the temperature \bar{T}_w which is the wall temperature of the tube:

$$\bar{T}_w = \frac{1}{\Delta \ell} \int_0^{\Delta \ell} T_w(x) dx \quad \dots (21b)$$

The pressure drop is then calculated from the formula:

$$\Delta P = \xi \frac{(\rho u)^2 \Delta \ell}{2 \rho d} + \overline{(\rho u)^2} \left(\frac{1}{\rho_{out}} - \frac{1}{\rho_{in}} \right) \quad \dots (22)$$

Thus, when the equation (22) is applied outside the near-critical region and the physical properties of the flow do not change drastically, the equation can reduce to the form:

$$\Delta P = \xi \overline{(\rho u)^2} \Delta \ell / 2 \rho d \quad \dots (23)$$

Based on the correlation in equation (19) for heat transfer, the formula in equation (22) for pressure drop, the energy equation, and the continuity equation, a computer program was designed to calculate the wall temperatures, bulk fluid temperatures, and pressure drop along a heated pipe with a given heat flux as a function of distance from the entrance.

The basic assumptions in the program are: (1) the pipe is hydraulically smooth; (2) the heat transfer coefficient is a function of local conditions only; (3) the flow is turbulent and fully developed; and (4) pressure is constant at a cross section. An additional factor $f(x/d)$ allows for the

increase in heat transfer in the initial portion of the pipe^[55]:

$$f(x/d) = 0.95 + 0.95(x/d)^{-0.8} \quad \dots (24)$$

All required equations for the calculation are listed in Figure 12. The flow chart for the program is shown in Figures 13 and 14, and details of the procedure are given in Appendix I.

The program was first tested against the experimental data of Jackson and Evans-Lutterodt^[60]. As shown in Figure 15, the program accurately predicts the wall and bulk temperatures along the heated pipe for the case in which buoyancy forces do not exist. Both the bulk and wall temperatures along the pipe are below the pseudo-critical temperature.

This program was also used to predict heat transfer to super-critical flow in pipes under other conditions as shown in Figures 16, 17, and 18. Figure 16 compares predicted values with the experiments of Kranoshchekov et al.^[49]. In this case, both the bulk and wall temperatures along the pipe are above the pseudo-critical temperature. The difference between the calculated wall and bulk temperature profiles is within $\pm 10\%$ of the experimental values. Figure 17 shows data from Kranoshchekov et al.^[55] in which the bulk temperatures along the pipe are less than the pseudo-critical temperature and the wall temperatures are greater than the pseudo-critical temperature. The computed results correspond amazingly well with the experimental data. The heat flux and wall temperatures in Figure 17 are beyond the range of limits first suggested for the correlation. Figure 18 shows the special case of Schnurr^[42], in which the fluid bulk temperature spans the pseudo-critical temperature. However, the calculated results still match well with the experimental data.

In general, the program predicts heat transfer rates within the expected accuracy of the correlation. Accuracy increases in regions further away from the critical state, but calculated temperatures are higher than the actual at an intermediate distance from the critical state. Under the latter condition, the correlation factor in equation (19) may still be less than a unity. In conclusion, the program based on the correlation in equation (19) and the conservation equations is suitable for analyses of the supercritical CO₂ cooling loop in this study.

5.3 Heat Transfer to Single Phase Fluids in Fuel Bundles

Heat transfer in fuel bundles (see Figure 4) can be classified as either single or two-phase. The work in each class is further divided into theoretical and experimental studies. In this section, only previous studies on the prediction of heat transfer to single phase fluids in bundles are discussed. The single phase fluids of concern are compressed liquids and subcritical gases.

The theoretical works mainly involve prediction of performance characteristics of clustered rod bundles under conditions of fully developed heat transfer to axially uniform heat flux, together with the related hydrodynamic problems for longitudinal flows. The coolant can be in laminar, turbulent, or slug flow.

There are three methods for analysing heat transfer in bundles currently in use: fundamental, equivalent annulus, and lumped parameter. The fundamental method for theoretical prediction of heat transfer to single phase fluids in bundles is based on solution of the momentum and energy equations. This approach has gained certain success for laminar

flow, where analytical solutions have been found for the velocity fields of: (a) infinite rod clusters, (b) semi-infinite rod clusters, and (c) some special geometry finite rod clusters. Based on the known velocity fields, heat transfer rates can be determined for laminar longitudinal flow in an infinite rod cluster. In the case of turbulent flows, heat transfer has also been successfully analysed for infinite rod clusters. There are three approaches in these analyses: (1) both velocity and temperature fields are computed by iterative procedures; (2) the velocity field is first determined graphically and used in the differential form of the energy balance, which is numerically integrated by finite difference procedures; (3) both the differential forms of the momentum and energy balance are integrated numerically by finite difference procedures to obtain the velocity and temperature fields. Despite the fairly accurate predictions made for simple geometries, the fundamental method is not so easy to apply to more complex flow geometries.

In the equivalent annulus method, the complicated rod cluster is divided into many annuli. An equivalent model can be used to describe the entire array of rods in the bundle as shown in Figure 19a^[67]. The bundle is approximately divided into annuli, with some being heated from both sides and others from one side only. The basic solution for the concentric annulus is then applied to each region. This method is mainly used by designers to adjust rod spacing to obtain the desired flow split between regions, and has been found to be quite satisfactory for relatively widely spaced bundles.

Another equivalent annulus model considers individual rods in parallel rod arrays. As seen in Figure 10b^[68], the hexagonal flow passage defined by zero shear planes around a rod may be approximated by a circular

tube of equivalent area. This flow passage (bounded by the rod and the zero shear planes) is assumed to be equivalent to the region between the center tube and the zero shear plane of an annulus.

The advantage of the equivalent annulus model is that heat transfer rates can be easily calculated by applying available solutions for the concentric circular tube annulus. The principal limitation, of course, is how well the equivalent annulus represents the actual flow. The experimental data shows that the equivalent annulus method is only roughly correct^[69,70]. The analogy tends to underestimate the Nusselt number at high Reynolds number, and breaks down completely at close rod spacing (i.e., Pitch/Rod Diameter ~ 1.1) because the circular shear plane is no longer a good approximation to the actual zero shear planes.

In the lumped parameter type of analysis, the flow in the array is divided into many subchannels as shown in Figure 20^[71]. The characteristic dimension of each subchannel is expressed as the equivalent hydraulic diameter:

$$D_h = \frac{4 \times \text{Cross-sectional Area}}{\text{Wetted Perimeter}} \quad \dots (25)$$

The axial pressure gradient in each subchannel is then determined on the basis of the equivalent hydraulic diameter and a friction factor which is calculated from a given correlation. The flow is balanced for all subchannels in the array by equating the pressure drops. The fluid bulk temperature in each subchannel is calculated from the known heat flux distribution and inter-subchannel mixing rates. Based on the equivalent hydraulic diameter, subchannel flow rate and local fluid bulk temperature, the local heat transfer coefficient and wall temperature can be calculated from a

given correlation.

The lumped-parameter method can deal with large and complicated geometry rod arrays incorporating non-uniform heating from rod to rod as well as in the axial direction, and easily accommodates fluid property changes. Many computer programs have been developed based on this approach. The work of Oldaker^[71] is a typical example of computer programs developed by AECL to study the performance of Canadian fuel bundles. However, the lumped-parameter method requires judgement in defining subchannels and determining friction and heat transfer correlations. The application of this method must be incorporated with experiments, since experiments are needed to determine mixing rates between subchannels.

Besides mixing rate experiments, many other experiments have been carried out in order to predict heat transfer in bundles and supplement the analytical works, especially in the early state of the development of nuclear power reactor designs. Experiments have been conducted not only on the effects of rod cluster geometry on heat transfer but also the effects of rod spacers, bearing pads, and end-plates of fuel bundles. Today, the accumulated and combined knowledge from the analytical and experimental works is adequate for predicting the performance of fuel in preliminary designs. However, the actual performance of a new fuel bundle design must still be checked by experiments.

5.4 Heat Transfer to Supercritical CO₂ in Fuel Bundle

5.4.1 Specifications and Assumptions

Heat transfer to supercritical carbon dioxide in fuel bundles has

not been studied before. However, reasonable estimates can be based on the separate studies of heat transfer to supercritical carbon dioxide in heated pipes and heat transfer to single phase fluids in bundles. This section will discuss the approach and the assumptions of the analysis of heat transfer to supercritical carbon dioxide in CANDU-type fuel bundles.

Because of the complicated geometry of CANDU fuel bundles, the fundamental method discussed in the previous section is not useful. Because of the small ratio of pitch to rod diameter for CANDU fuel bundles, the equivalent annulus method is also not suitable. Therefore, the lumped-parameter method was the only method used for analysis of heat transfer to supercritical carbon dioxide in bundles. Certain assumptions were made in order to put the method into use. Because there is no available experimental data for supercritical carbon dioxide mixing rates between subchannels of fuel bundles, the first assumption was that of zero mixing between subchannels. The mixing can be caused by turbulent interchange, diversion cross-flow, flow scattering, and flow sweeping^[72]. Turbulent interchange results from eddy diffusion between subchannels and can be characterized by the eddy diffusivity of momentum. Diversion cross-flow is the direct flow caused by radial pressure gradients between adjacent subchannels. These gradients may be induced by gross differences between the subchannel heat flux distributions, and the differences in subchannel equivalent hydraulic diameters. Flow scattering refers to the non-directional mixing effects associated with spacers, bearing pads, and end-plates. Flow sweeping is the direct cross-flow effect associated with mechanisms designed to create mixing between subchannels. These mechanisms are mainly wire wrap spacers, helical fins, contoured grids, and mixing vanes, but they are not used in present CANDU fuel bundles. Therefore,

if supercritical carbon dioxide were used as a coolant for the CANDU reactor, mixing due to flow sweeping does not exist, but strong mixing due to the effects of the other three causes can be expected.

Mixing can balance the enthalpies and average the fluid bulk temperatures of subchannels. If there is no mixing, the bulk temperature of the coolant in the particular subchannel which has the maximum linear heat rate can be over-predicted. Also, because the local wall temperature depends on the local fluid bulk temperature for a given flux, the wall temperature is then over-predicted. Evidently, the zero mixing assumption is not only untrue but also a very serious assumption. It will cause under-estimation of the performance of a fuel bundle in an analysis when maximum withstanding temperature of the fuel bundle is used as the upper limit for design.

The second assumption is that the rod bundle is smooth. Therefore, turbulence created by spacers, bearing pads, and end-plates is not taken into account in this analysis. The structural arrangements in fuel bundles create not only mixing between subchannels, but also high eddy diffusivity of momentum and heat in each subchannel. The eddy diffusivity is closely related to heat transfer. As the degree of diffusivity increases, the heat transfer coefficient increases. Hoffman et al.^[73] found that spacers improve the local heat transfer by tripping the boundary layer. This results in starting a new thermal entry length as shown in Figure 21. Other mechanisms also can improve the general heat transfer throughout the entire bundle as well as local heat transfer. For example, Figure 22^[73] shows that the Nusselt numbers in a fuel bundle with wire wrap spacers are greater than Nusselt numbers calculated from the correlation for single

phase fluids flowing in circular smooth tubes. Hence, the second assumption will over-predict the wall temperature profiles in subchannels. In other words, the "smooth bundle" assumption will under-estimate the performance of fuel bundles in term of maximum withstanding operating temperature.

The smooth bundle assumption may also under-predict pressure drop through the bundle. The increase of turbulence created by the fuel bundle structure increases the skin friction along the fuel bundle. In addition, the direct drag due to the structure can cause further pressure drop.

On the other hand, Figure 23^[74] shows that the friction factor in a closely packed bundle (pitch to rod diameter, $p/d = 1.141$) may actually be less than that of a smooth circular tube. This phenomenon is apparently due to the effect of close-packing. The decrease of friction factor in a closely packed bundle (such as a CANDU fuel bundle) may counter balance the increase of friction factor due to the effect of end plates and other parts of the fuel bundle structure. Therefore, as a first approximation, the friction factor used in this work was calculated from a correlation for supercritical carbon dioxide flowing in a smooth tube.

The last assumption in applying the lumped-parameter method is that subchannels are continuous throughout the reactor core. In other words, it was assumed that the relative orientation of bundles in the reactor core does not affect heat transfer or hydrodynamics of coolant flow in subchannels. Fortunately, experiments^[75,76] confirm that although there may be discontinuities in subchannels between fuel bundles, the relative orientation of fuel bundles has little effect on average heat transfer. Figure 24^[77] shows calculated results of wall temperature

discontinuities due to change in orientation of fuel bundles, and the general shape of the wall temperature profile when the subchannel is assumed to be continuous.

Similar to the analysis of heat transfer to single phase fluids in circular pipes, heat transfer coefficients for supercritical carbon dioxide flow in fuel bundles are assumed to depend only on the local conditions. Also, the coolant flow in subchannels is assumed to be fully developed (but with a factor $f(x/d)$ as in equation (23) allowing for increase in heat transfer in the initial portion of the subchannel). In addition, the effect of the ratio p/d can be taken into account for heat transfer by using Figure 25*.

From the above discussion, despite the many assumptions, an analysis of heat transfer to supercritical carbon dioxide in the CANDU-type fuel bundles can be made. Moreover, the result of this analysis should be on the conservative side, that is the maximum calculated sheath temperatures should be larger than actual expected values.

5.4.2 Fuel Bundle Geometry and Subchannel Analysis

As discussed previously, fuel bundle design must be based on balance of subchannel enthalpies for optimum performance. This enthalpy balance can minimize temperature differences between subchannels, and reduce the axial increase of bulk temperature in a particular subchannel which has the maximum heat rate.

*Figure 25: Kay^[78] summarized the effect of the ratio p/d on Nusselt number for fully developed, turbulent flow parallel to a bank of smooth circular rods.

Enthalpy balance can be controlled by creating mixing with specially designed mechanisms such as wire-wrap spacers. Mixing also can be created by properly arranging the geometry of the fuel bundles.

Figure 26^[12] shows the geometry of an existing fuel bundle used in the CANDU 500 reactor at Pickering. Because of the different cross-sectional areas of subchannels, subchannel flow rates and velocities are different. This can result in cross-sectional pressure gradients, hence, subchannel mixing. Figure 8 shows the subchannel temperature profiles for a given axial and radial heat flux distribution. Because of the enthalpy balance due to mixing, the temperature differences between flows are very small.

However, this same bundle cannot achieve sufficient enthalpy balance when supercritical carbon dioxide is used as a coolant. Because of the low density of supercritical carbon dioxide at high temperature and resulting high flow speed, the resistance in subchannel 4 does not allow adequate flow for a given heat output. Therefore, despite the mixing between subchannels, the enthalpy, bulk temperature, and hence the wall temperature in this subchannel will increase rapidly. The wall temperature may eventually exceed the limiting value.

A similar problem has been encountered in the development of the CANDU boiling reactor, fog reactor, and once-through reactor, in which low density light water is used as a coolant^[79]. In order to solve the problem of rapid axial increase of temperature due to enthalpy unbalance, fillers (or blockers, see Figure 27) are introduced to block subchannel passages which have too large a flow area. Tube-in-shell fuel elements (see Figure 28) have also been suggested. The geometries of these fuel elements allow coolant distribution according to subchannel heat rate, and resulting

good enthalpy balance and small temperature differences between subchannels.

In order to find a suitable fuel bundle geometry for the proposed supercritical carbon dioxide cooled CANDU reactor, the subchannel dimensions must be determined. If necessary, fillers have to be introduced into the fuel bundle to assist subchannel flow balance. The subchannel dimensions are governed by heat transfer rates and a relationship must be found between the coolant flow rate and the maximum subchannel wall temperature with a given operating condition.

Figure 29 is a plot of subchannel maximum wall temperatures versus inlet coolant temperatures for a given axial heat flux distribution and a given outlet coolant temperature. The heat flux distribution is the average axial value for the CANDU reactor at Pickering. Each curve represents the relationship between the maximum wall temperature and the inlet coolant temperature for a constant equivalent hydraulic diameter. The inlet temperature can be interpreted as the coolant flow rate which can be expressed as:

$$M = \frac{\int_0^{\ell} (\text{Axial Heat Flux Distribution}) d\ell}{h(T_{\text{out}}) - h(T_{\text{in}})}, \quad \dots (26)$$

where: ℓ is the length of the subchannel,

$h(T_{\text{out}})$ is the outlet coolant enthalpy, which is a function of the outlet coolant temperature, T_{out} ,

$h(T_{\text{in}})$ is the inlet coolant enthalpy, which is a function of the inlet coolant temperature, T_{in} .

When the axial heat flux distribution and the outlet temperature is fixed, the flow rate is approximately proportional to the inlet coolant temperature.

The outlet temperature was first chosen to be 775°K. However, when the equivalent diameter is larger than 1.4 D_o (7.4 cm), the maximum wall temperature exceeds the safety limit of 550°C which has been discussed previously. Therefore, a lower coolant outlet temperature of 750°K was chosen. A similar plot is also used to show the relationship between the inlet temperature, i.e. the flow rate, and pressure drop as shown in Figure 30.

Figures 29 and 30 show that for a given equivalent hydraulic diameter of a subchannel, the total pressure drop increases, and the maximum wall temperature decreases with increase of the inlet coolant temperature; i.e., the flow rate or velocity in a subchannel. For a very small equivalent diameter subchannel, the final pressure drops below the critical pressure. Therefore, the coolant cannot be maintained in a supercritical state throughout the cooling loop. For a large equivalent hydraulic diameter subchannel, the pressure drops less quickly, which allows higher inlet coolant temperature; i.e., higher flow rates. The high coolant flow rate will produce high heat transfer rates and guarantees a maximum wall temperature below the safety limit. High inlet coolant temperature is also very desirable for steam generation as will be discussed in a later chapter. However, use of large subchannel equivalent hydraulic diameters will require large diameters for fuel bundles and coolant channels. Coolant channels which have large diameters and fixed wall thickness cannot withstand higher pressures, and fail to meet the

criteria of compactness for reactor design. Today, only small diameter coolant channels are used in the CANDU reactor.

Because this work is only a preliminary study, without any attempt being made to optimize the coolant performance in bundles in terms of power station efficiency, an equivalent subchannel hydraulic diameter of $0.75 \text{ cm} = 1.44 D_o$ and a coolant inlet temperature of 400°K were chosen for this study. These values were chosen on the basis of maximum wall temperatures and reasonable flow rates and therefore, relatively low pressure drop. As a result, the fuel bundles can be operated safely, and the carbon dioxide coolant can be kept in a supercritical state throughout the cooling loop.

For given inlet and outlet coolant temperatures, and a specified heat flux distribution, the relationship between the equivalent hydraulic diameter and maximum wall temperature, and also the final pressure for a given inlet pressure can be studied. Figure 31 shows that for a constant flow rate, the equivalent hydraulic diameter increases with maximum wall temperature and final pressure. The upper limit of equivalent hydraulic diameter occurs when $1.02 \text{ cm} = 2.3 D_o$ and the maximum wall temperature reaches the safety limit of 550°C . The lower limit to achieve compact fuel bundles is approximately $0.75 \text{ cm} = 1.44 D_o$, since the final pressure drops drastically from this point. An equivalent hydraulic diameter of 0.75 cm was chosen to make the design as safe and compact as possible.

5.4.3 Predicted Heat Transfer to Supercritical Carbon Dioxide in 32-element Fuel Bundles

An equivalent subchannel hydraulic diameter of 0.75 cm was chosen

coolant. However, specifying the equivalent hydraulic diameter does not uniquely determine the exact geometry of subchannels since equivalent hydraulic diameter depends on flow area and wetted perimeter in a subchannel. Final design selections must also take into account overall compactness of the bundle.

When the subchannel equivalent hydraulic diameter is chosen to be 0.75 cm and with 1.52 cm diameter fuel rods (the same as those at Pickering), the most compact subchannel geometry is the square array. Figure 32 shows the geometry of a 32-element fuel bundle with a square array of fuel rods, along with pertinent dimensions. The overall diameter of this 32-element fuel bundle is approximately equal to the existing fuel bundle used in CANDU reactors (Pickering type). This ensures that the basic design of the CANDU reactor would remain the same if supercritical carbon dioxide were used as a coolant. This type of fuel bundle is not the best when considering the coolant enthalpy balance. In the CANDU reactor, the heat flux distribution within a fuel bundle increases away from the center of the bundle. Therefore, the proposed fuel bundle fails to distribute coolant flow according to the radial heat flux distribution. However, blockers can be used to reduce the large flow area subchannels which are near the coolant tube wall.

Heat transfer performance of this 32-element fuel bundle was analysed in a typical case when using supercritical carbon dioxide as a coolant for the CANDU reactor. The heat flux distribution was based on data obtained during steady operation of the Pickering station^[12]. The axial heat flux distribution is:

$$Q(x) = q(n) \cdot \sin (kx + \phi) , \quad \dots (27)$$

where: $Q(x)$ is the axial heat flux distribution for a subchannel as a

function of distance from the inlet, in KW/M,

$q(n)$ is the maximum linear heat rate of a subchannel n , in KW/M,

x is the distance from the inlet of a subchannel, in M,

k is a constant, 0.51504,

ϕ is a constant, 0.25744.

The maximum linear heat rate $q(n)$ is based on the radial neutron flux distribution in the Pickering 28-element bundle shown in Figure 33^[83]. The formula for the calculation is:

$$q(n) = \frac{f}{0.96} \cdot \frac{TWP - CWP}{4.775} \cdot 35.8, \quad \dots (28)$$

where: f is the normalized neutron flux at the radial distance of the center of the subchannel,

TWP is the total wetted perimeter in cm,

CWP is the cold (unheated) wetted perimeter in cm.

Based on the assumptions and lumped parameter method discussed previously, heat transfer to supercritical carbon dioxide in the proposed 32-element bundle was studied in detail. The computer program used was similar to that already described for circular tubes, with the exception that subchannel flow rates were balanced to produce equal subchannel pressure drops. Typical results are shown in Figures 34 to 36. The coolant temperature profiles in individual subchannels are shown in Figure 34. Wall temperature profiles are shown in Figure 35. Pressure drop along the coolant tube is shown in Figure 36. When the inlet temperature of supercritical coolant was 400°K (260°F), the final bulk temperature at the outlet of the coolant channel was found to be 730.7°K (855.6°F).

These results will be summarized and discussed in Chapter 7.

6. POSSIBLE STEAM CYCLES

6.1 General

The ultimate goal of this study is to study ways to improve the overall efficiency of the CANDU reactor. Accordingly, it is important to investigate potential steam cycles in association with the CANDU reactor when supercritical carbon dioxide is used as a coolant.

The coolant temperature is one of the most significant parameters in steam generation. The higher the coolant temperature, the higher will be the thermal efficiency of the cycle, and hence, the lower will be the fueling cost. Coolant temperatures fix the steam temperature and the associated saturation pressure as shown in Figure 37. Line "e-g" in Figure 37 represents the state points of the CO_2 as it cools down in the steam generator from "e" to "g". This is approximately a straight line since $dH = M \cdot C_p \cdot dT$ for high temperature supercritical carbon dioxide and the specific heat at constant pressure varies only slightly with temperature. The line "a-b-c-d" represents constant pressure heating of the water-steam system. Because of the second law of thermodynamics and its limitation on direction of heat flow, the saturation temperature of the water must be lower than the temperature of the CO_2 , approximately at the point where the coolant line intercepts the saturation curve on the enthalpy versus temperature diagram. Therefore, the cycle pressure is also fixed according to the saturation temperature. In other words, although only the entry temperature of the coolant into the steam generator determines the maximum temperature of the steam, both the entry and exit temperatures determine the steam pressure. Because the maximum temperature

as well as the pressure of the steam cycle determine the efficiency of the reactor power plant, high coolant entry and exit temperatures are desirable.

The problem of low coolant exit temperature is often encountered in nuclear reactor power generation. In order to solve the problem of low steam pressure due to the low coolant exit temperature, Wooten et al.^[80] suggested a dual-pressure steam cycle. Figure 38 shows the paths of the different processes with dual-pressure steam generation. It is necessarily drawn on a different basis from that of Figure 37 which has enthalpy of water as an abscissa, and instead, the abscissa of Figure 38 is the distance along the steam generator from the entrance to the exit.

In the dual-pressure steam generation cycle, feedwater is separated into two branches where it is pumped by two feedwater pumps to two different pressures. The temperatures of the feedwater entering the steam generator are equal in both branches. As shown in Figure 38, the low pressure feedwater is further heated in the economizer from "a" to "b", evaporated at a particular constant pressure and temperature from "b" to "c", superheated in the superheating section from "c" to "d", and then fed to a low pressure turbine stage.

The high pressure water is heated in a second economizer from "a'" to "b'", in which it is subjected to the same downstream coolant as the low pressure feedwater economizer. It is further heated in a third economizer from "b'" to "c'", evaporated from "c'" to "d'", then superheated from "d'" to "e'" by the incoming coolant. Finally, it is fed to the high pressure turbine inlet. In this process of dual-pressure steam generation, the coolant heats the high and low pressure steam alternatively.

The dual-reheat steam generation cycle was also discussed by Wooten et al. [78]. Dual-reheat steam generation is similar to dual-pressure steam generation, except that the expanded high pressure steam from the high pressure turbine is joined with the low pressure feedwater and superheated together before expansion through the low pressure turbine stage.

The dual-pressure steam cycle can result in higher thermal efficiencies than the single-pressure steam cycle. Of course, the more complicated dual-pressure steam cycle circuit increases the capital cost of the plant. The dual-reheat cycle has the additional advantage of lower moisture content at turbine exhaust and higher work output per unit mass of working fluid. However, the advantages of the dual-pressure steam system are reduced when the coolant exit temperature increases and approaches the temperature of coolant entering the steam generator.

6.2 Steam Cycle for the Supercritical Carbon Dioxide Cooled CANDU Reactor Plant

This section discusses the possible steam cycles with supercritical carbon dioxide coolant conditions based on the previous calculated results of heat transfer in the 32-element bundle. The previously calculated outlet temperature of the supercritical carbon dioxide coolant is 855.6°F (730.7°K), and the inlet temperature was chosen to be 260°F (400°K). For some heat loss, the coolant entry temperature into the steam generator was chosen to be 845°F. The coolant temperature leaving the steam generator was chosen to be 280°F, which assures heat exchange in the recuperator.

In analyzing steam cycle performance, only pressure drop across the reactor and turbine stages was taken into account. The pressure losses in piping, recuperator, and steam generator were not considered. The latter pressure losses depend on structural details, but with good engineering design, these pressure drops can be kept small. For example, the pressure drop for gaseous carbon dioxide flowing through the steam generator at the Hinkley Point gas-cooled power plant is only 1.6 psia^[81].

The single-pressure steam cycle was analyzed first. From the temperature versus enthalpy diagram in Figure 37, when the entry and exit temperatures are 845°F and 280°F respectively, the generated steam has a pressure of 130 psia and a maximum temperature of 815°F. Based on the turbine circuit, shown in Figure 39, the ideal overall plant efficiency is only 26.73%. The low efficiency is mainly due to the low steam pressure, which in turn is due to the low exit temperature.

The dual-pressure cycle was also studied as a potential energy-conversion cycle. Figure 38 shows the supercritical carbon dioxide coolant and steam paths in the steam generator for the case of high to low pressure ratio of 600/70.3 (psia). Figure 40 shows the corresponding turbine circuit. This cycle gives an ideal overall plant efficiency of 29.42%; higher than the single-pressure cycle.

To study the effect of high to low pressure ratio on the efficiency of the cycle, the case of the dual-pressure cycle of 1200/70.3 (psia) was also analyzed. Figures 41 and 42 show steam generation and enthalpy balance for the turbine circuit respectively. The ideal overall plant efficiency for this case is 29.87%, which is about the same as the previous dual-pressure cycle. In the dual-pressure cycle, the ratio of flow rates

of high pressure to low pressure steam decreases when the pressure ratio increases. Therefore, the ideal overall efficiency of the dual-pressure cycle remains approximately constant under given coolant conditions.

To study the further possible improvement of efficiency with given coolant conditions, a new dual-reheat steam cycle having a pressure ratio of 1200/70.3 (psia) is proposed. Figure 43 shows the steam generation loop. Figure 44 shows the heat balance for the turbine circuit. In this cycle, the expanded high pressure steam is joined with low pressure feedwater and evaporated together in the steam generator to become the low pressure steam. In this case, the high and low pressure feeds are heated in a parallel fashion instead of alternatively as in the dual-pressure (non-reheat) cases. This reheating method is somewhat different from the method suggested by Wooten et al.^[80]. Because of parallel heating, the large temperature difference between the coolant and the feeds is eliminated. This decreases the irreversibility of the steam generation process. Therefore, the ideal overall plant efficiency of the new dual-reheat cycle is increased for a given coolant condition. The ideal overall plant efficiency of the dual-reheat cycle of this case was calculated to be 33.02%.

The results of cycle performance are summarized and discussed in the next chapter. Comparisons are also made with the performance of the existing Pickering station.

7. RESULTS AND DISCUSSION

7.1 Typical Heat Transfer in Bundles

The fluid dynamic and heat transfer conditions of supercritical carbon dioxide in the subchannels of the 32-element fuel bundles are summarized in Figure 45. This figure shows that the highest subchannel maximum wall temperature occurs in subchannel 6, which has the highest enthalpy among all the subchannels. The lowest subchannel maximum wall temperature is only 409.0°C , which is 137.0°C lower than the highest subchannel maximum wall temperature. The great difference between the subchannel wall temperatures and between the subchannel coolant temperatures shows that the assumption of zero mixing between subchannels has a major effect on subchannel enthalpy balance. Therefore, the maximum operating temperature of the 32-element fuel bundles, i.e. the highest subchannel maximum wall temperature, is over predicted.

The overall performance of supercritical carbon dioxide coolant in the 32-element fuel bundles is summarized in Figure 46. For the purpose of comparison, the typical overall performance of heavy water coolant in the 28-element fuel bundles for Pickering Station is also listed. Because of the high heat extraction per unit mass for supercritical carbon dioxide coolant, the total mass flow rate is much lower than for heavy water coolant at a given channel power. Since there is no dryout when using supercritical carbon dioxide as a coolant, the allowable operating temperature of the fuel bundle is much higher. As a result, the coolant temperature is much higher than the existing case of heavy water coolant. However, the pressure drop in the case of supercritical carbon dioxide coolant may be

underestimated as pointed out in the previous discussion.

The detail sizes of the proposed 32-element fuel bundle and the existing 28-element Pickering fuel bundle are shown in Figure 47 for comparison. The overall dimensions of these two fuel bundles are approximately the same; this satisfies the design restraint that the basic structure and reactor physics of the CANDU reactor remain the same. The 32-element fuel bundle has a slightly larger radius but contains more fuel, thereby reducing the required number of fuel channels for a given reactor power. Thus, the larger radius and thicker coolant tubes may not increase the total weight of structural material in the reactor core.

To balance the excess flow in the outer subchannels, flow restricting blockers are used in the 32-element fuel bundle. This results in an increase in reactor structural material and hence a possible decrease of neutron economy, which determines the fueling cost. However, this can be minimized by selecting blockers which are fairly transparent to neutrons although impermeable to coolant flow (possibly high temperature plastic or ceramics). Optimum design of fuel bundle geometry would allow for subchannel enthalpy balance. In other words, the subchannel flow areas should allow for subchannel flow rates proportional to the subchannel linear heat rates. If blockers are not used in the 32-element fuel bundle and subchannel enthalpies are balanced, the average flow area of each subchannel would be larger than proposed here. This allows higher flow rate of the coolant, and hence, higher inlet coolant temperature into the reactor; i.e., higher exit temperature from the steam generator. Therefore, the plant efficiency can be increased.

7.2 Typical Steam Cycles

The steam conditions for the thermal cycles which were analysed previously are summarized in Figure 48. For purposes of comparison, the corresponding steam conditions of the Pickering generating station^[12] are also listed. The performance of these thermal cycles is summarized in the table of Figure 49. The ideal overall plant efficiency of the Pickering generating station is 33.94%, which is based on the turbo-generation heat balance as shown in Figure 50^[12], and the actual plant efficiency is only 29.1%.

One of the conditions which strongly effects the ideal results and is not usually noted, is the turbine efficiencies assumed in the calculation. The efficiency of the low pressure turbines in both cases of the dual-pressure cycle is assumed to be 88.5%. This is based on the existing efficiency of the low pressure turbines of the Pickering Station. For the low pressure turbine of the dual-reheat cycle and the high pressure turbines of all cycles using supercritical carbon dioxide, turbine efficiencies are assumed to be 90%. This is justified on the basis of higher inlet-steam pressures and temperatures and lower outlet moisture content.

The steam condition when using supercritical carbon dioxide as a coolant is very much different from the steam condition of the Pickering generating station because of the different coolant conditions. However, the steam condition also depends on the method of generation. Therefore, despite similar coolant conditions in the three cases of the single pressure, dual-pressure, and dual-reheat cycles, the efficiencies are different. The calculated ideal overall plant efficiency of the dual-reheat

cycle is 33.02% which is competitive with the calculated ideal overall plant efficiency of the Pickering generating station. This shows that the use of supercritical carbon dioxide coolant may improve the existing thermal efficiency of CANDU reactor power plants when the performance of supercritical carbon dioxide coolant is optimized further from the design of this study.

Another positive result of this study shows the advantage of the concept of pumping in the supercritical cooling loop; the pumping power required by the supercritical carbon dioxide is small. Despite that supercritical carbon dioxide is assumed to be pumped at a temperature of 90°F, which is slightly lower than the pseudo-critical temperature of 99.5°F at 1240 psia, the ideal pump work is only slightly larger than for heavy water coolant of the Pickering Station. The annual average temperature of lake or river water in Southern Canada is approximately 48°F. Therefore, the estimate of pumping power for the supercritical carbon dioxide coolant is very conservative.

8. SUMMARY AND CONCLUSIONS

This study indicates the technical feasibility of using supercritical carbon dioxide as a coolant for a CANDU-type reactor. The reactor is cooled by a single phase coolant, which is pumped at a high density liquid-like state. The supercritical-fluid-cooled reactor may have the combined advantage of avoiding dryout as in gas-cooled reactors, and the advantage of low coolant circulation power as for liquid-cooled reactors.

As a result of eliminating dryout, the maximum operating temperature of the fuel sheath can be increased to 550°C (1021°F) for existing Canadian fuel bundles. The coolant temperature in the case study of this work was calculated to be 855°F. This high temperature coolant can produce steam at a temperature and pressure comparable to that of conventional fossil-fuel plants. However, since the exit coolant temperature from the steam generator may be as low as 280°F, a portion of the supercritical carbon dioxide coolant is used to produce low pressure steam.

In the cases of single pressure and dual-pressure cycles, the steam generation process irreversibility is high, and as a result, the useful energy extracted from the supercritical coolant is low. The ideal overall plant efficiencies of the single pressure, dual-pressure 600/70.3 (psia), and dual-pressure 1200/70.3 (psia) cycles are 26.73%, 29.42%, and 29.87% respectively, compared to 33.94% for the Pickering generating station.

A new dual-reheat cycle is proposed to reduce the high degree of

irreversibility in the steam generation process. In the new dual-reheat cycle, the coolant heats the low and high pressure feeds in a parallel manner instead of alternative heating as in dual-pressure cycles. The ideal overall plant efficiency of the new proposed dual-reheat cycle is 33.02%, which is comparable to that of the Pickering generating station.

The present result is conservative since the performance of supercritical carbon dioxide has been underestimated because of the assumptions of: (1) no mixing between subchannels, and (2) smooth and continuous subchannels. Mixing can improve heat transfer coefficients and also minimize the coolant and wall temperature rise in the particular subchannel having the maximum linear heat rate. For a given maximum fuel bundle sheath temperature, the no-mixing assumption underpredicts the inlet and outlet temperature of the reactor (i.e., the exit and entry temperature of the steam generator respectively). The smooth and continuous subchannel assumption also contributes to the underprediction of the performance of supercritical carbon dioxide by underestimating the heat transfer coefficient and overestimating the difference between wall and bulk temperatures. Therefore, the calculated ideal overall plant efficiency of the dual-reheat cycle is a conservative estimate.

The performance of supercritical carbon dioxide has not been optimized in this work. If fuel bundle geometry was designed to achieve subchannel enthalpy balance without using blockers, the net flow area in a given diameter coolant channel could be larger. A larger net flow area allows higher flow rates, i.e. higher reactor inlet coolant temperatures without higher pressure drops. The optimization of fuel bundle geometry should be included in future research.

While the technical feasibility of using supercritical carbon dioxide as a reactor coolant has been demonstrated in the present work, a great number of other factors must be considered in the design of an actual power station. Logistics of coolants supply and storage, safety, supporting hardware designs and overall cost must be considered. The complexity of financing a modern electrical generating station would demand serious study in its own right. It was not possible to consider all of these features in a preliminary study like the present. It might be noted, however, that because of the great cost involved in heavy water production, the use of carbon dioxide may also offer an economic advantage. Evidently, a great deal of research on this matter is required.

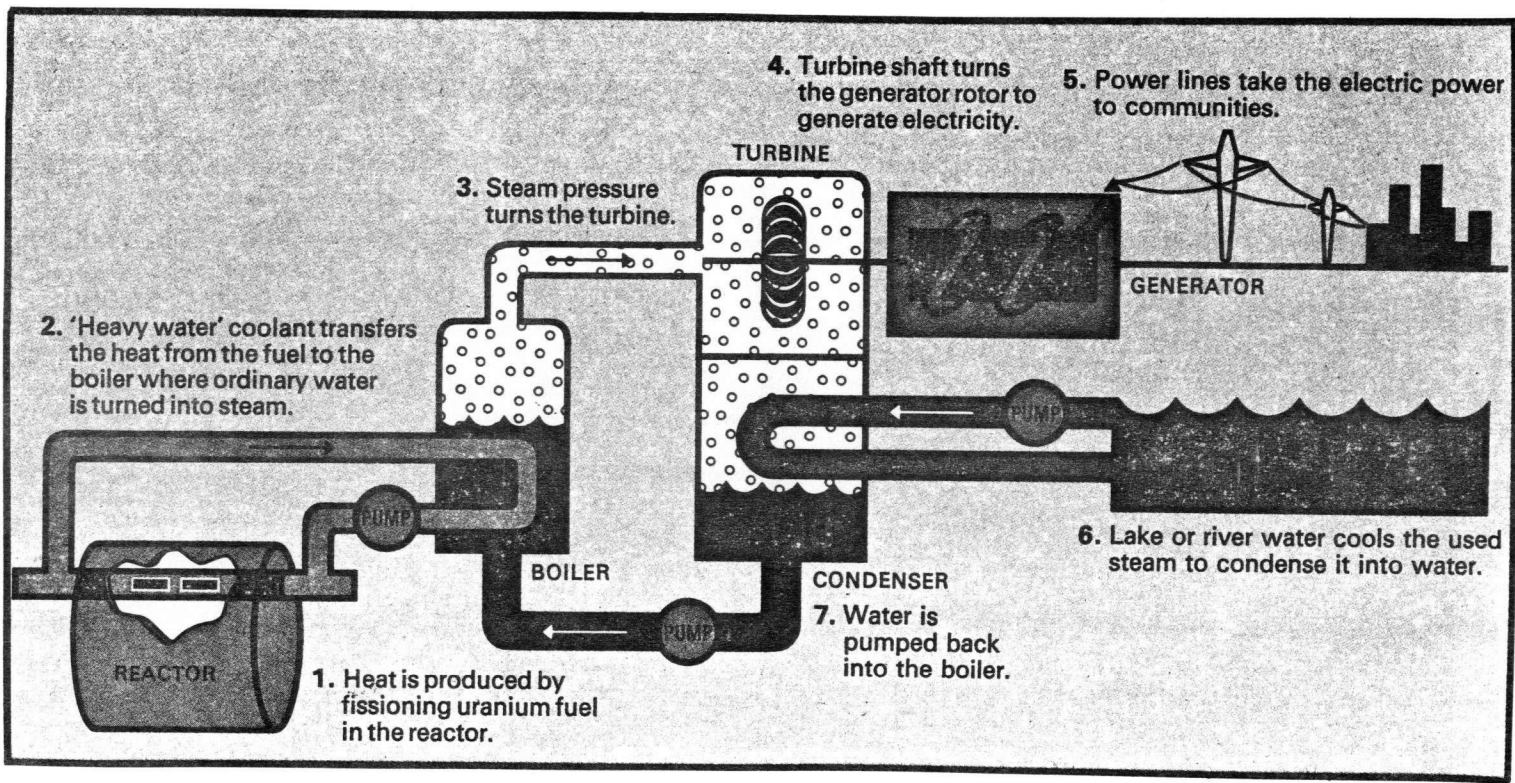


Figure 1. Thermo-Hydraulic Features of PHW CANDU Reactor Power Plant

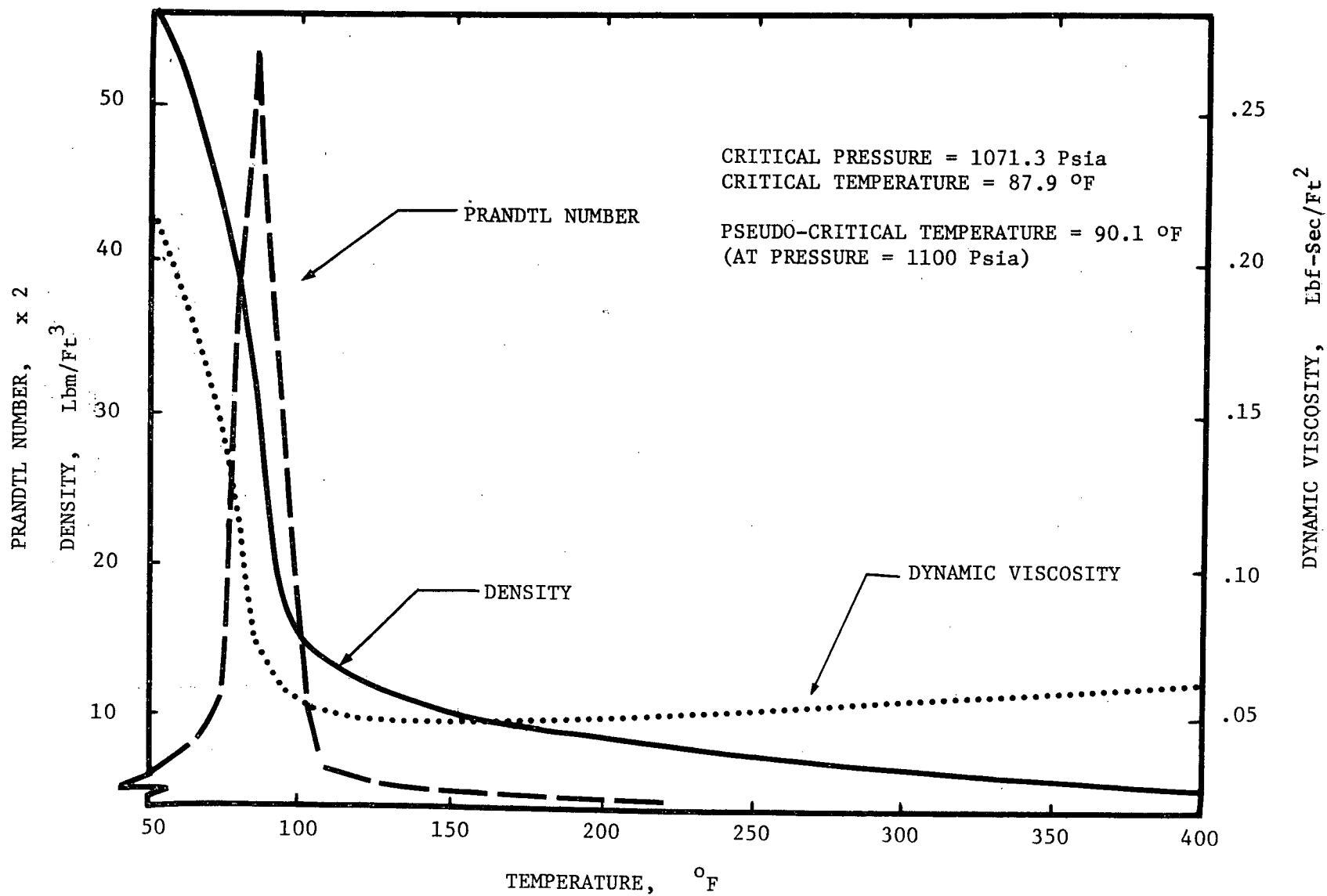


Figure 2. Typical Property Variations in Near-Critical Carbon Dioxide



Figure 3. Process Path of Supercritical Cooling Loop on P-V Diagram

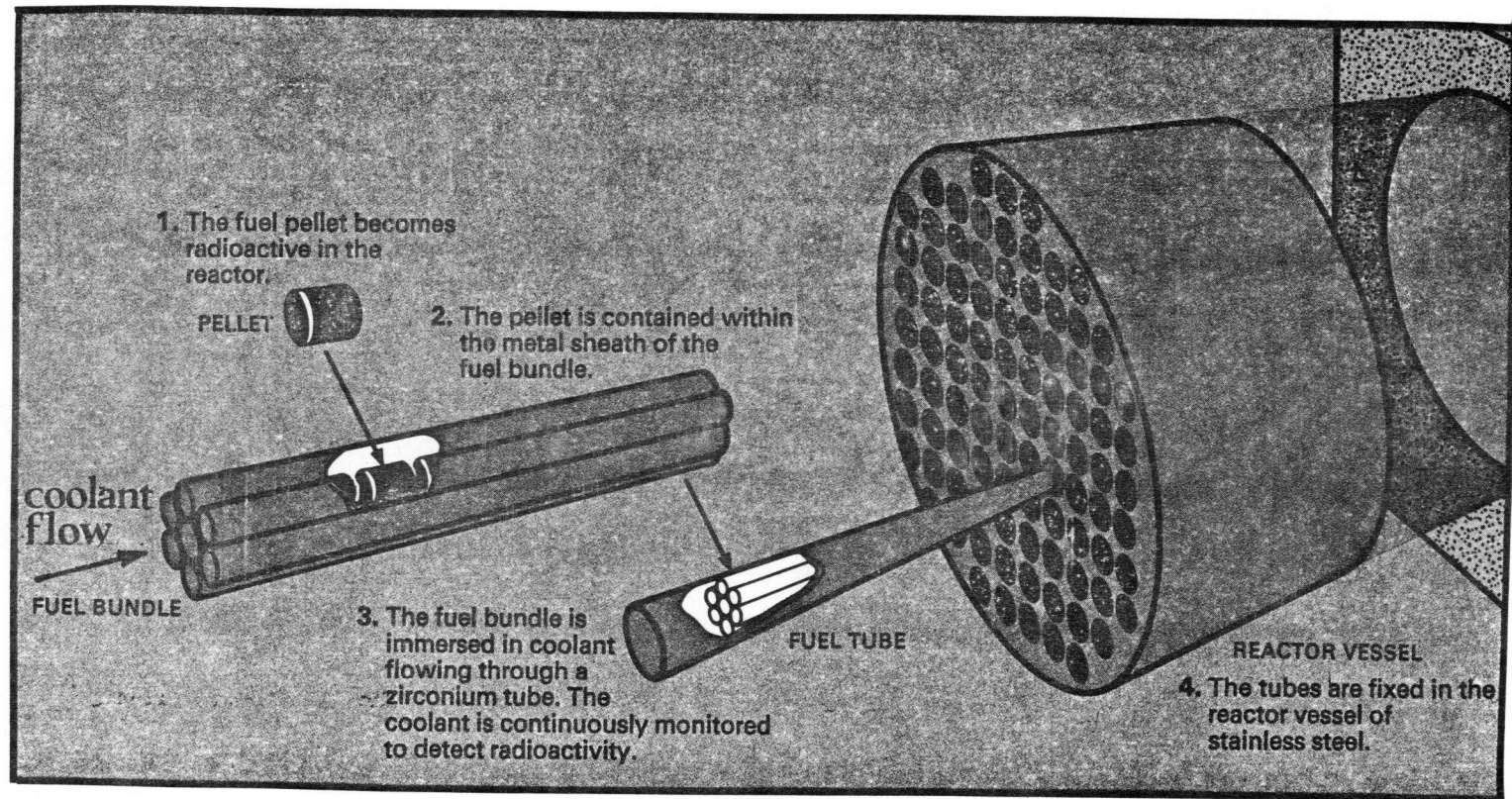


Figure 4. PHW CANDU Reactor Arrangement

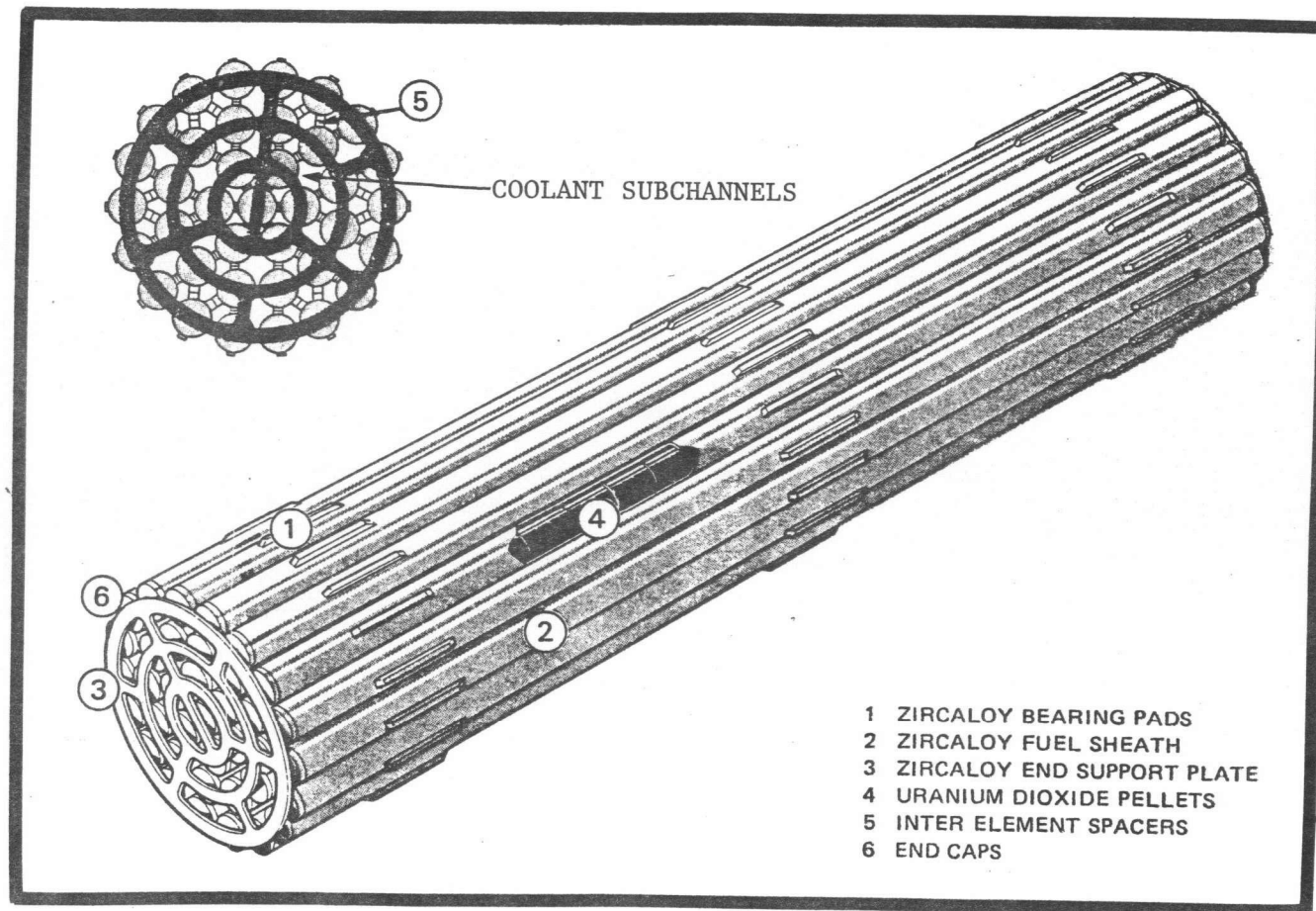


Figure 5. Fuel Bundle

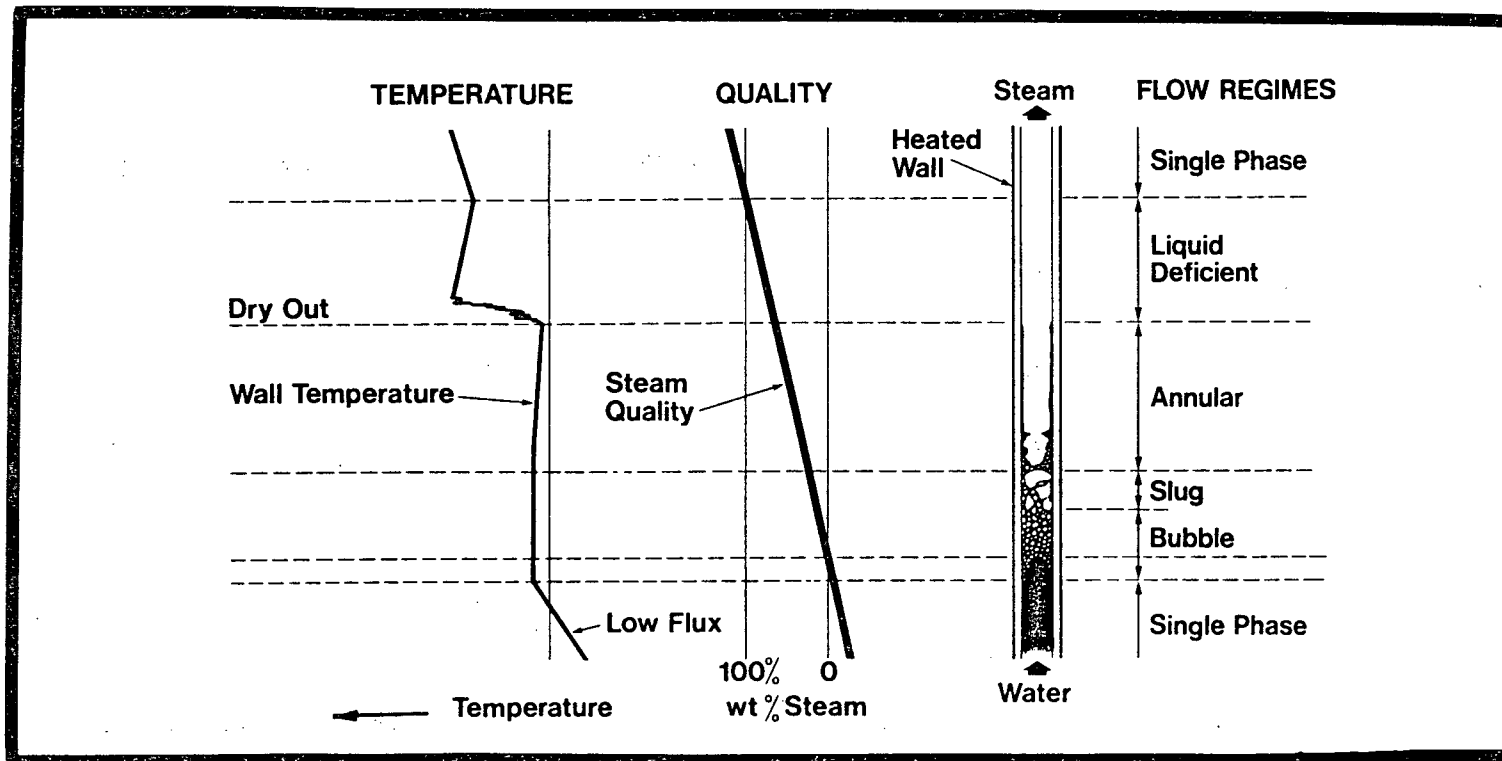


Figure 6. Thermal Hydraulic Regions in a Boiling Channel

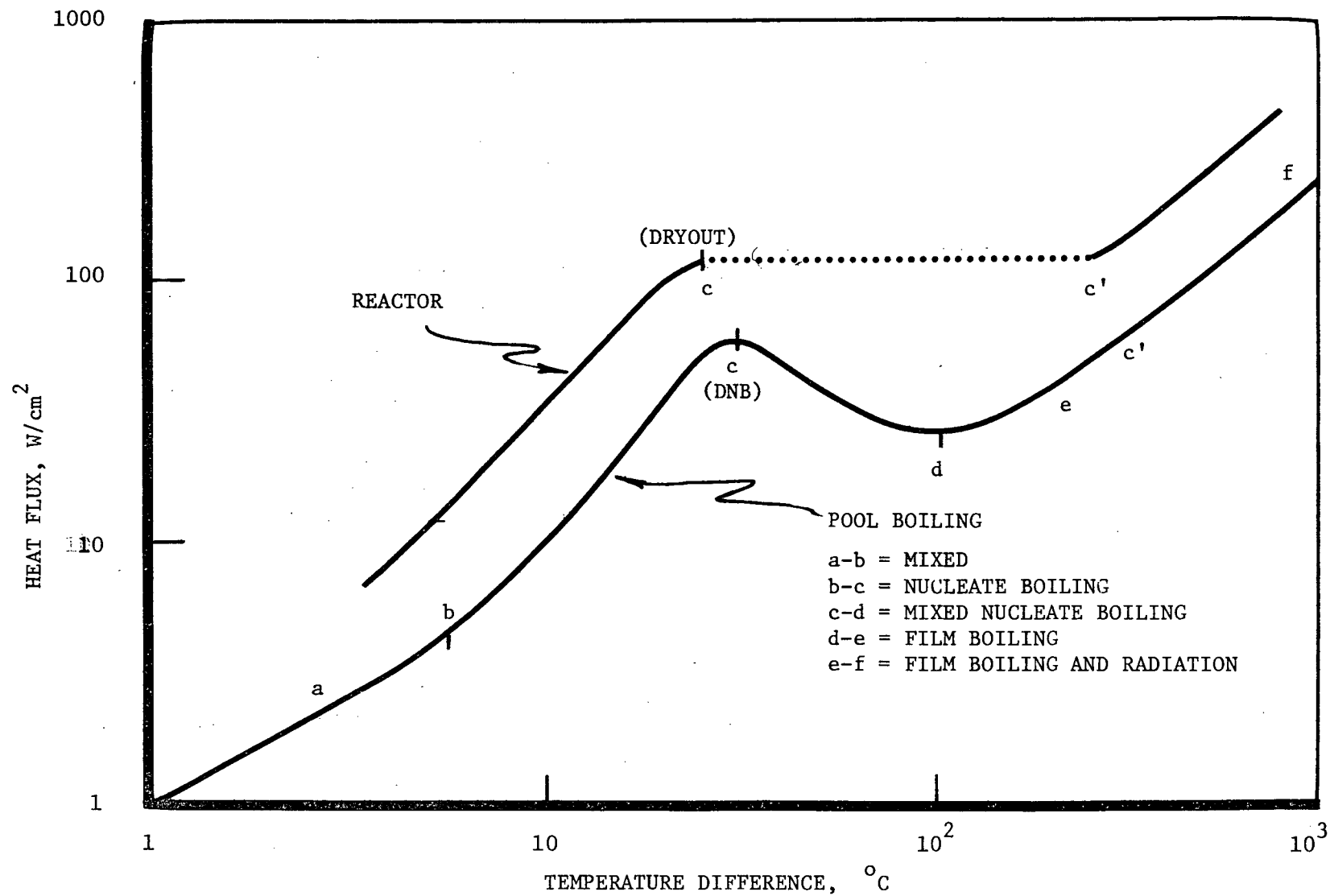


Figure 7. Boiling Regions

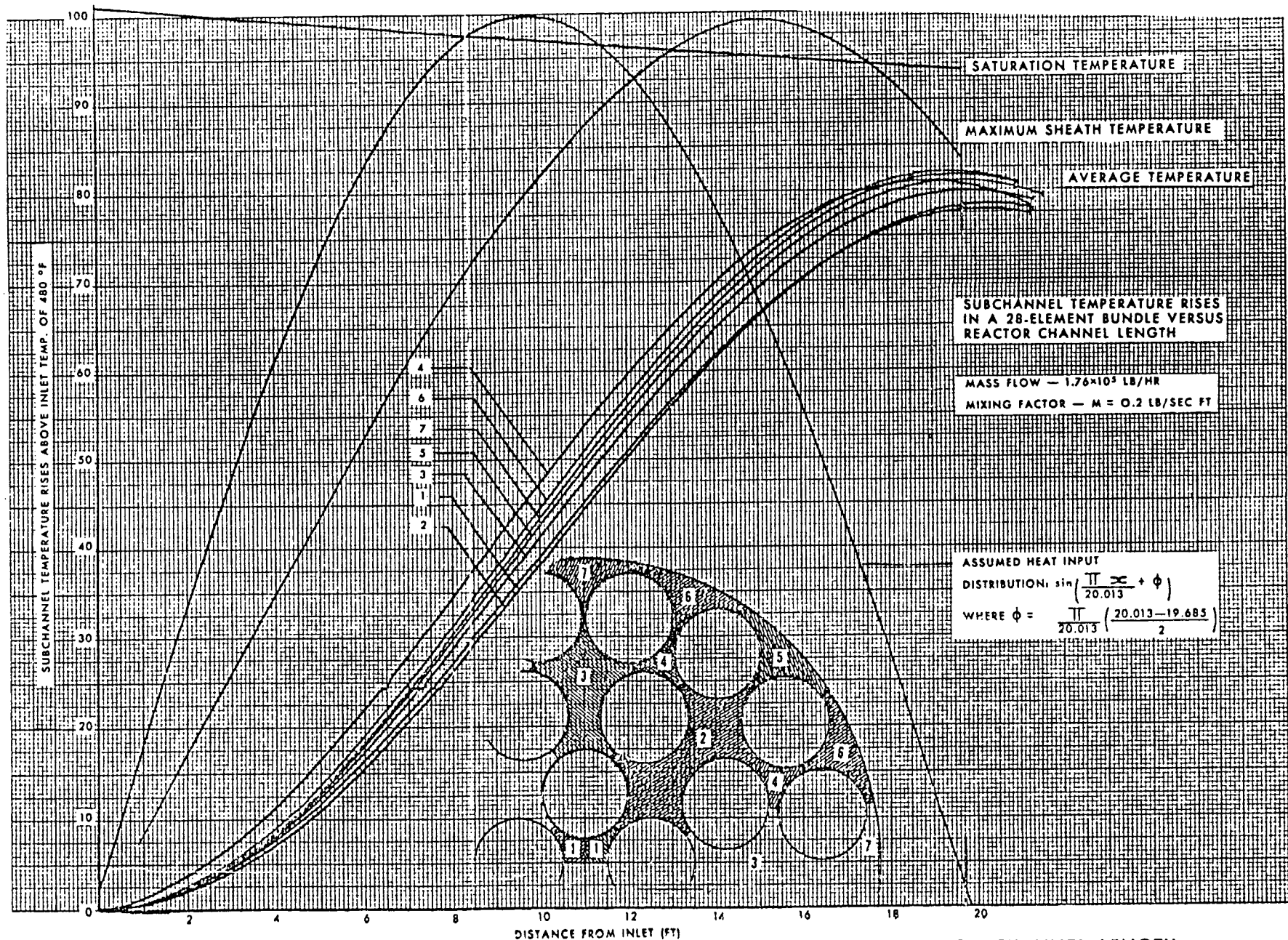


Figure 8. SUBCHANNEL TEMPERATURE RISES IN A 28 ELEMENT BUNDLE VERSUS REACTOR CHANNEL LENGTH
(FROM [12])

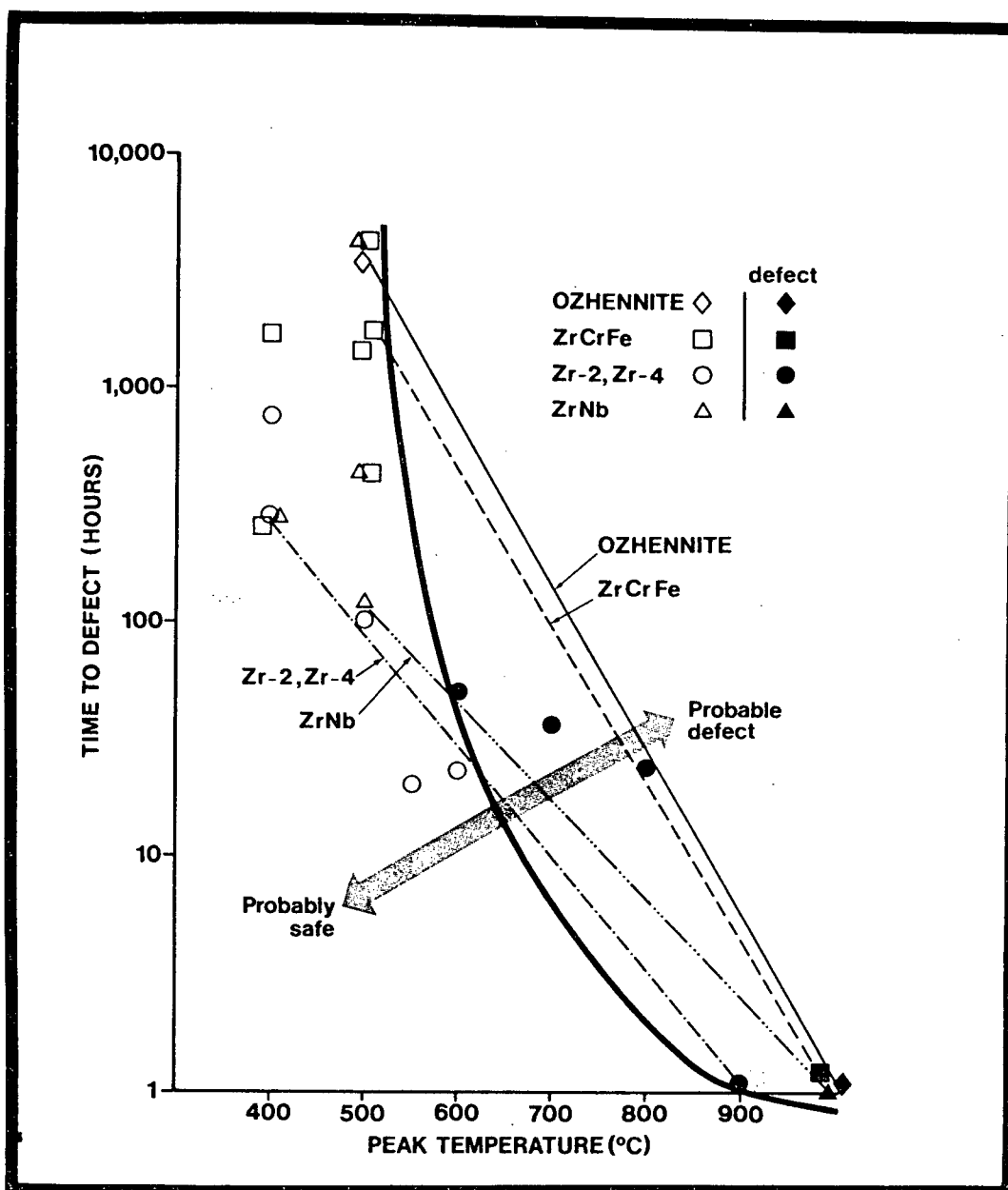


Figure 9. High Sheath Temperature Operation vs Time for Various Zirconium Alloy Fuel Elements (from [13])

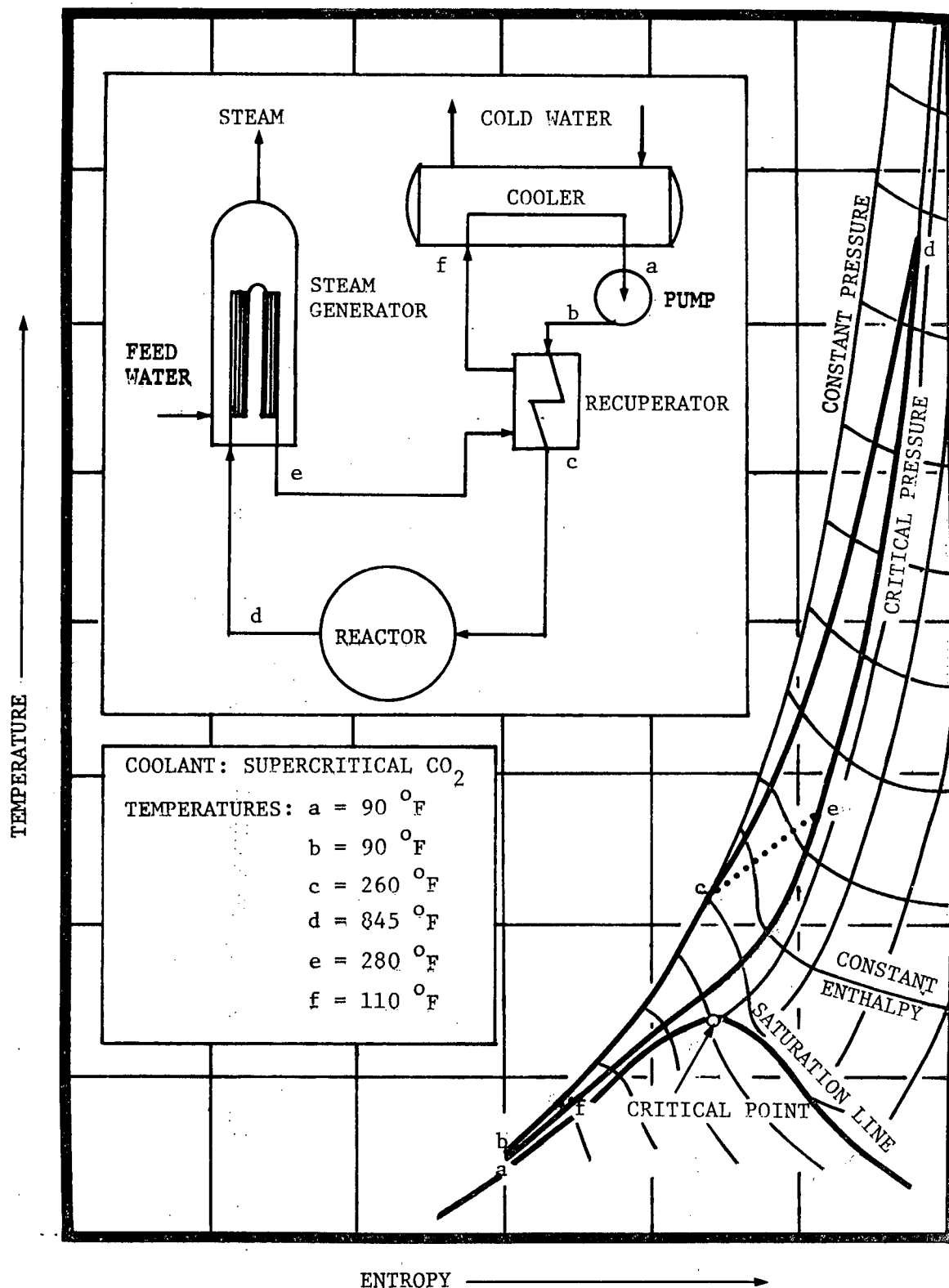


Figure 10. Proposed Supercritical CO₂ Cooling Loop

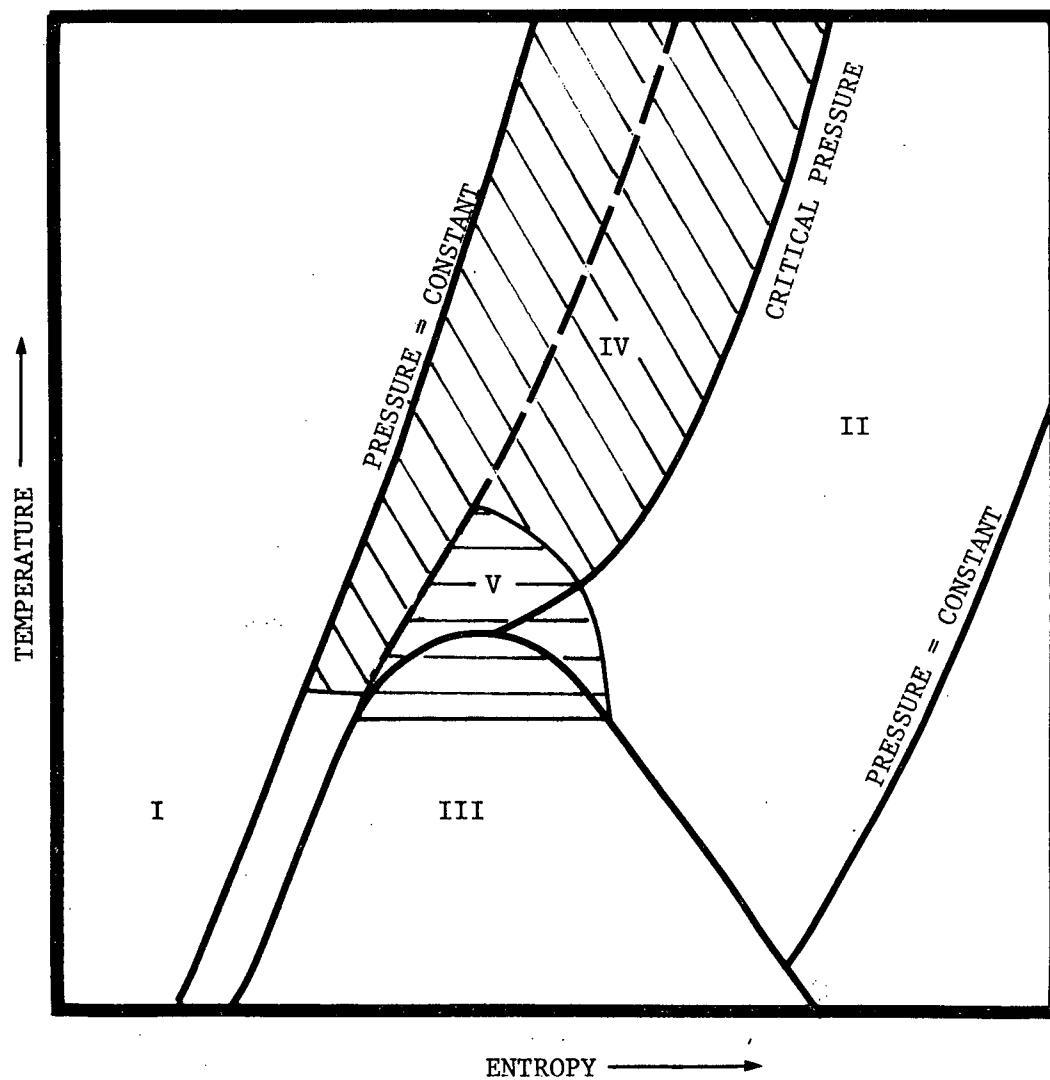
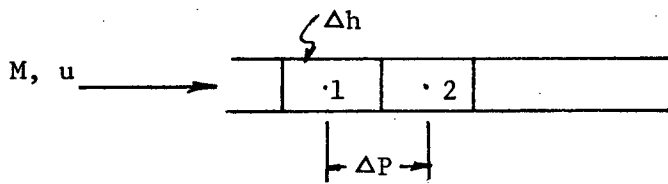


Figure 11. Heat Transfer Regions: I - Liquids, II - Subcritical Gases, III - Two-Phase, IV - Above-Critical Fluids, V - Near-Critical Fluids. (from [18])



1. Continuity

$$M = \text{Constant.}$$

2. Energy Conservation Equation:

$$h_2 = h_1 + \Delta h$$

3. Friction Factor Correlation for Constant Property Flow:

$$\xi_o = [1.82 \log (Re_b) - 1.64]^{-2}.$$

4. Heat Transfer Correlation for Constant Property Flow:

$$Nu_o = \frac{(\xi_o/8) Re_b Pr_b}{12.7 \sqrt{\xi_o/8} (Pr_b^{2/3} - 1) + 1.07}.$$

5. Pressure Drop Equation for Supercritical Flow:

$$\Delta P = \xi \frac{(\rho u)^2 \Delta \ell}{2 \rho d} + \overline{(\rho u)^2} \left(\frac{1}{\rho_2} - \frac{1}{\rho_1} \right),$$

$$\xi = \xi_s = \xi_o (\mu_w / \mu_b)^{0.22} \quad \text{for} \quad Gr/Re_b^2 \leq 5 \times 10^{-4},$$

$$\xi = \xi_s 2.15 (Gr/Re_b)^{0.1} \quad \text{for} \quad 5 \times 10^{-4} < Gr/Re_b^2 \leq 3 \times 10^{-1},$$

$$\bar{\rho}, \bar{\mu}_b \text{ evaluated at } P = P_1 + \frac{1}{2} \Delta P, T = (T_{b1} + T_{b2})/2,$$

$$\bar{\mu}_w \text{ evaluated at } P = P_1 + \frac{1}{2} \Delta P, T = (T_{w1} + T_{w2})/2.$$

(FIGURE 12 continued on the following page.)

6. Heat Transfer Correlation for Supercritical Flow:

$$Nu = Nu_o (\rho_w/\rho_b)^{0.3} (\overline{Cp}/Cp_b)^n ,$$

$$n = 0.4 \quad \text{at} \quad T_b/T_m \leq 1 \quad \text{or} \quad T_b/T_m \geq 1.2 ,$$

$$n = n_1 = 0.22 + 0.18 (T_w/T_m) \quad \text{at} \quad 1 \leq T_w/T_m \leq 2.5 ,$$

$$n = n_1 + (5n_1 - 2)(1 - T_b/T_m) \quad \text{at} \quad 1 \leq T_b/T_m \leq 1.2 .$$

Figure 12.. List of Equations

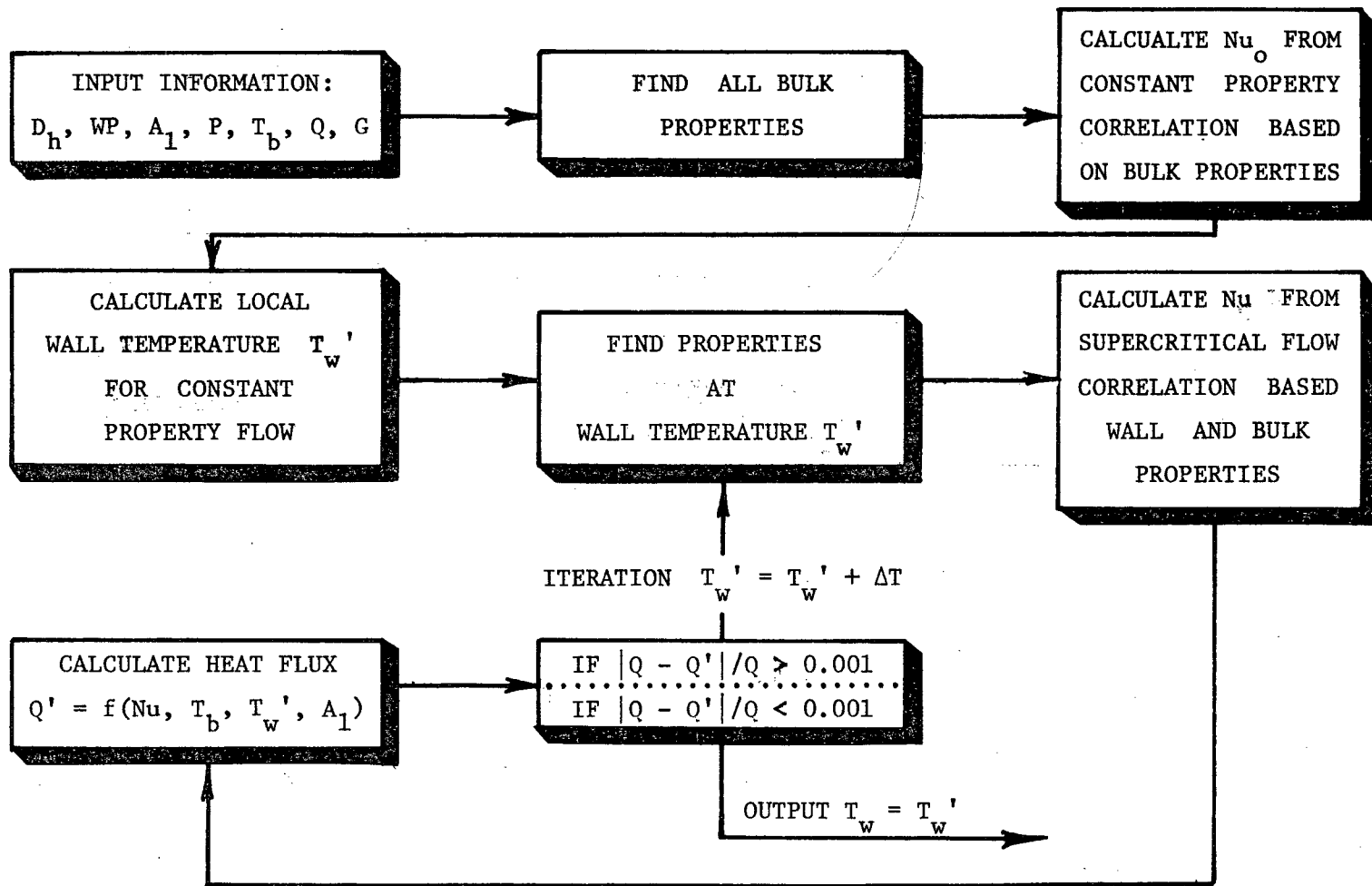


Figure 13. Routine for Calculating Wall Temperature

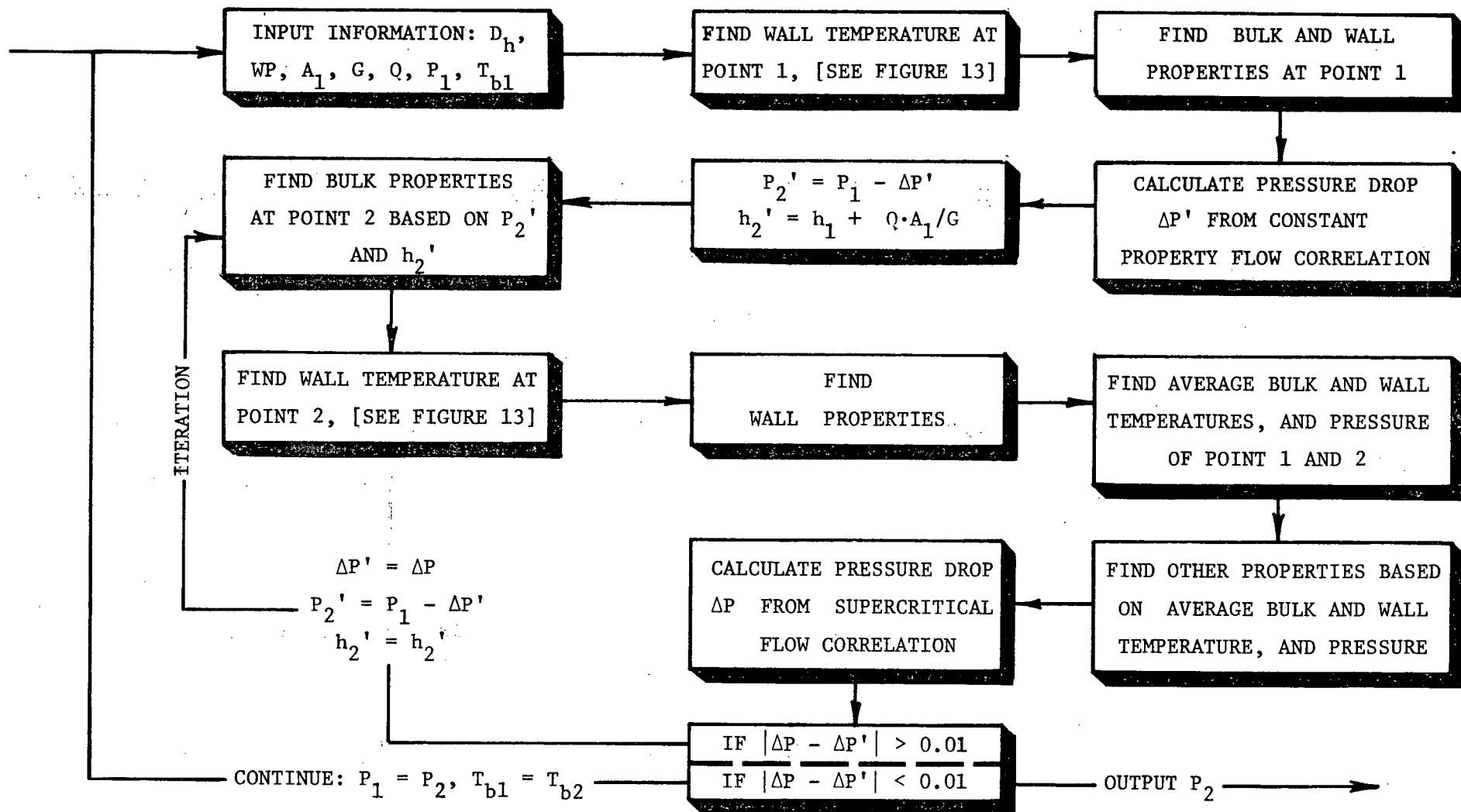


Figure 14. Computer Program Flow Chart for Calculating Heat Transfer to Supercritical Flow in Heated Pipes

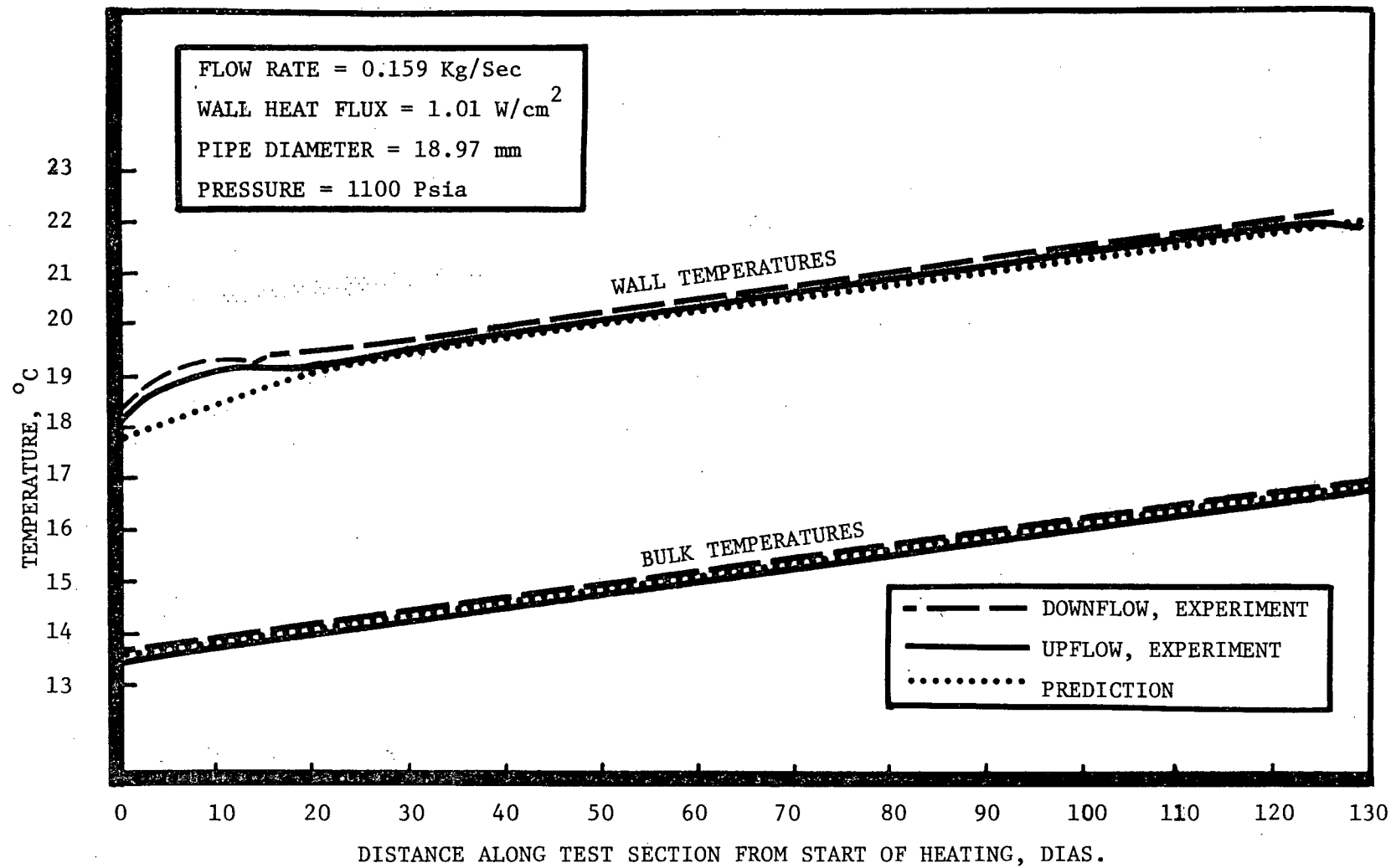


Figure 15. Prediction of Heat Transfer to Supercritical Flow, Experimental Results from [60]

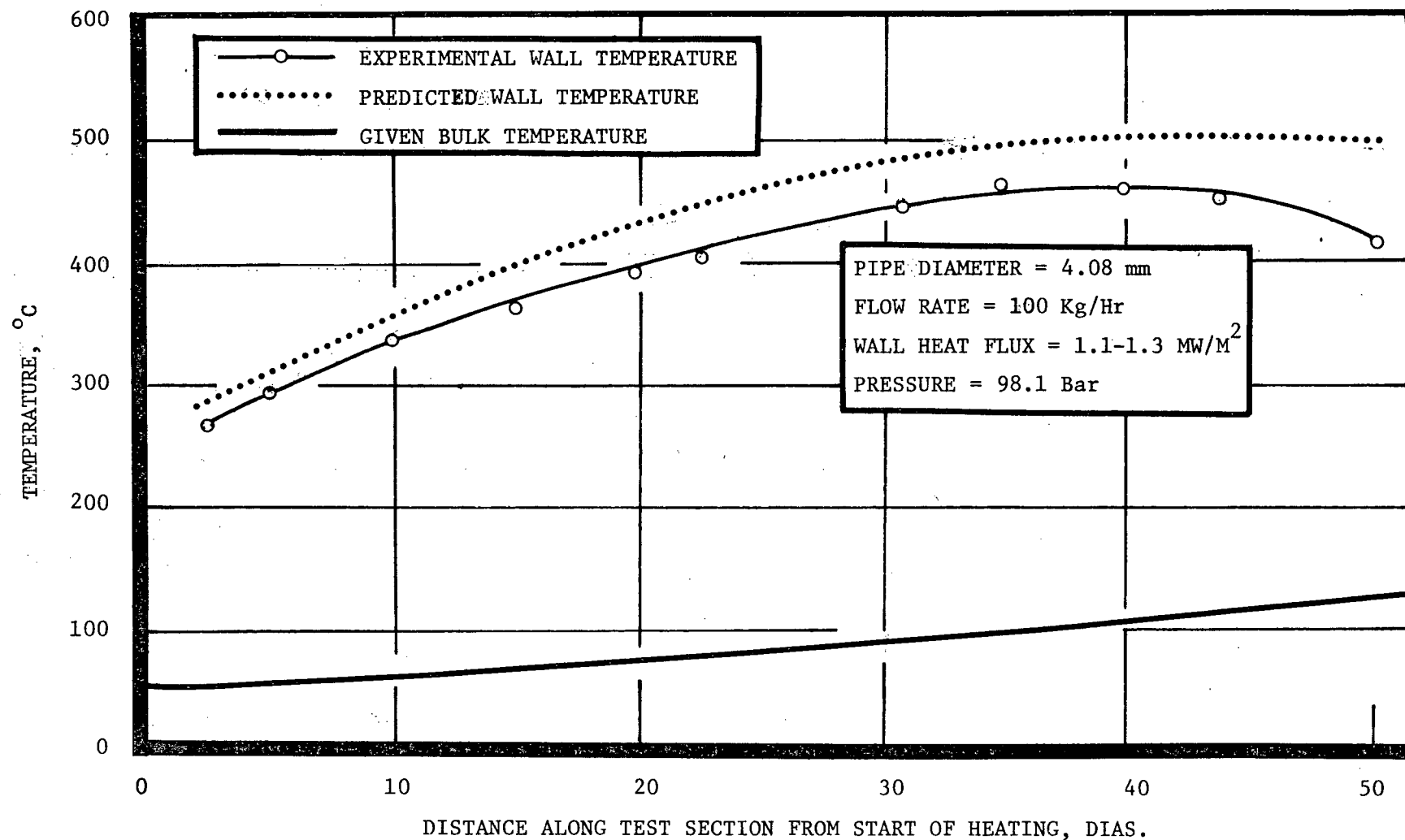


Figure 16. Prediction of Heat Transfer to Supercritical Flow, Experimental Results from [49]

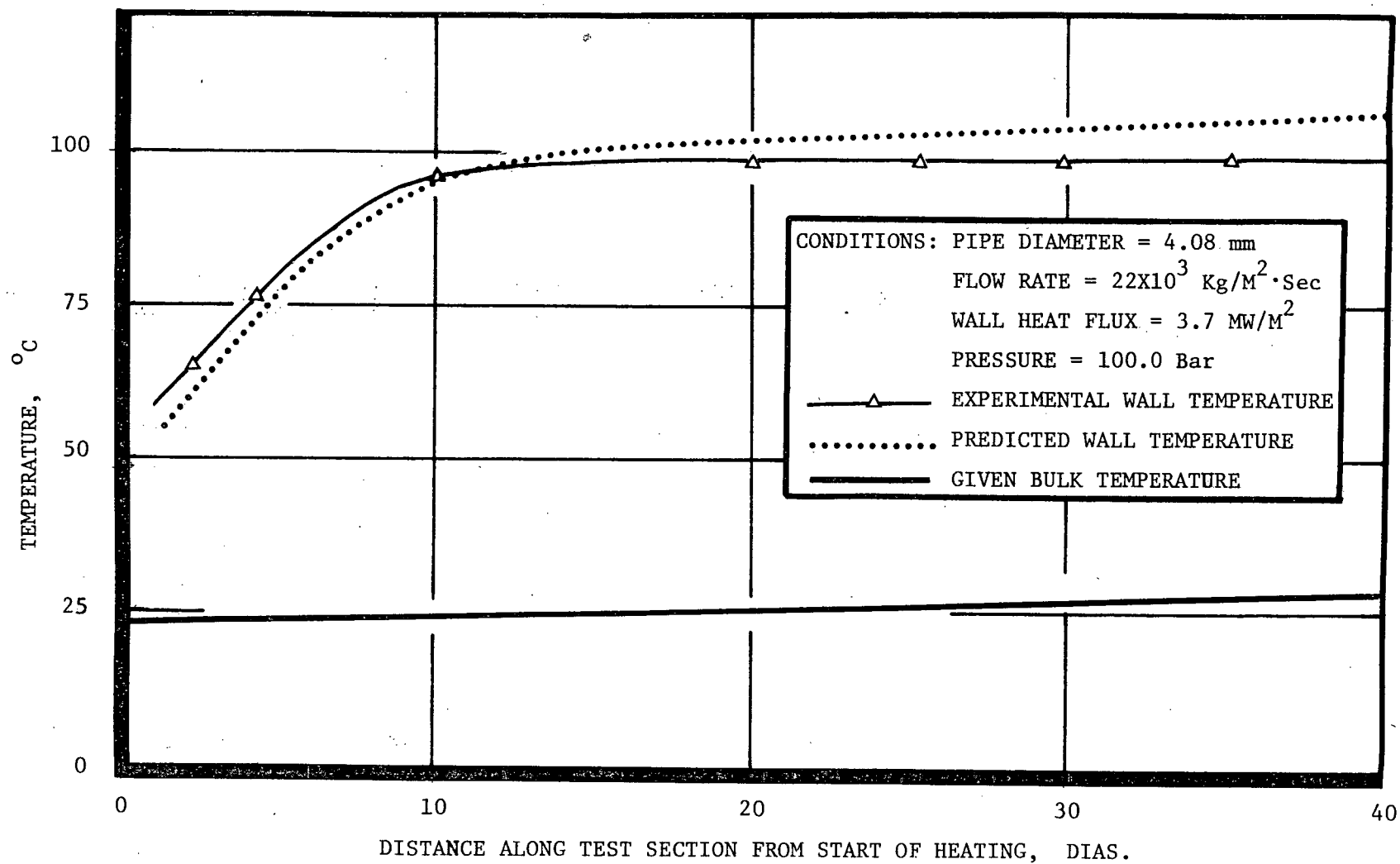


Figure 17. Prediction of Heat Transfer to Supercritical Flow, Experimental Results from [55]

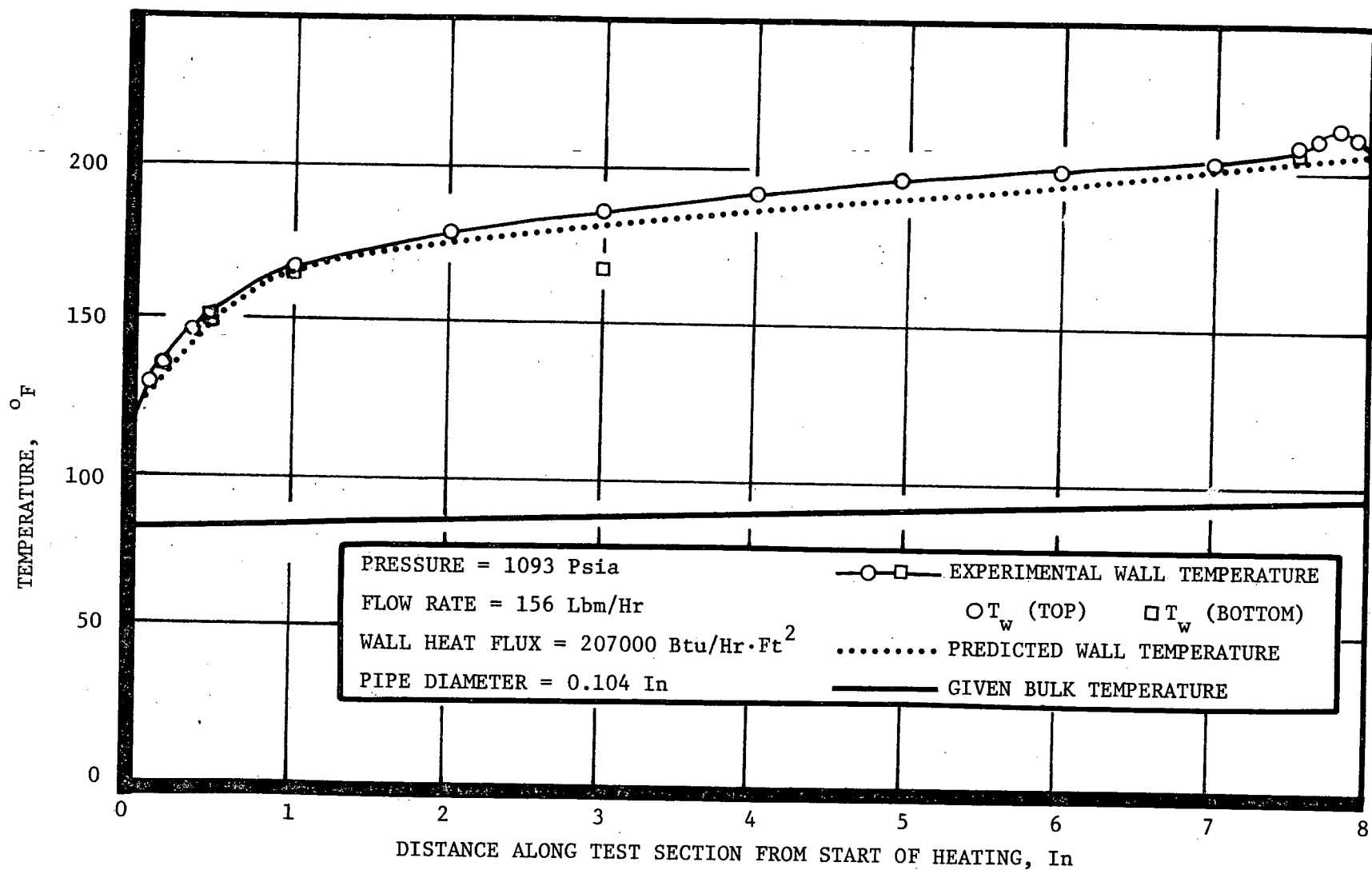
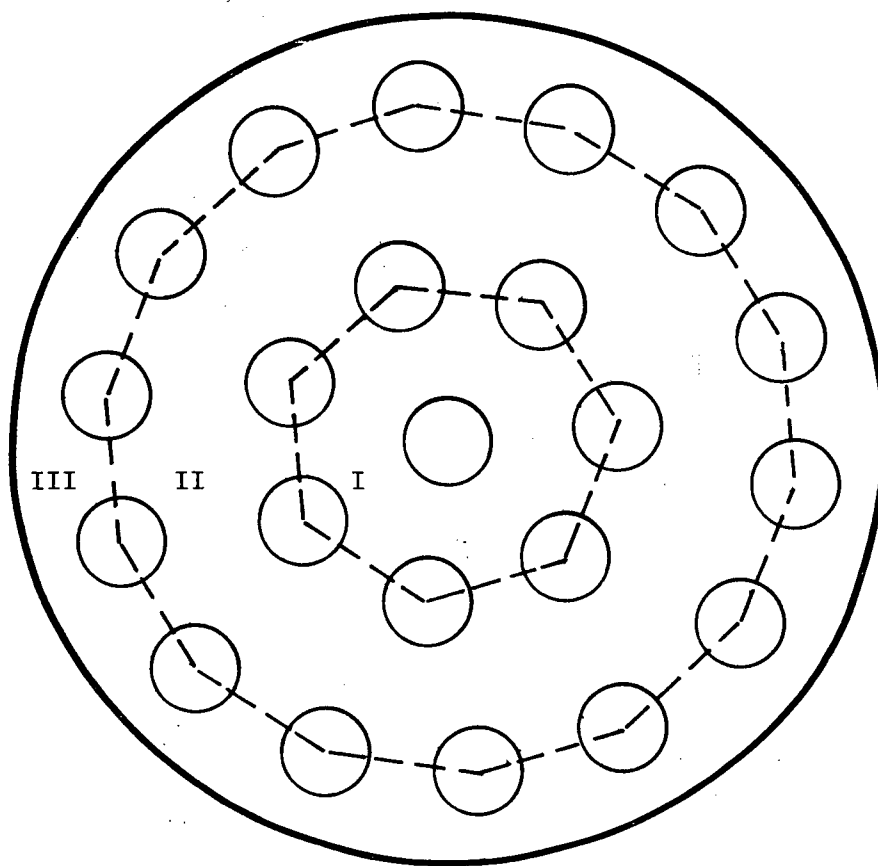
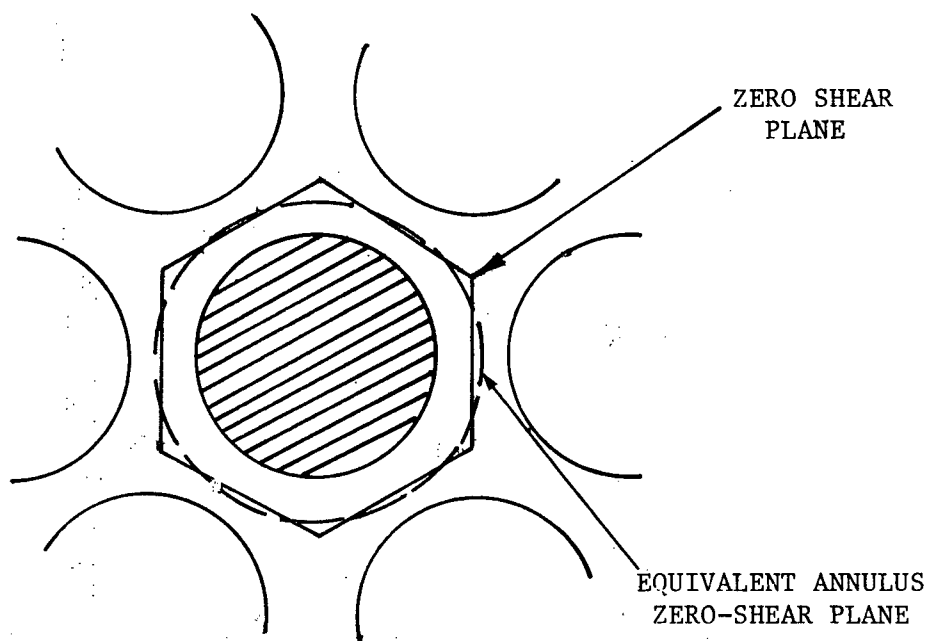


Figure 18. Prediction of Heat Transfer to Supercritical Flow, Experimental Results from [42]

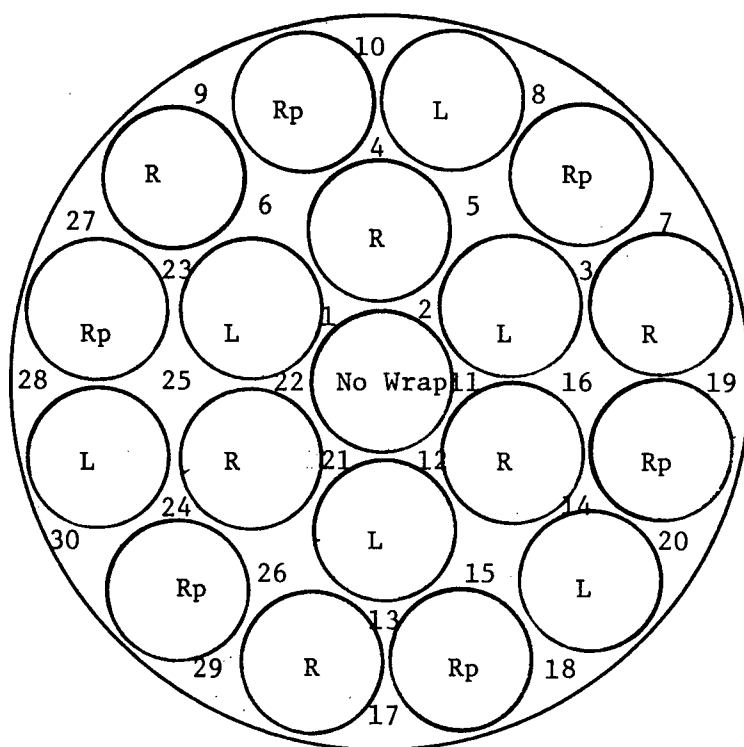


(a) Entire Array Equivalent Annulus [67]



(b) Single Rod Equivalent Annulus [68]

Figure 19. Equivalent Annulus Models for Rod-Bundles



19-ELEMENT WIRE-
WRAPPED BUNDLE

L LEFT-HAND WRAP
R RIGHT-HAND WRAP
Rp PARTIAL RIGHT-
HAND WRAP
(OUTER 120°)

Wire wrap is used to increase mixing between subchannels which are divided at the minimum spacings between fuel-rods. The subchannels are classified and designated with numbers, according to their geometry and mixing condition.

Figure 20. Lumped Parameter Model for Rod Bundles (from [71])

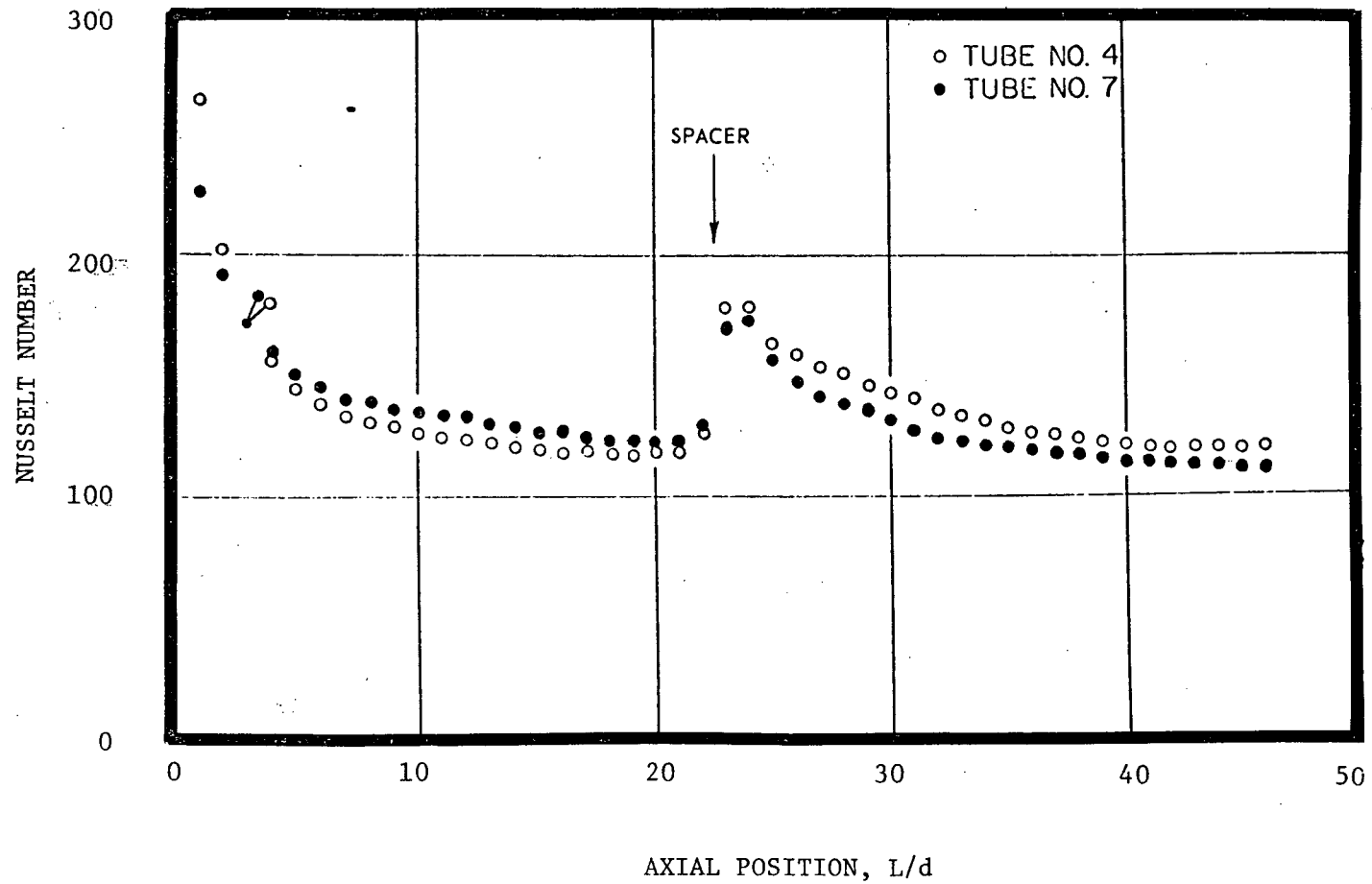


Figure 21. Thermal Entrance Following a Grid Type Spacer (from [73])

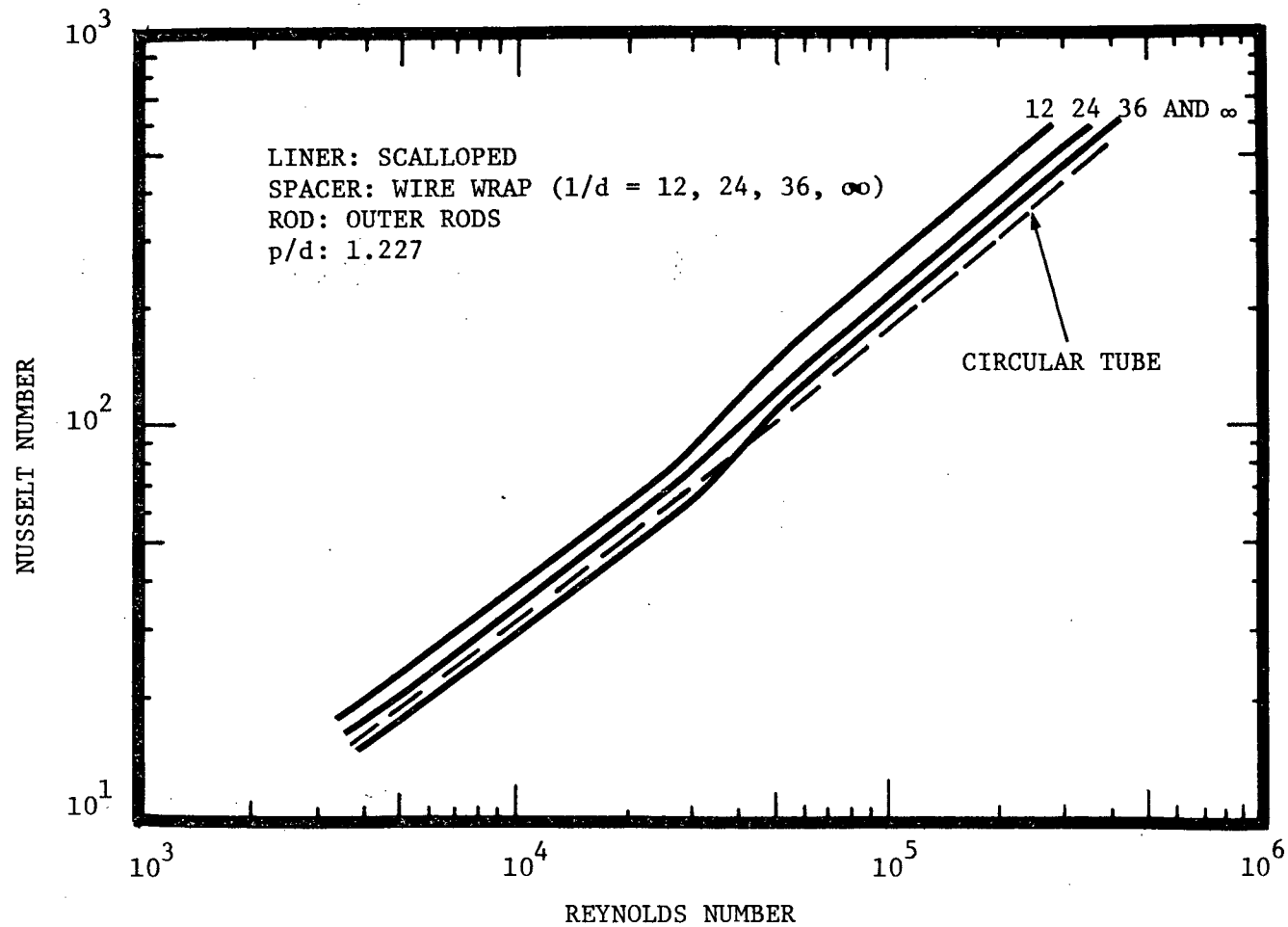


Figure 22. Comparison of Heat Transfer Data in a Uniformly Heated Seven-Rod Bundle ($Pr = 0.7$) with Wire-Wrap Spacers (from [74])

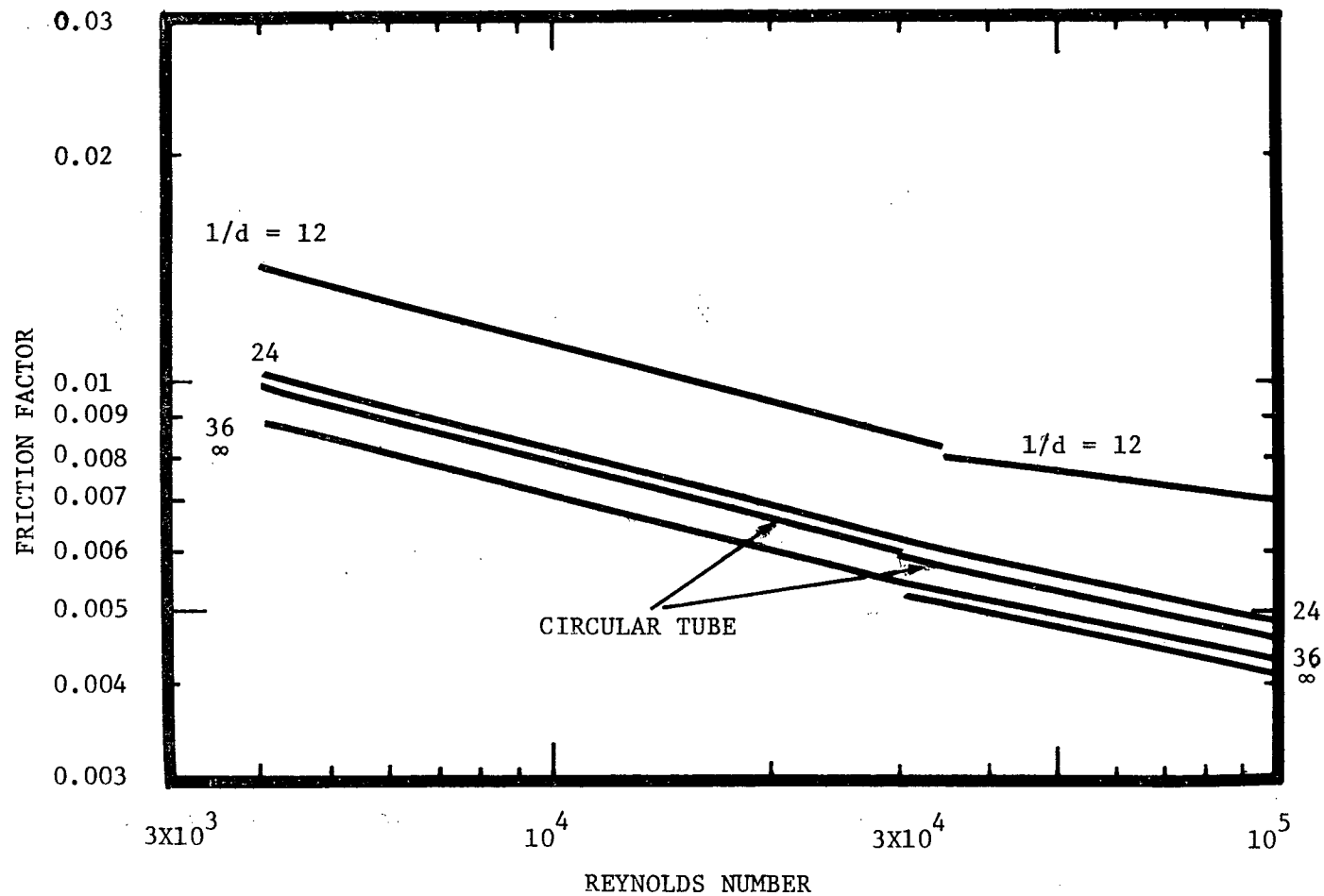


Figure 23. Comparison of Friction Factors for Seven-Rod Bundle with Wire-Wrap Spacers ($1/d = 12, 24, 36, \infty$) in a Scalloped Liner ($p/d = 1.237$) (from [74])

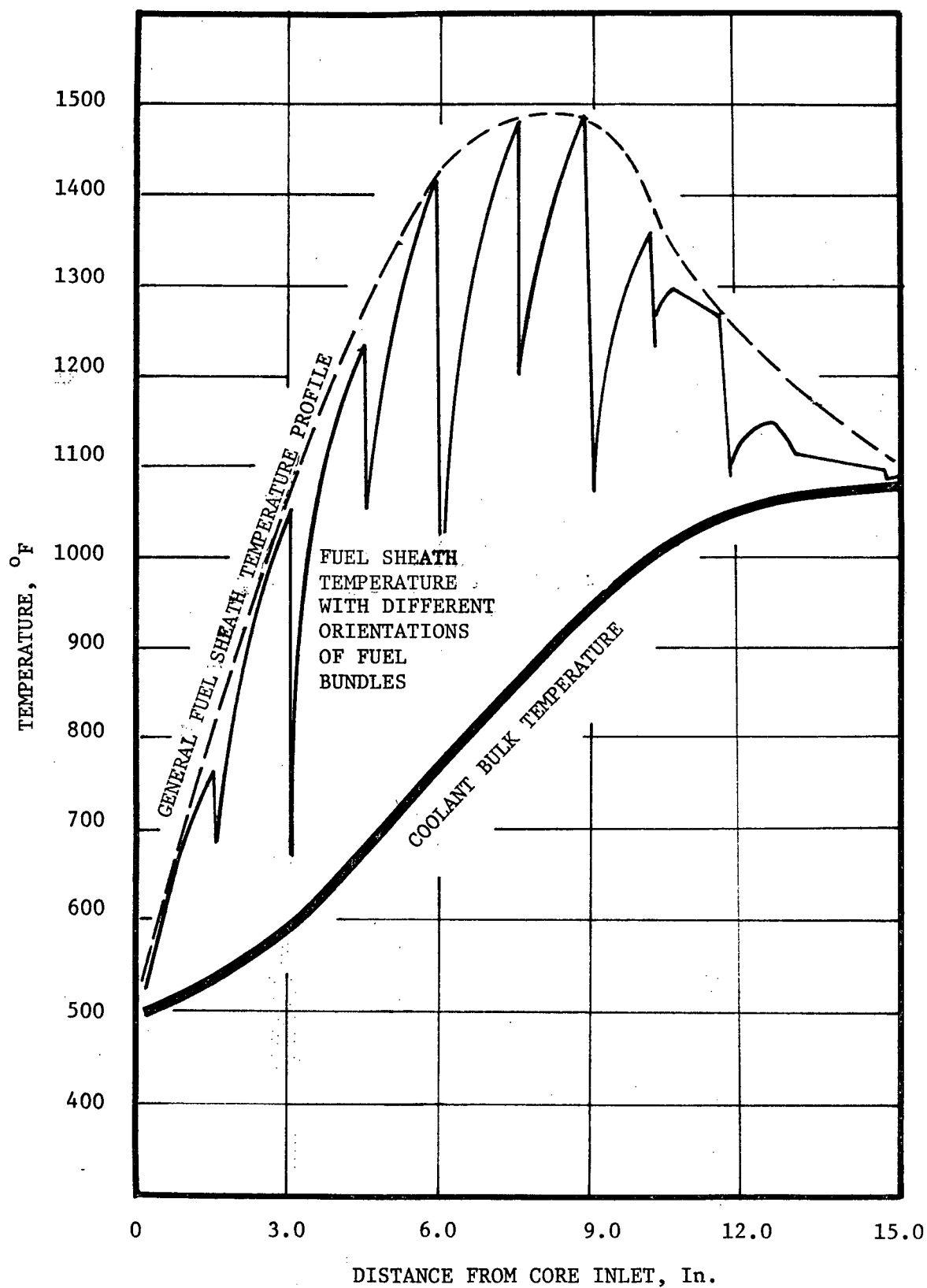


Figure 24. Temperature Profiles in Coolant Channel with Different Fuel Bundle Orientation(from [77])

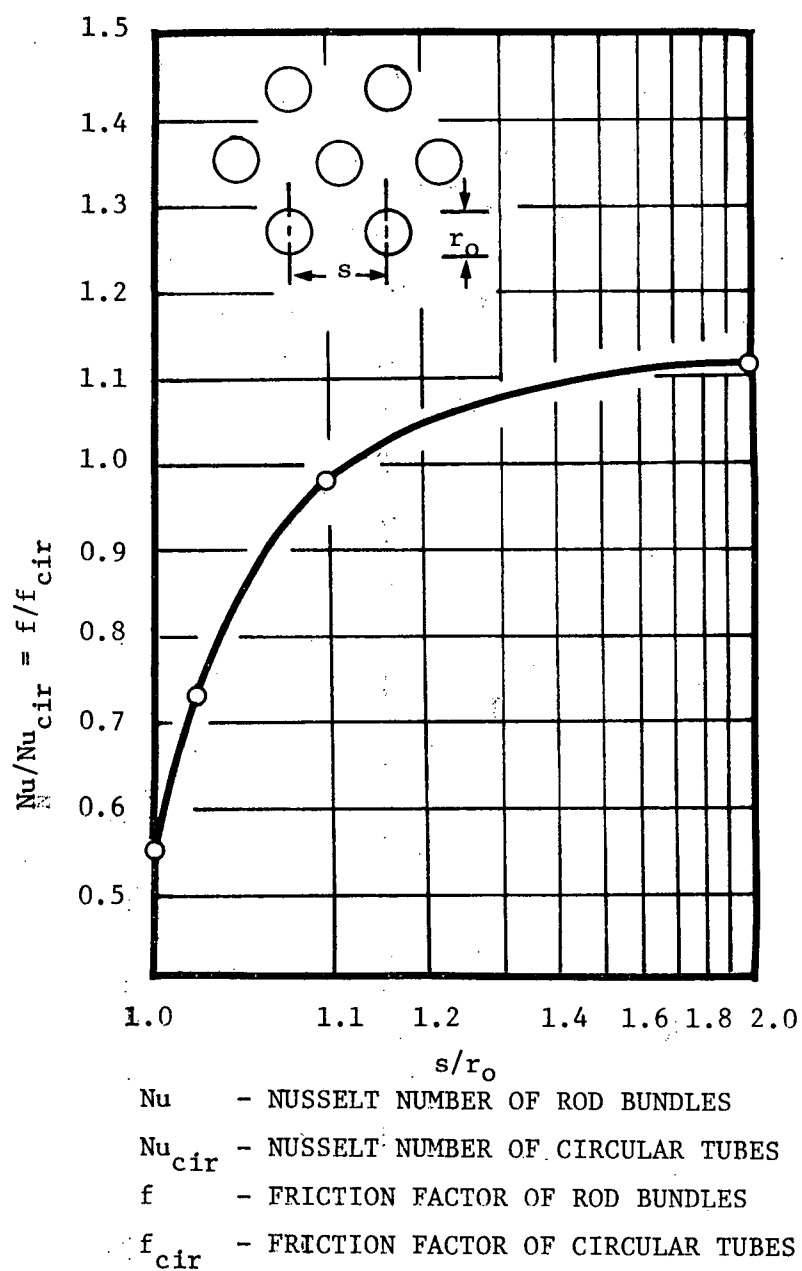
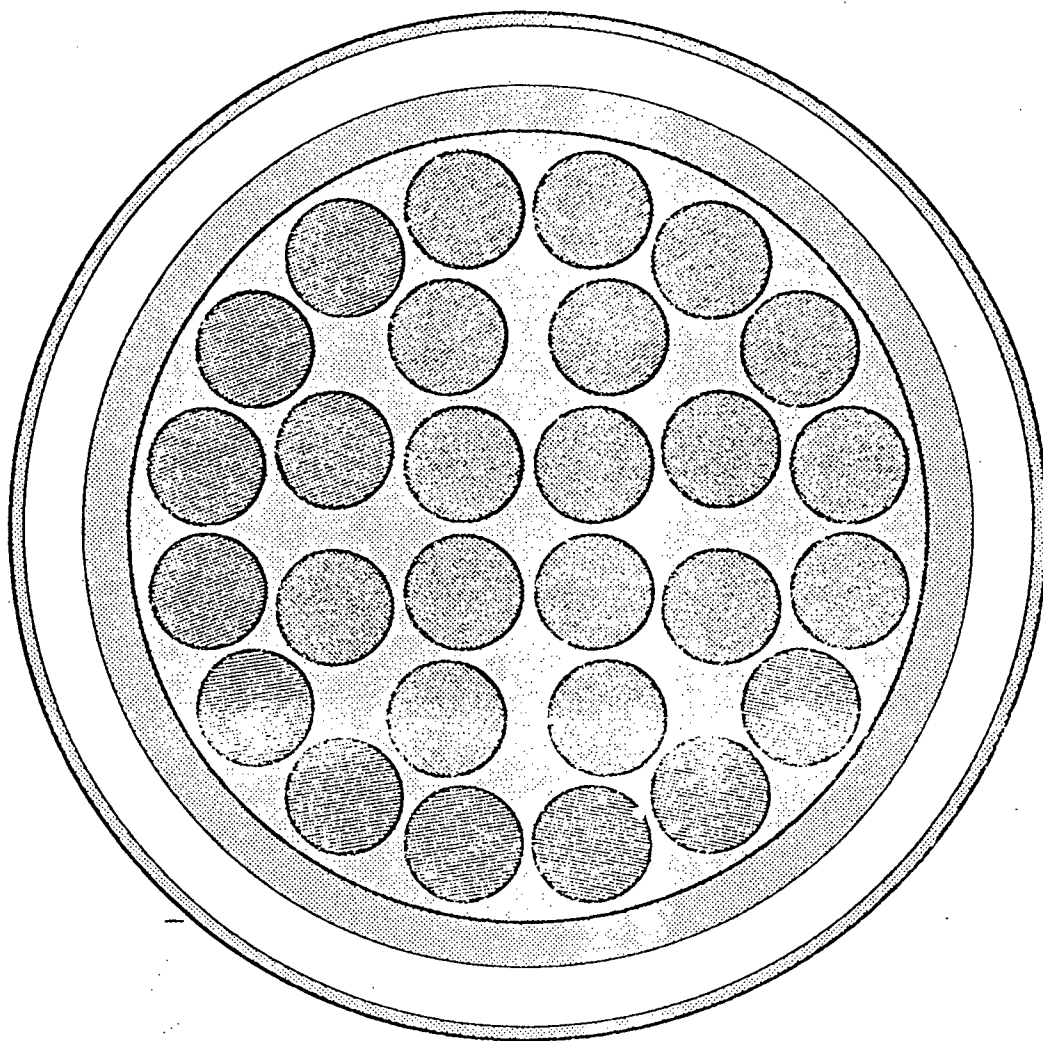


Figure 25. Effect of Ratio of Pitch to Rod Diameter on Nusselt Number and Friction Factor (from [78])



28. ELEMENT BUNDLE

FULL SCALE CROSS SECTION
OF FUEL AND COOLANT TUBE

Figure 26. CROSS SECTION OF FUEL AND COOLANT TUBE
(FROM [12])

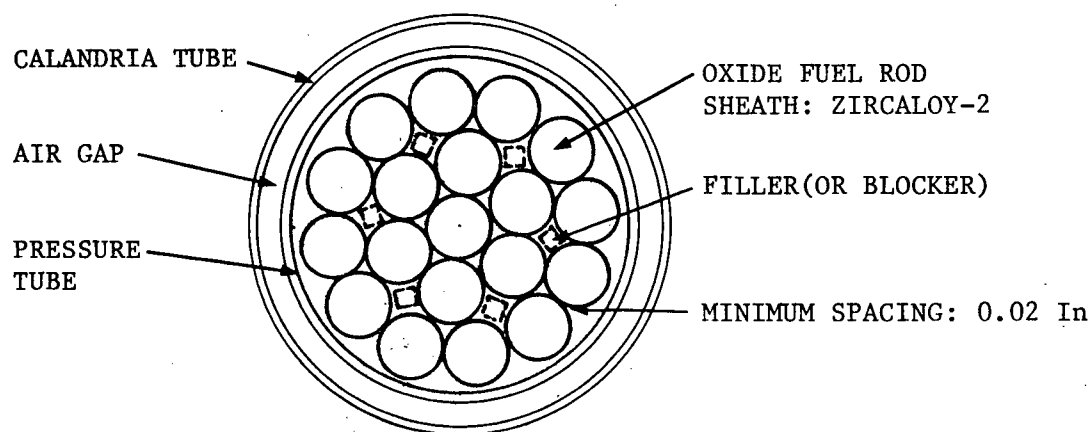


Figure 27. Channel for Boiling Reactor (from [79])

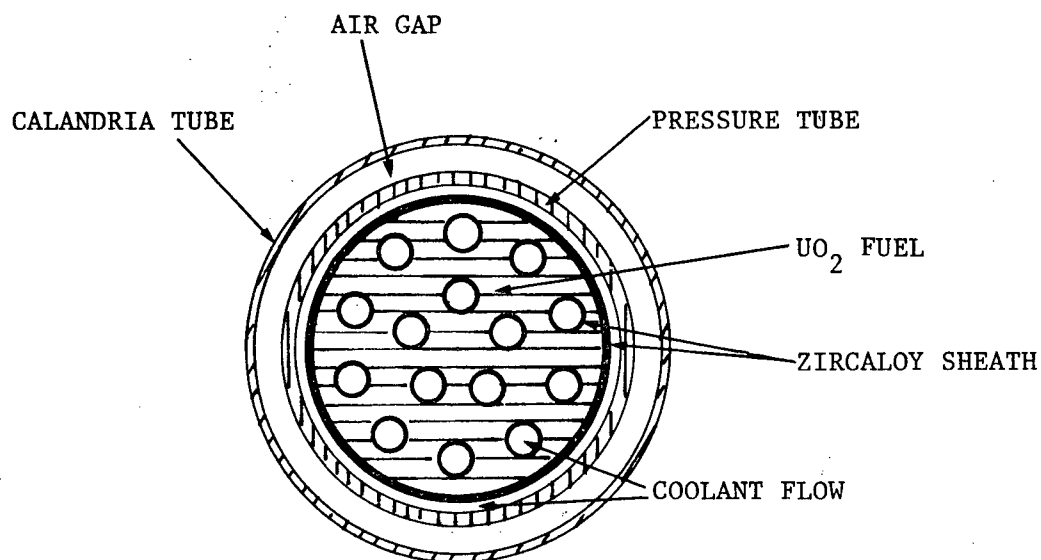


Figure 28. Tube-in-Shell Fuel Element (from [79])

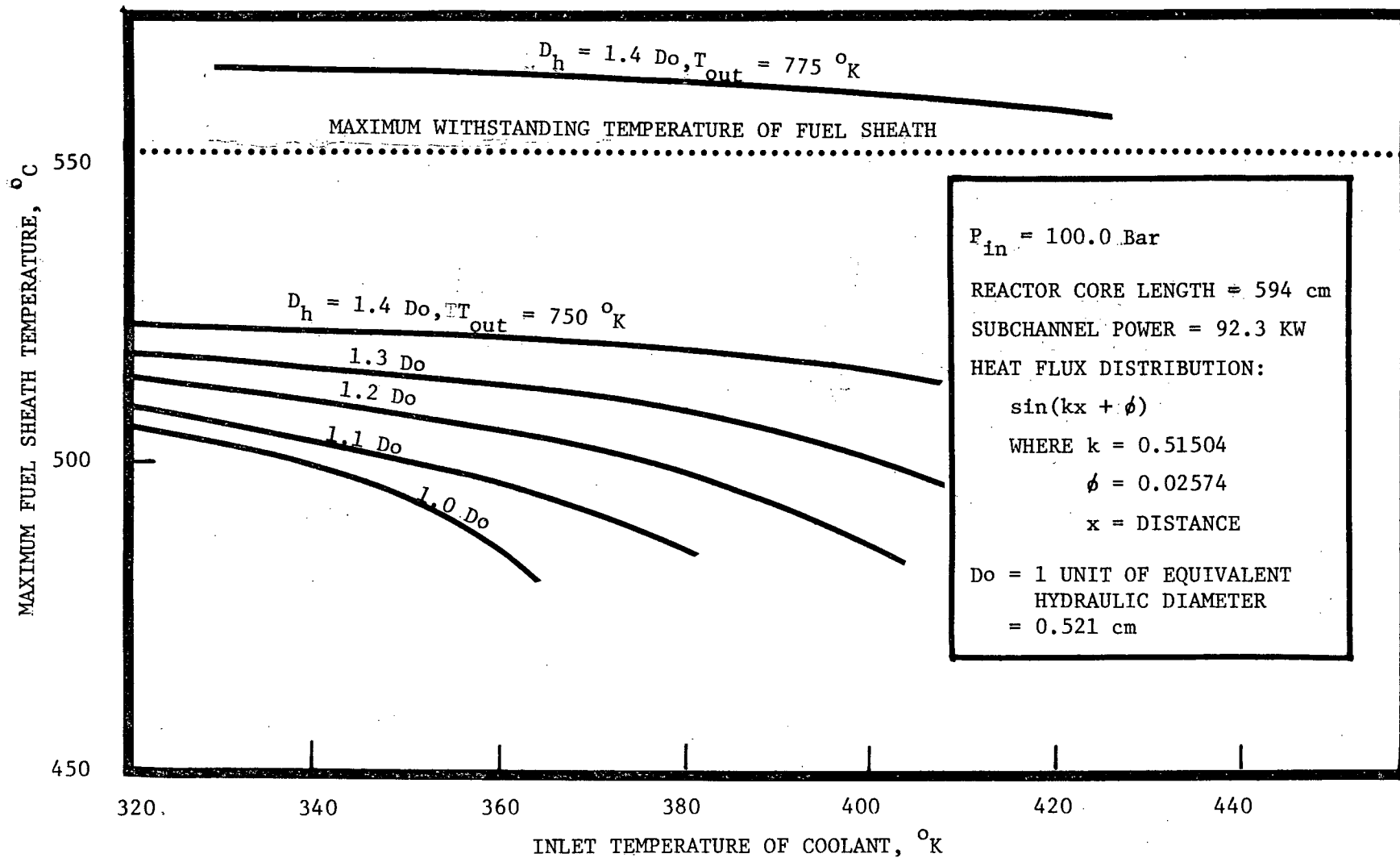


Figure 29. Maximum Operating Temperature Versus Inlet Coolant Temperature

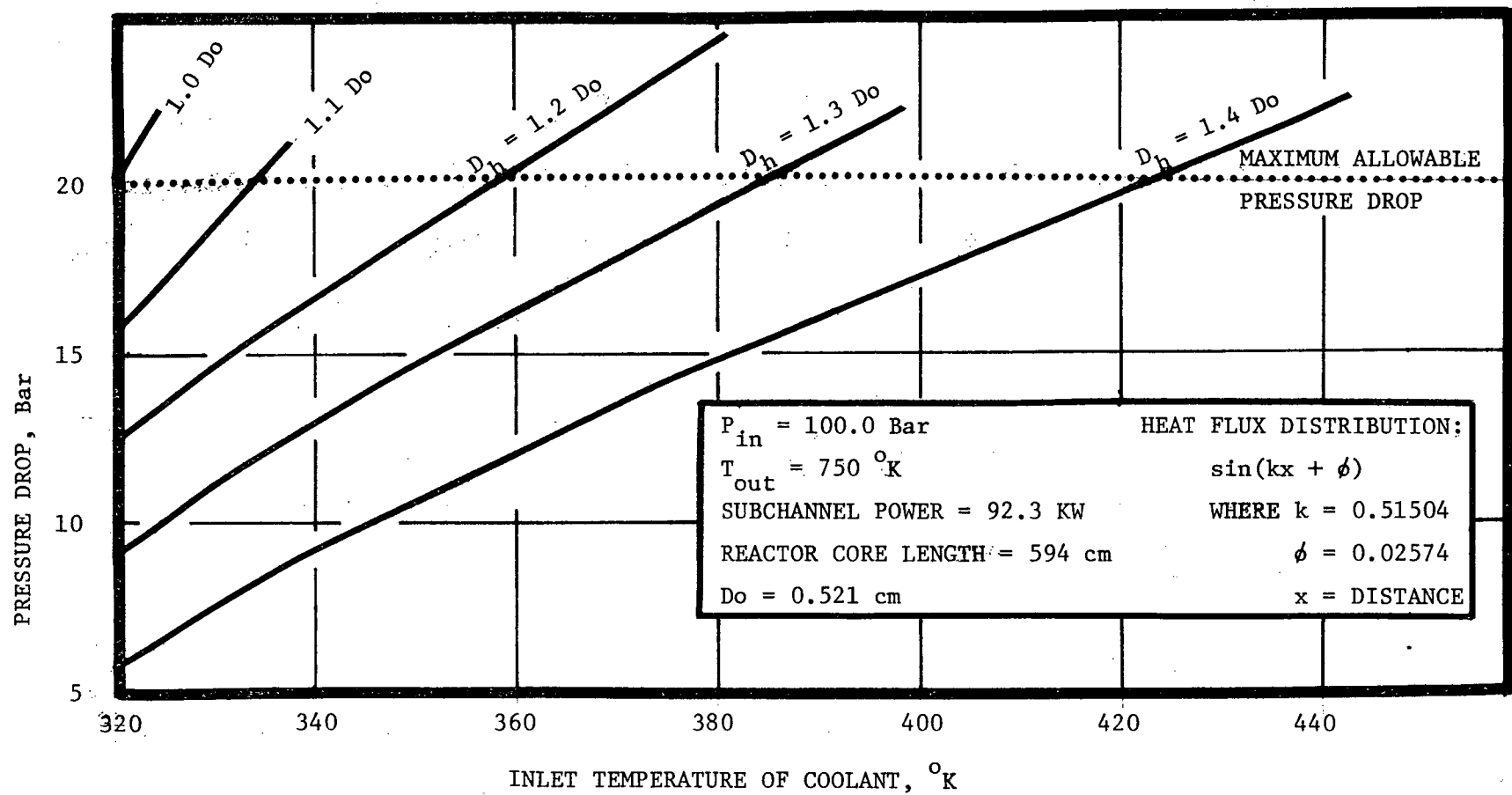


Figure 30. Pressure Drop Versus Inlet Coolant Temperature

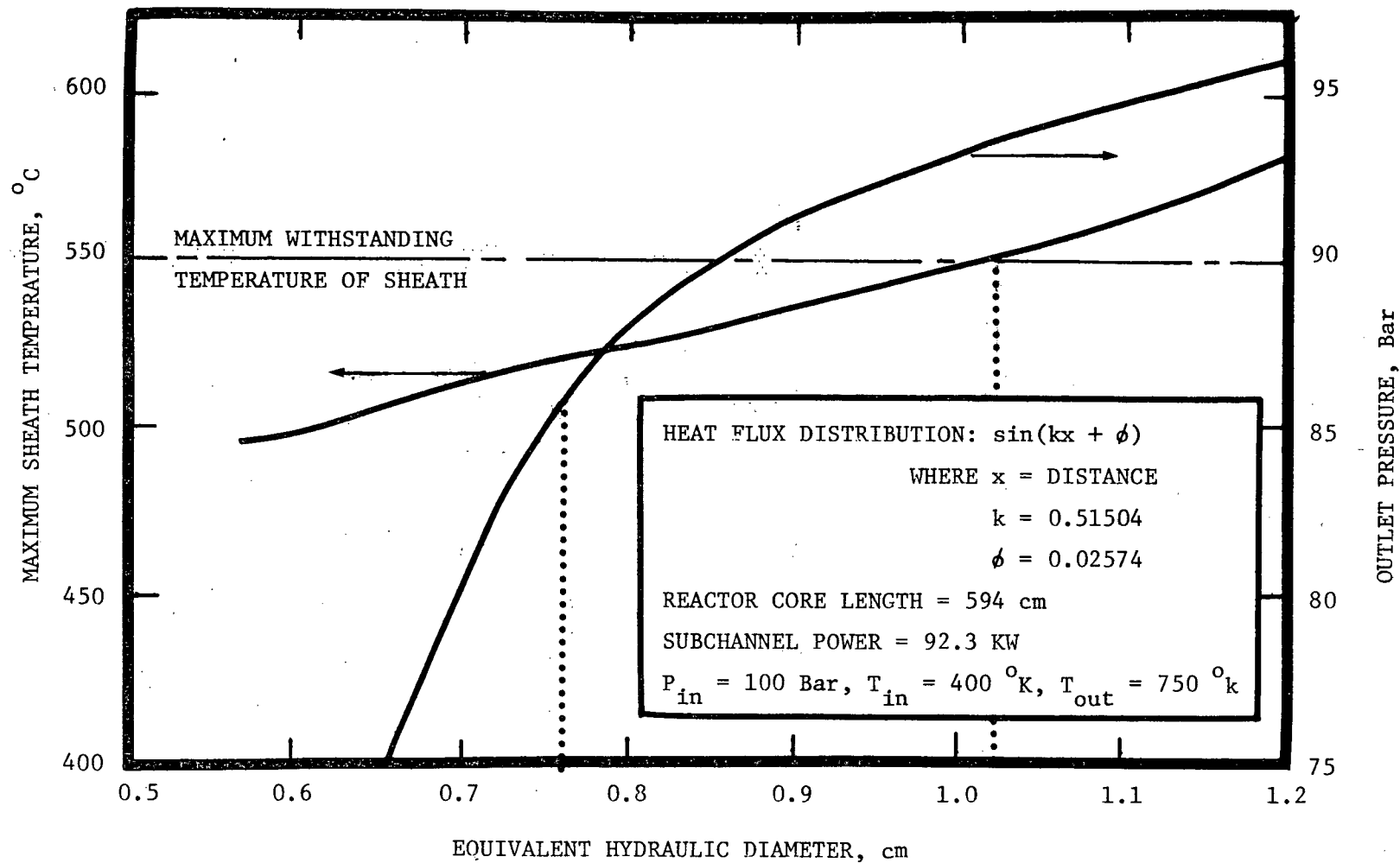
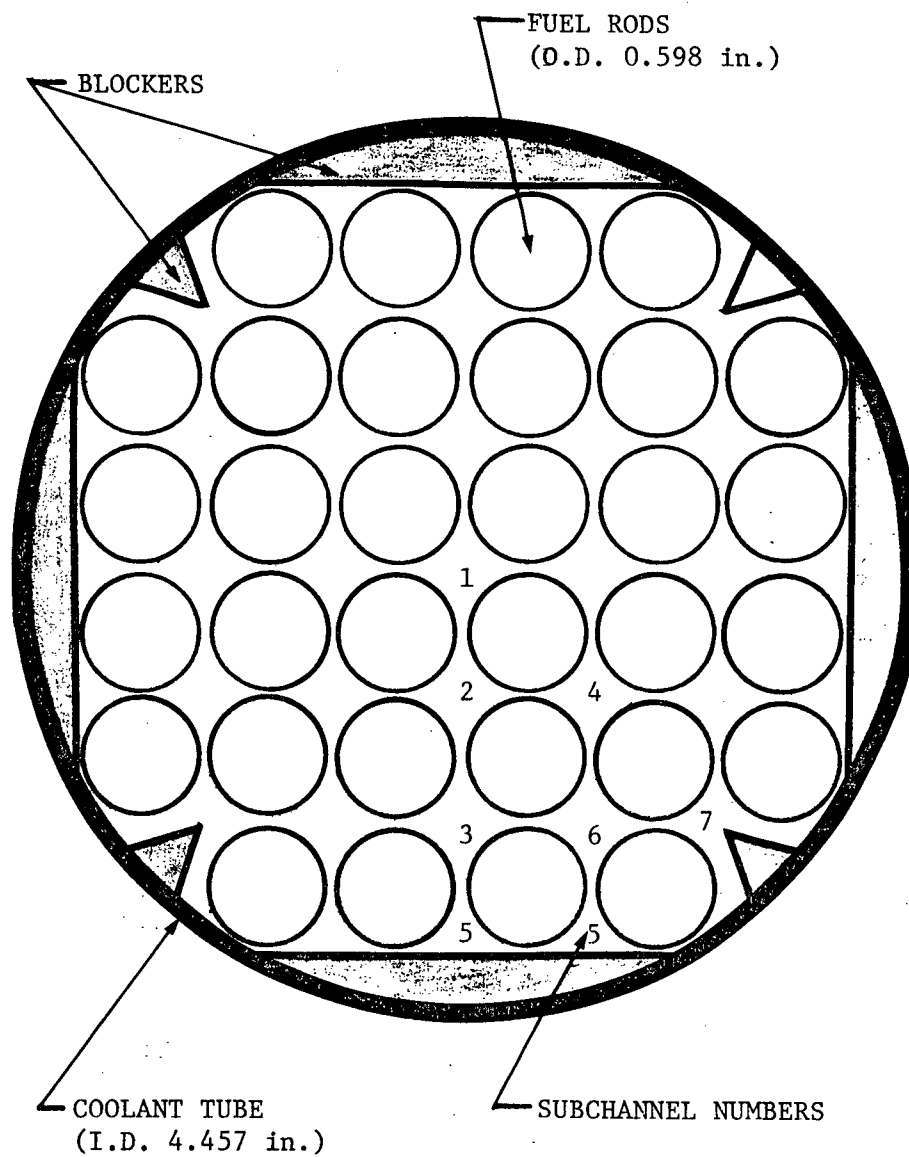


Figure 31. Selection of Minimum Equivalent Hydraulic Diameter



FULL SCALE CROSS SECTION
OF FUEL BUNDLE AND COOLANT TUBE

Figure 32. Cross Section of 32-Element Fuel Bundle

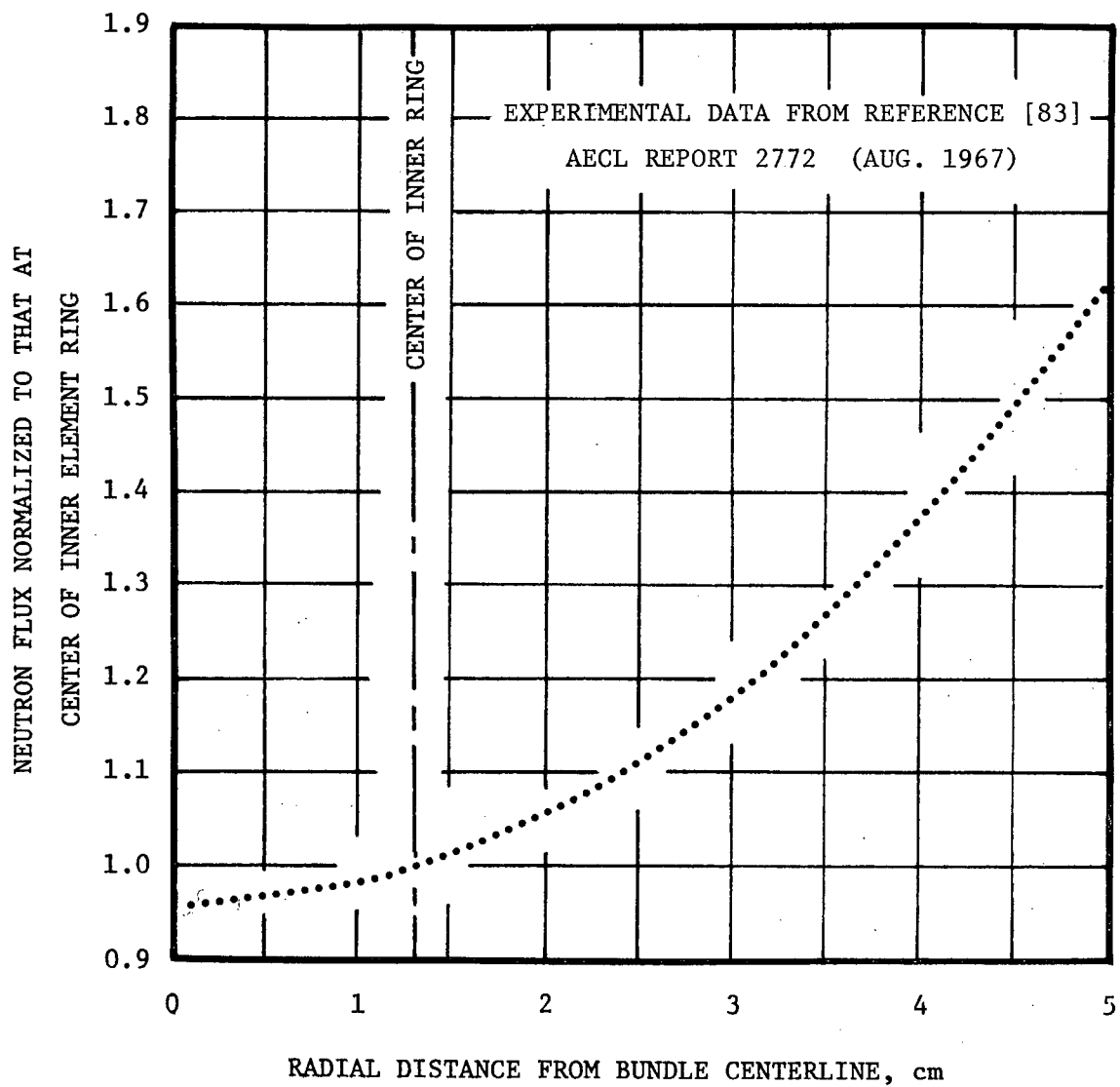


Figure 33. Radial Neutron Flux Distribution in Fuel Bundle

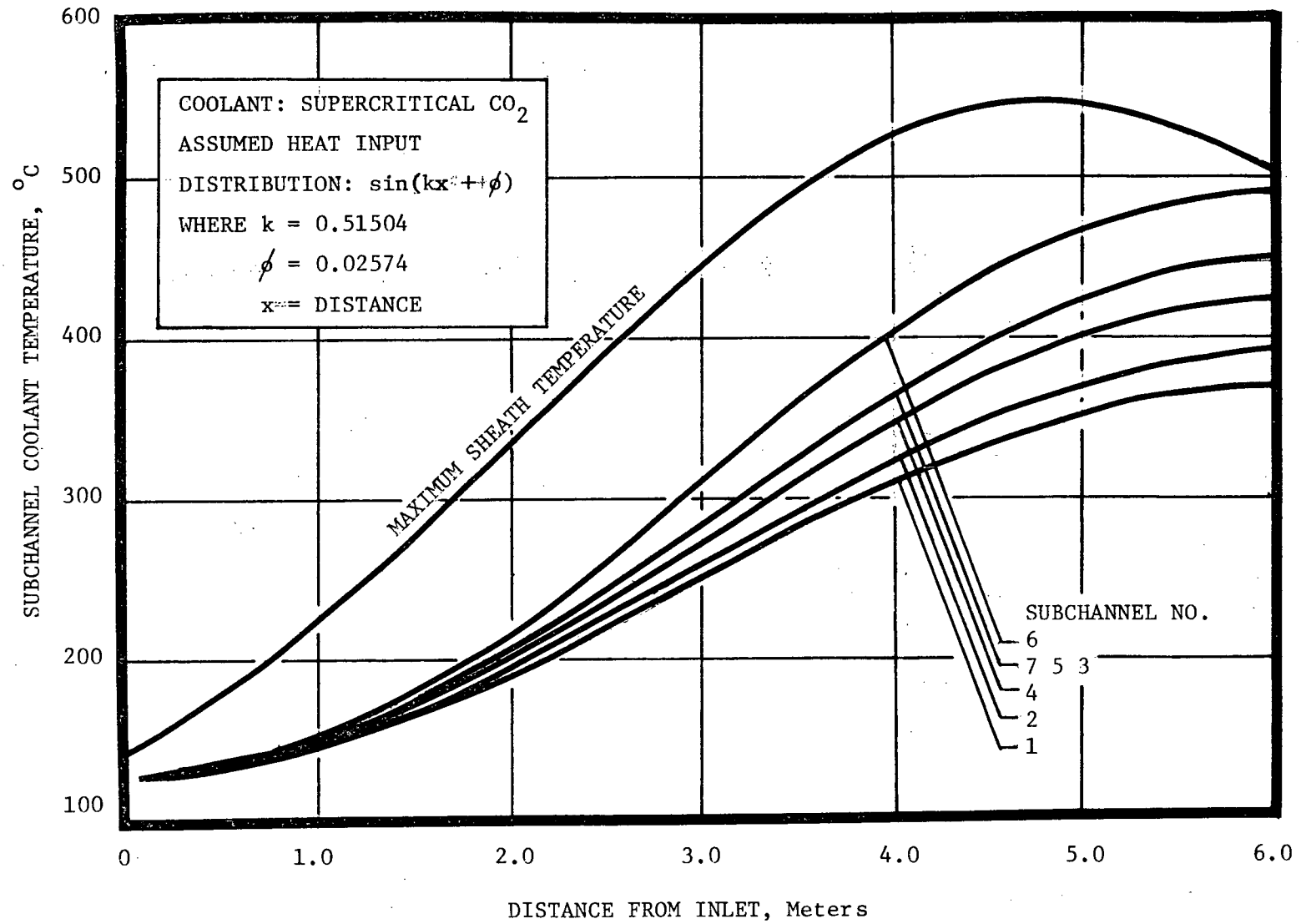


Figure 34. Subchannel Coolant Temperature Rise in 32-Element Fuel Bundles Versus Reactor Channel Length

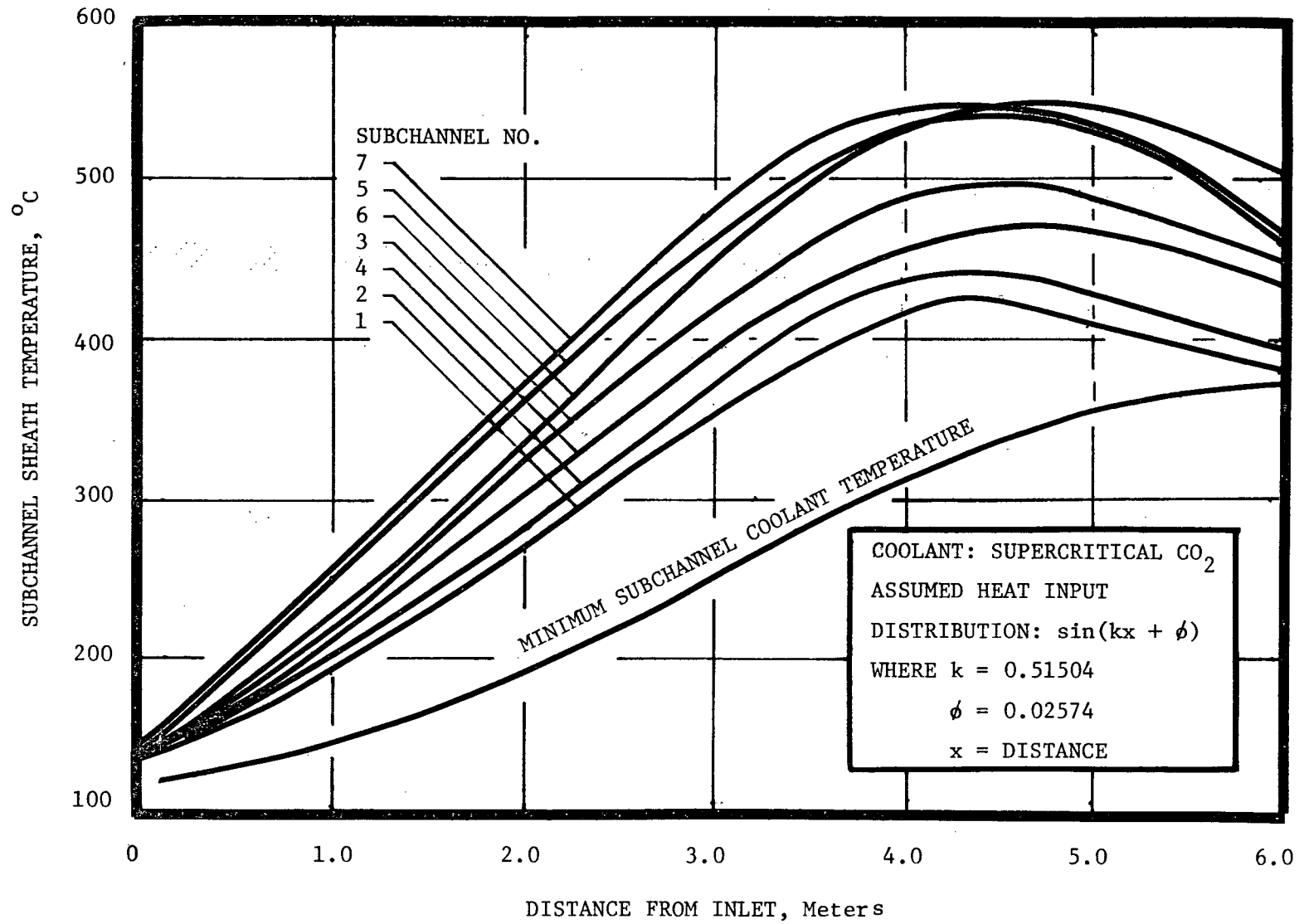


Figure 35. Subchannel Sheath Temperature Rise in 32-Element Fuel Bundles Versus Reactor Channel Length

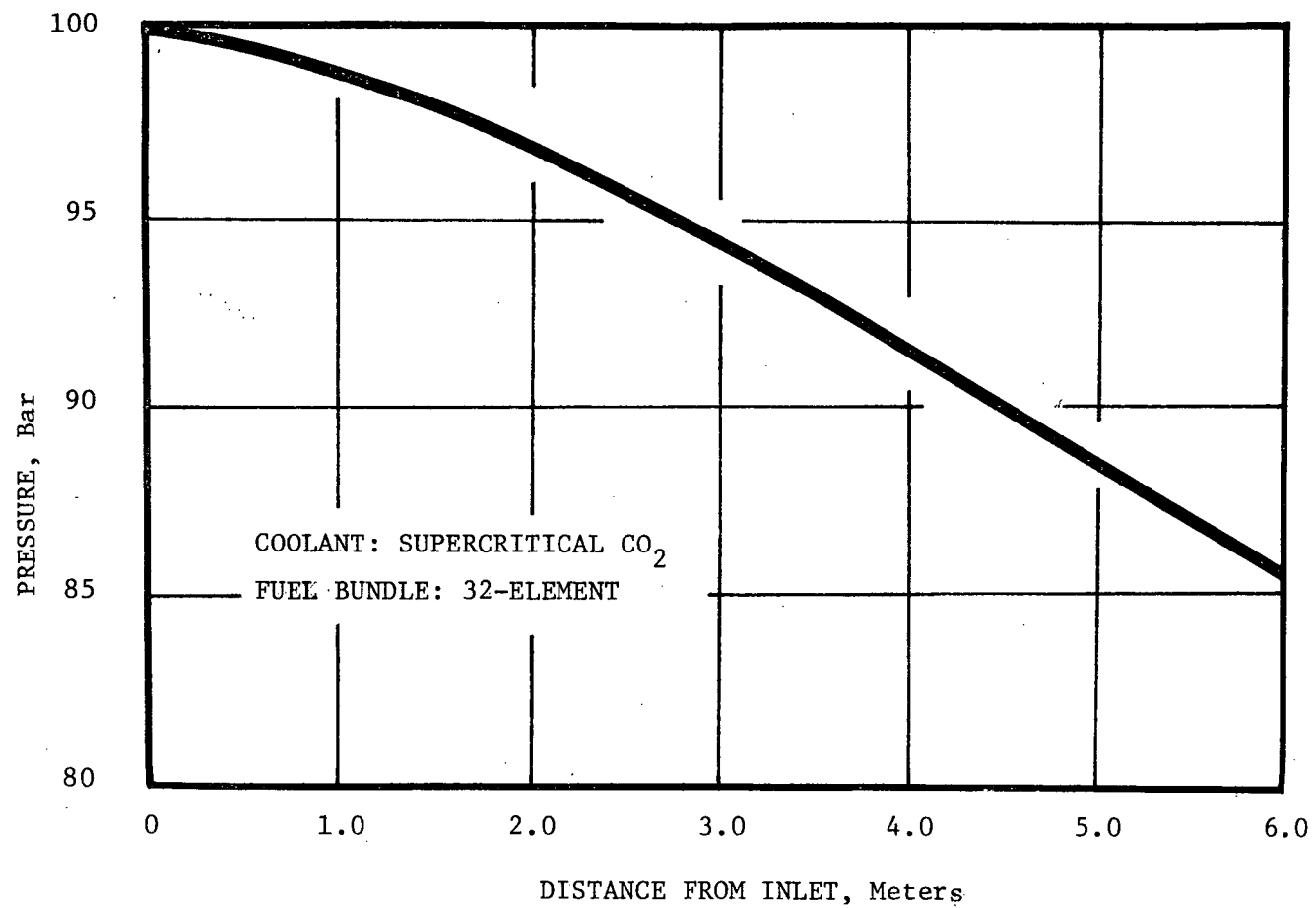


Figure 36. Pressure Drop Along Reactor Channel Length

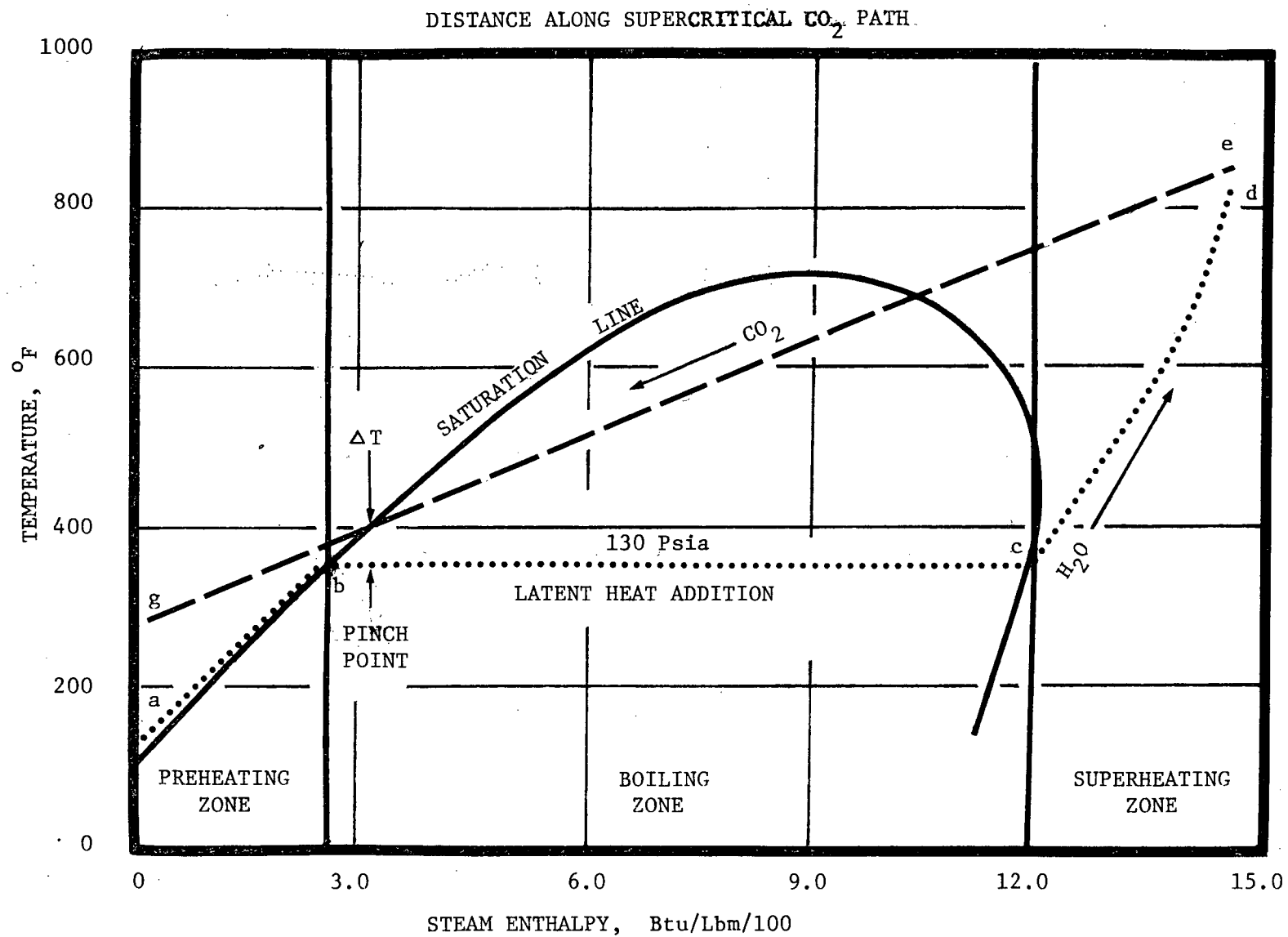
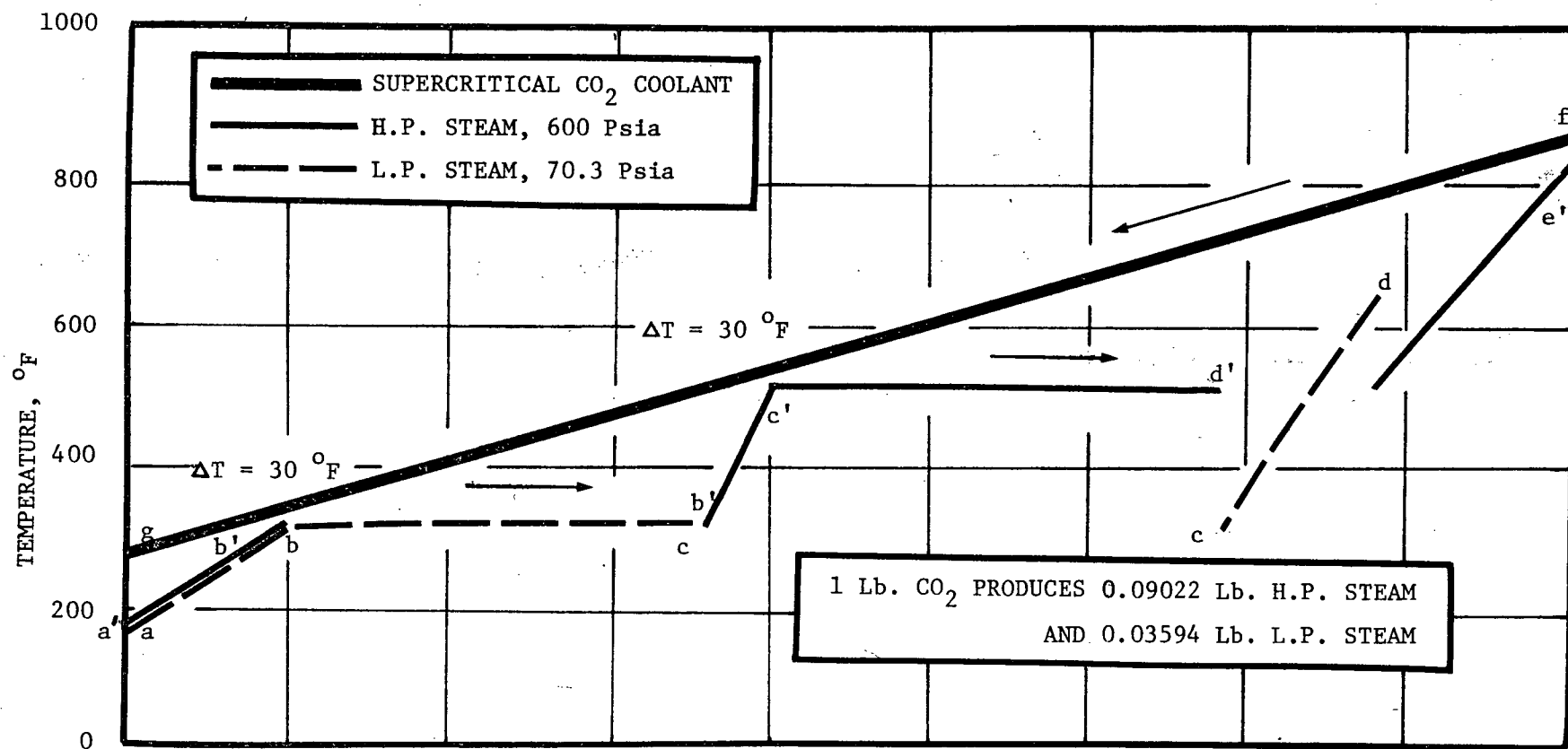


Figure 37. Single Pressure Steam Generation



REPRESENTATIVE POSITION IN STEAM GENERATOR

Figure 38. Dual-Pressure 600.0/70.3 (psia) Steam Generation

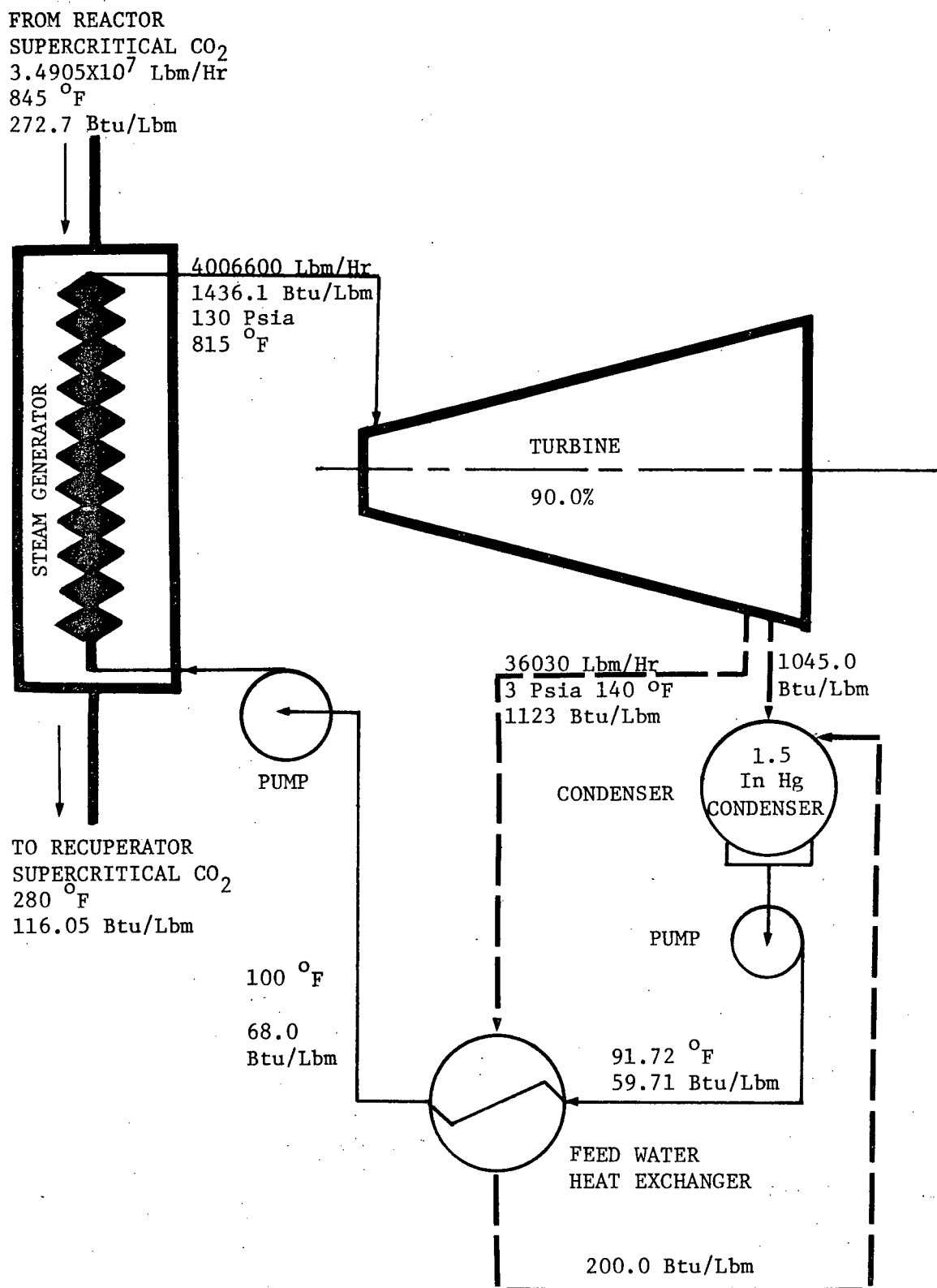


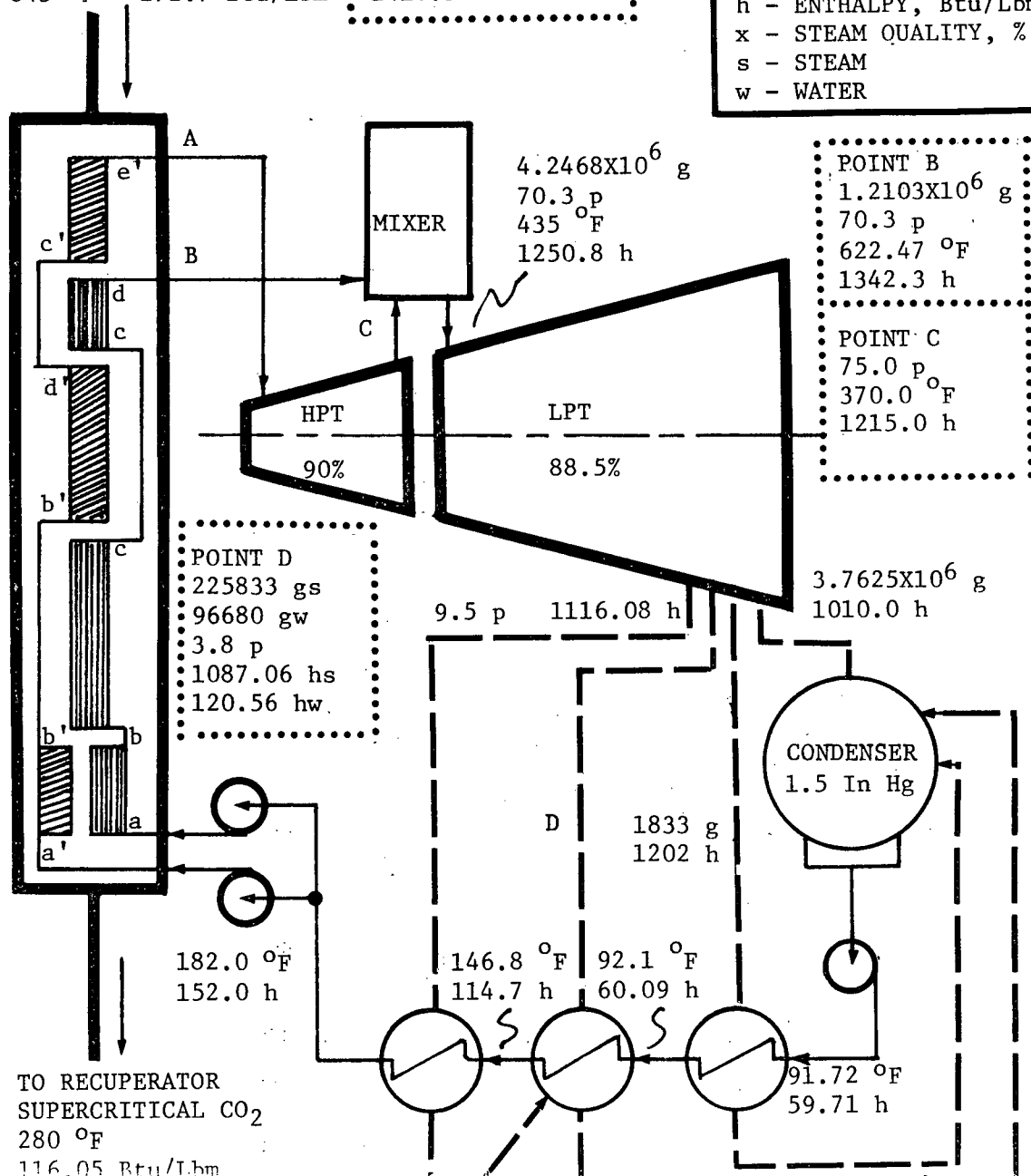
Figure 39. Turbine Circuit Heat Balance of Single Pressure Cycle

FROM REACTOR
 SUPERCRITICAL CO₂
 3.4905×10^7 Lbm/Hr
 845 °F 272.7 Btu/Lbm

POINT A
 3.0365×10^6 g
 600.0 p 815 °F
 1416.5 h

LEGEND:

g - FLOW RATE, Lbm/Hr
 p - PRESSURE, Psia
 h - ENTHALPY, Btu/Lbm
 x - STEAM QUALITY, %
 s - STEAM
 w - WATER



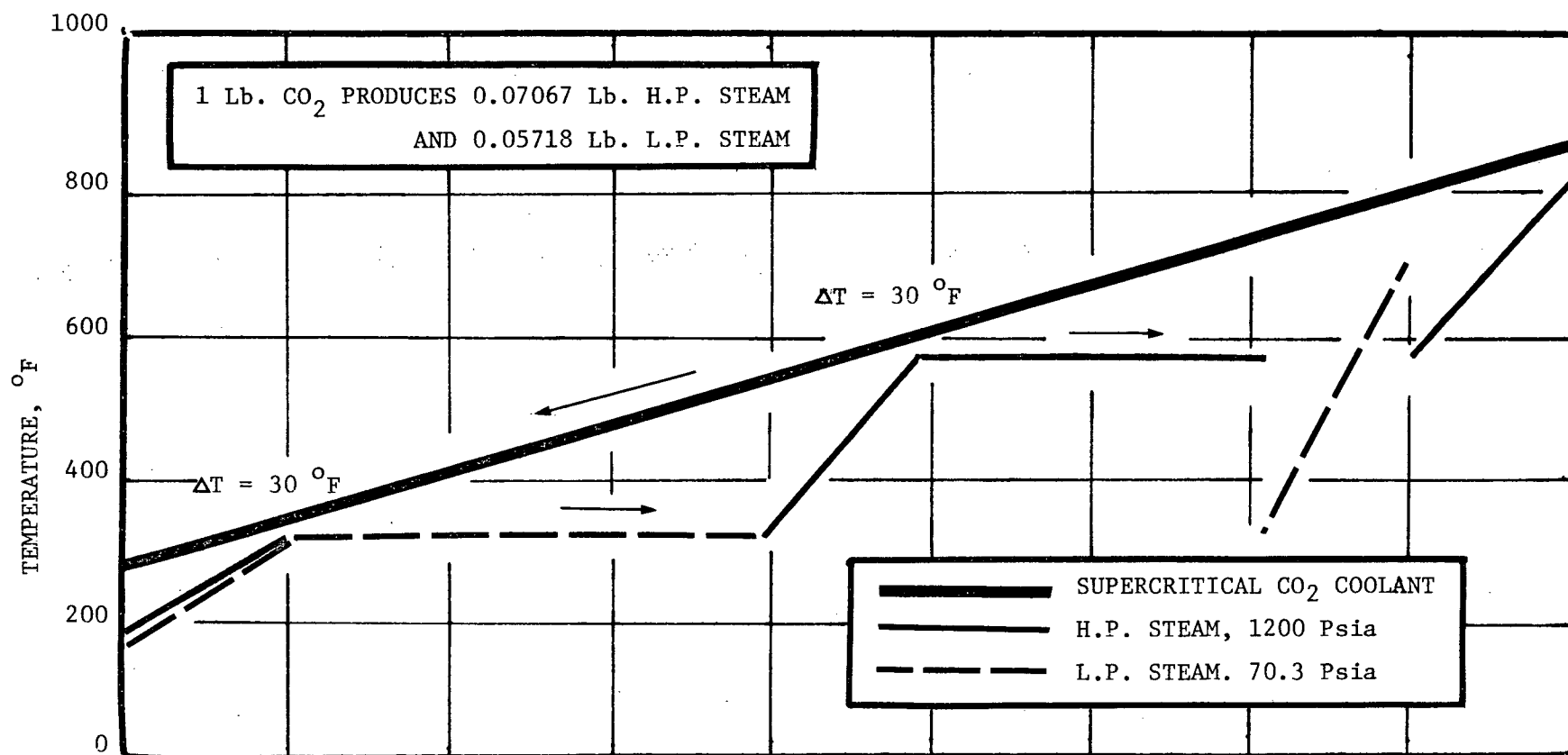


Figure 41. Dual-Pressure 1200.0/70.3 (psia) Steam Generation

FROM REACTOR
 SUPERCRITICAL CO₂
 3.4905×10^7 g
 845 °F, 272.7 h

POINT A
 2.4547×10^6 g
 1200 p, 815 °F
 1389.03 h

LEGEND:

g - FLOW RATE, Lbm/Hr
 p - PRESSURE, Psia
 h - ENTHALPY, Btu/Lbm
 x - QUALITY OF STEAM
 s - STEAM
 w - WATER

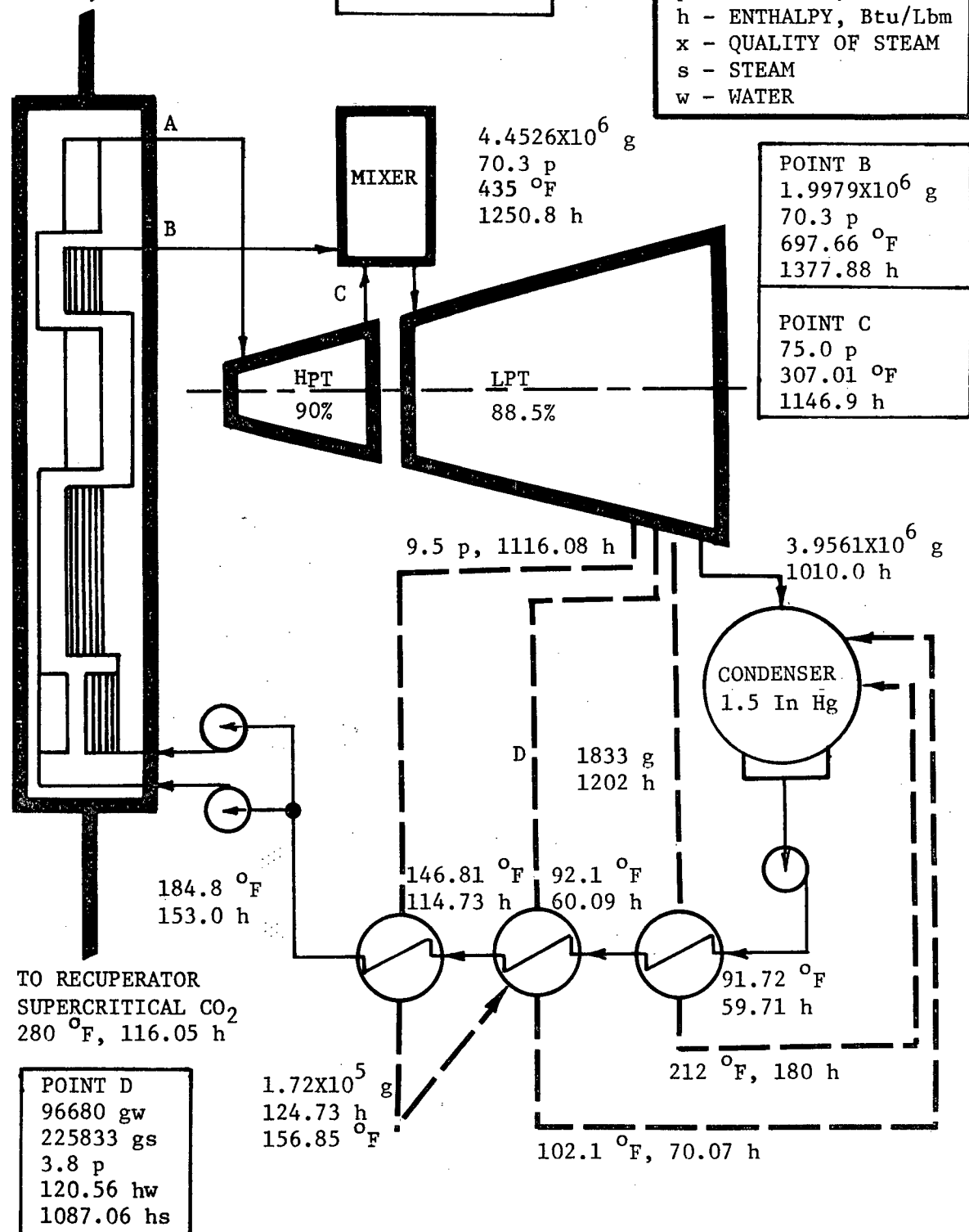


Figure 42. Turbine Circuit Heat Balance of Dual-Pressure 1200.0/70.3 (psia) Cycle

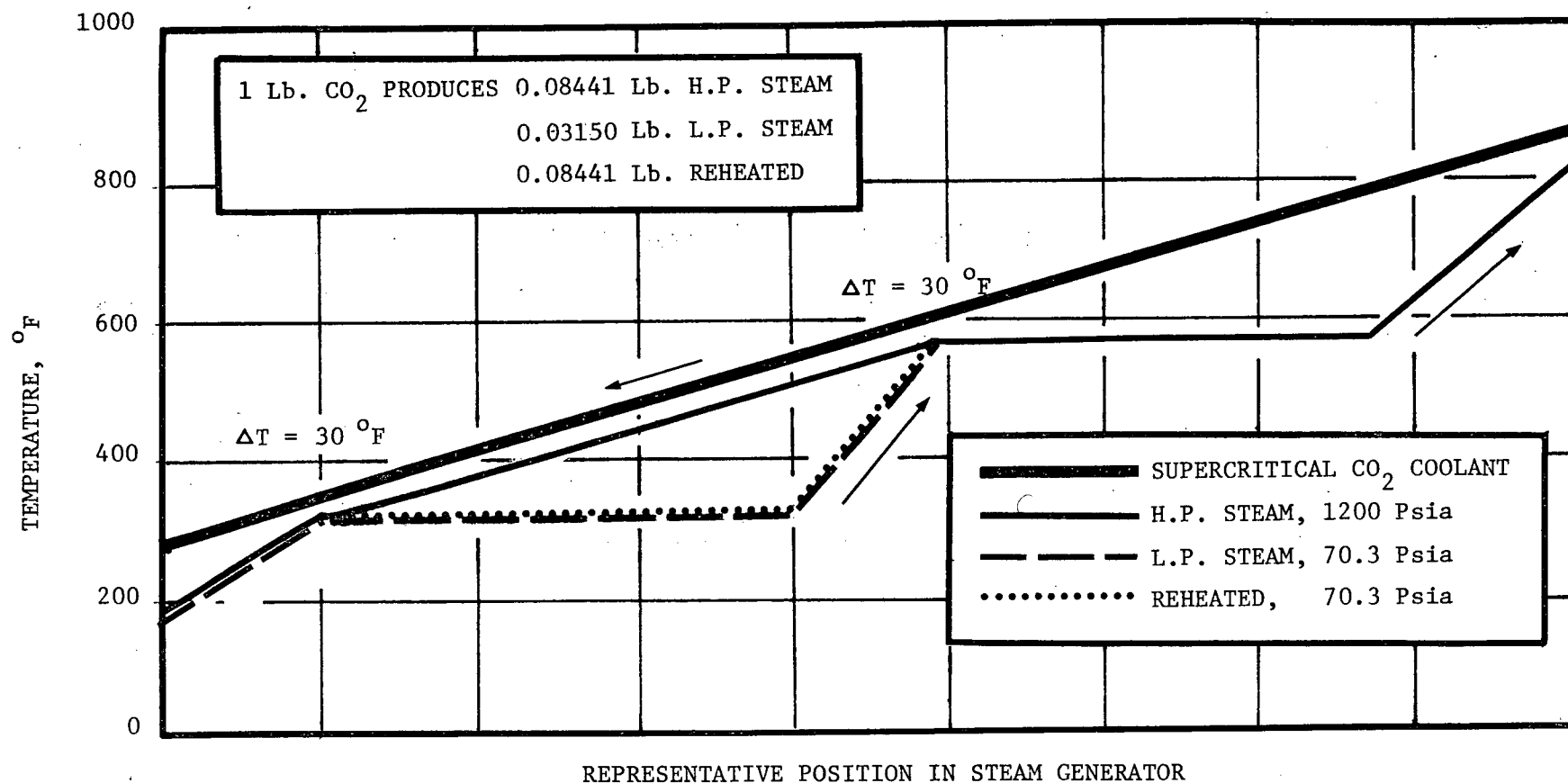


Figure 43. Dual-Reheat 1200.0/70.3 (psia) Steam Generation

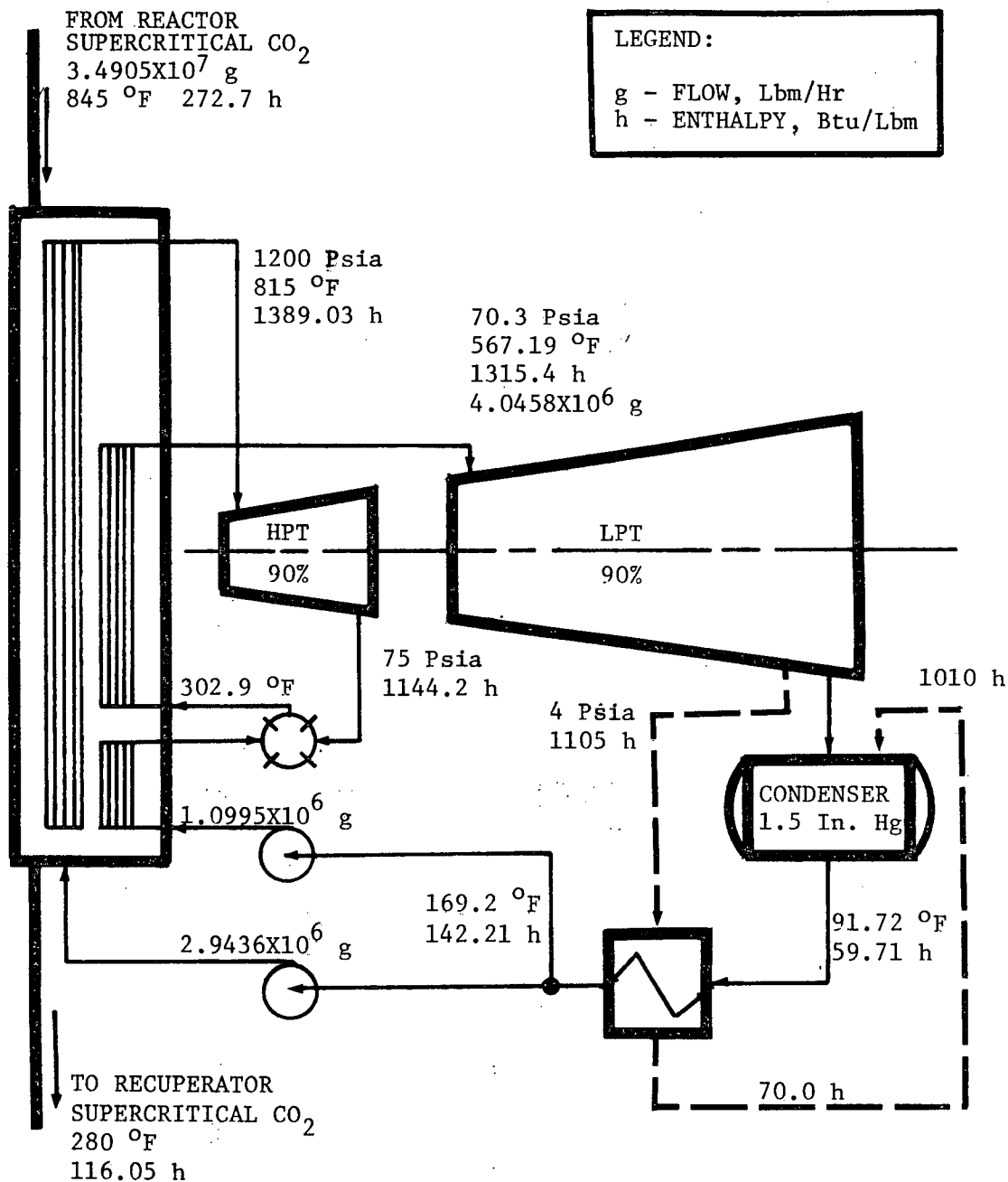


Figure 44. Turbine Circuit Heat Balance of Dual-Reheat 1200/70.3 (psia) Cycle

SUB-CHANNEL	NO. OF SUB-CHANNELS	FLOW AREA cm ²	TOTAL WET. PER. cm	UNHEATED WET. PER. cm	HEAT RATE Q, KW/M	POWER KW	MAX. TEMP. °C	FLOW RATE Kg/Sec	FINAL ENTHALPY KJ/Kg	ENTHALPY CHANGE KJ/Kg
1	1	0.8947	4.775		35.8	143.0	409.0	0.4651	545.8	298.3
2	4	0.8947	4.775		37.8	151.0	426.0	0.4638	563.7	316.2
3	4	0.8947	4.775		44.5	177.8	505.0	0.4238	650.5	403.0
4	4	0.8947	4.775		39.7	158.6	457.0	0.4394	598.2	350.7
5	12	0.6571	3.777	1.116	31.4	125.6	532.0	0.3018	651.7	404.2
6	8	0.8947	4.775		48.2	192.7	546.0	0.4178	695.3	411.8
7	4	1.3872	8.921	3.773	60.8	242.9	538.0	0.5839	651.7	404.2

ASSUMED HEAT INPUT DISTRIBUTION: $q = Q \cdot \sin(kx + \phi)$

WHERE $k = 0.51504$

$\phi = 0.02547$

$x = \text{DISTANCE}$

INLET CONDITION:

PRESSURE = 100 Bar = 1450 Psia

TEMPERATURE = 126.85 °C = 260 °F

ENTHALPY = 247.5 KJ/Kg = 110.26 Btu/Lbm

TOTAL COOLANT CHANNEL POWER: 6113 MW

TOTAL COOLANT CHANNEL MASS FLOW RATE: 15.091 Kg/Sec

OUTLET CONDITION:

PRESSURE = 85.5 Bar = 1240 Psia

TEMPERATURE = 457.8 °C = 855.6 °F

ENTHALPY = 640.9 KJ/Kg = 275.60 Btu/Lbm

Figure 45. Results of Heat Transfer to Supercritical CO₂ Coolant in 32-Element Fuel Bundles

CHARACTERISTICS \ COOLANT	HEAVY WATER	CARBON DIOXIDE
INLET PRESSURE (Psia)	1443	1450
OUTLET PRESSURE (Psia)	1254	1240
PRESSURE DROP (Psia)	189	210
MAXIMUM SHEATH TEMPERATURE (°C)	304	550
COOLANT INLET TEMPERATURE (°C)	249	127
COOLANT OUTLET TEMPERATURE (°C)	293	458
COOLANT TUBE INNER DIA. (In.)	4.070	4.458
FUEL ELEMENT DIA. (In.)	0.598	0.598
NO. OF FUEL ELEMENTS IN A BUNDLE	28	32
MAXIMUM CHANNEL POWER(MW)	5.125	6.113
MAXIMUM CHANNEL MASS FLOW RATE	22.2 Kg/Sec	15.1 Kg/Sec
POSSIBILITY OF DRYOUT	YES	NO
COOLANT COST	HIGH	LOW
FUEL USED	UO ₂	UO ₂ UC

Figure 46. Overall Performance of Supercritical Carbon Dioxide Coolant

	PICKERING	NEW DESIGN
COOLANT	HEAVY WATER	SUPERCRITICAL CO ₂
CORE LENGTH	19 Ft. 6 In.	19 Ft. 6 In.
MAXIMUM CHANNEL POWER	5.125 MW	6.113 MW
NO. OF FUEL RODS	28	32
O. D. OF SHEATH	0.598 In.	0.598 In.
O. D. OF FUEL BUNDLE	4.03 In.	4.358 In.
INTER-ELEMENT SPACING (MIN.)	0.05 In	0.496 In.
COOLANT TUBE X-SECTIONAL AREA	13.010 Sq. In.	15.605 Sq. In.
BLOCKER X-SECTIONAL AREA	NIL	1.622 Sq. In.
FUEL BUNDLE X-SECTIONAL AREA	7.864 Sq. In.	8.988 Sq. In.
COOLANT FLOW AREA	5.146 Sq. In.	4.995 Sq. In.
COOLANT TUBE I. D.	4.070 In.	4.457 In.

Figure 47. Overall Dimensions of 32-Element Fuel Bundle

	PICKERING	SINGLE PRES. CYCLE	DUAL PRESSURE CYCLE 600/70	DUAL PRESSURE CYCLE 1200/70	DUAL-REHEAT CYCLE 1200/70
TURBINE EFFICIENCY	H.P. 72.6% L.P. 88.5%	90.0%	H.P. 90.0% L.P. 88.5%	H.P. 90.0% L.P. 88.5%	H.P. 90.0% L.P. 90.0%
STEAM PRESSURE, Psia	H.P. 585 L.P. 70.3	130	H.P. 600 L.P. 70.3	H.P. 1200 L.P. 70.3	H.P. 1200 L.P. 70.3
MAXIMUM STEAM TEMPERATURE, °F	H.P. 483.5 L.P. 435.0	815.0	H.P. 815.0 L.P. 435.0	H.P. 815.0 L.P. 435.0	H.P. 815.0 L.P. 567.2
PRESSURE RATIO, H.P./L.P.	8.321		8.535	17.07	17.07
STEAM FLOW RATE Lbm/Hr	H.P. 5969862 L.P. 5550833	400600	H.P. 3036500 L.P. 4246800	H.P. 2454700 L.P. 4452600	H.P. 2946300 L.P. 4045800
STEAM FLOW RATE RATIO, H.P./L.P	1.075		0.7150	0.5513	0.7282
EXHAUST STEAM WETNESS	H.P. 11% L.P. 10%	5.4%	H.P. Super. L.P. 9%	H.P. 3.9% L.P. 9%	H.P. 3.9% L.P. 9%
EXHAUST STEAM PRESSURE, Psia	H.P. 70.3 Psia L.P. 1.5 In Hg	1.5 In Hg	H.P. 75.0 Psia L.P. 1.5 In Hg	H.P. 75.0 Psia L.P. 1.5 In Hg	H.P. 75.0 Psia L.P. 1.5 In Hg
TURBINE CYCLE EFFICIENCY	34.60%	27.6%	30.3%	30.7%	33.8%

Figure 48. Summary of Steam Conditions of Thermal Cycles

	PICKERING	SINGLE PRES. CYCLE	DUAL PRESSURE CYCLE 600/70.3	DUAL PRESSURE CYCLE 1200/70	DUAL-REHEAT CYCLE 1200/70
HEAT TRANSFERRED TO SECONDARY CIRCUIT, Btu/Hr	5.67×10^9	5.67×10^9	5.67×10^9	5.67×10^9	5.67×10^9
SHAFT WORK OUTPUT, Btu/Hr	1.9760×10^9	1.5640×10^9	1.7212×10^9	1.7504×10^9	1.9263×10^9
COOLANT FLOW RATE, Lbm/Hr	6.1300×10^7	3.4905×10^7	3.4905×10^7	3.4905×10^7	3.4905×10^7
PRIMARY PUMP WORK, Btu/ Hr	3.9365×10^7	4.3170×10^7	4.3170×10^7	4.3170×10^7	4.3170×10^7
FEED WATER FLOW RATE, Lbm/Hr	H.P. 5,969,862 DRAIN 489,525	4,006,600	H.P. 3,036,500 L.P. 1,210,300	H.P. 2,454,700 L.P. 1,997,900	H.P. 2,946,300 L.P. 1,099,500
SECONDARY PUMP WORK, Btu/Hr	1.2229×10^7	2.0030×10^6	6.7061×10^6	1.0443×10^7	1.0714×10^7
NET WORK OUTPUT, Btu/Hr	1.9224×10^9	1.5147×10^9	1.6672×10^9	1.6927×10^9	1.8724×10^9
IDEAL OVERALL EFFICIENCY	33.94%	26.73%	29.42%	29.87%	33.02%

Figure 49. Overall Performance of Thermal Cycles

MECHANICAL LOSSES 1347 KW
ELECTRICAL LOSSES 8162 KW
NET GENERATOR OUTPUT 543320 KW

LEGEND

g - Flow in lb/hr
a - Pressure in PSIA
f - Temperature in degrees F
h - Enthalpy btu/lb
x - Quality of steam in percent
lb/hr - Flow of steam
lb/rw - Flow of water
s - Enthalpy of steam - btu/lb

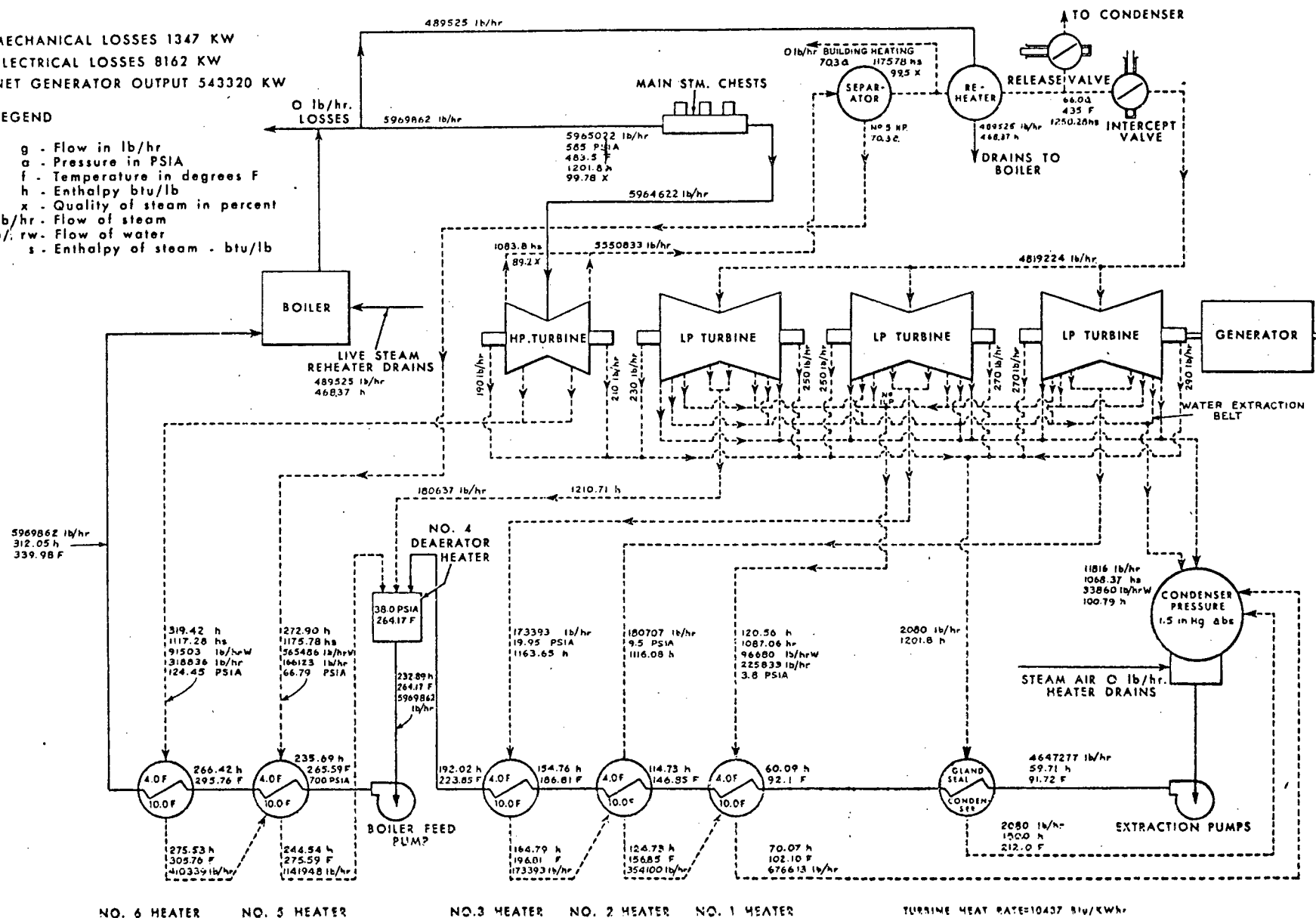


Figure 50. TURBO GENERATOR HEAT BALANCE (FROM [12])

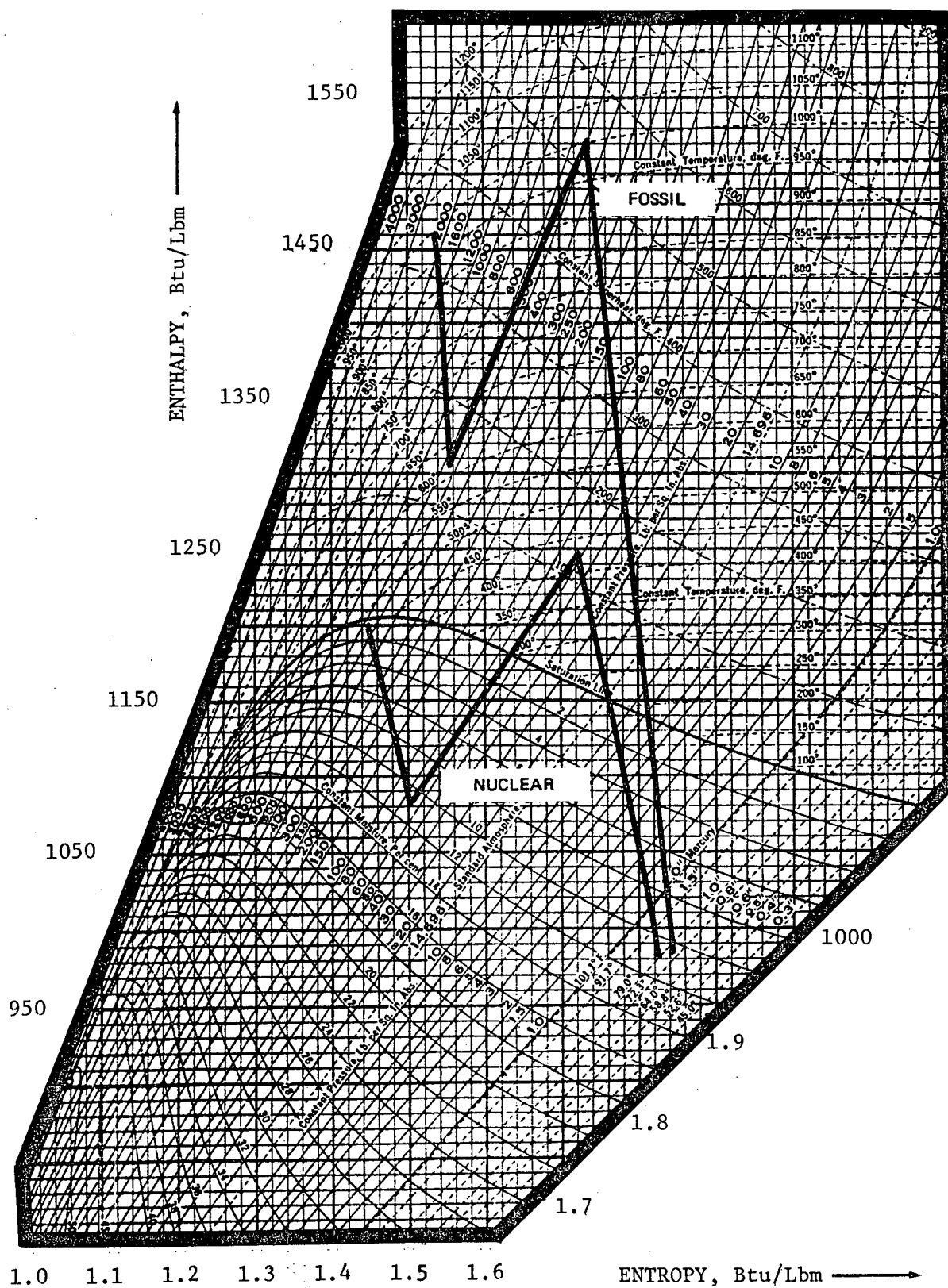


Figure 51. Expansion Line of CANDU reactor Turbine Stages (from [82])

REFERENCES

1. Mooradian, A.J.; "Nuclear Research and Development in Canada", Nuclear Engineering International, Survey of Canada, Pg. 13, June 1974.
2. McIntyre, H.C.; "Natural-Uranium Heavy-Water Reactors", Scientific American, Vol. 233, No. 4, Pg. 17, 1975.
3. El-Wakil, M.M.; NUCLEAR ENERGY CONVERSION, Intext Educational Publishers, Toronto, 1971.
4. Bate, D.L.S.; "Cost", AECL Nuclear Power Symposium, Lecture 16, 1971.
5. Eltham, B.E. and Bowen, J.H.; "Plant Survey", Chapter 3, THE DESIGN OF GAS-COOLED GRAPHITE-MODERATED REACTORS, Edited by Poulter, D.R., Oxford University Press, Toronto, 1963.
6. Wagman, D.D. et al.; "Heats, Free-Energies and Equilibrium Constants of Some Reactions Involving O₂, H₂, H₂O, C, CO, CO₂, and CH₄", J. Res. Nat. Bur. Stand., Vol. 34, Pg. 143, 1945.
7. Bridge, H. and Narin, J.S.; "Graphite", Chapter 7, THE DESIGN OF GAS-COOLED GRAPHITE-MODERATED REACTORS, Edited by Poulter, D.R., Oxford University Press, Toronto, 1963.
8. Harteck, I.P. and Dondes, S.; "Decomposition of Carbon Dioxide by Ionizine Radiation", J. Chem. Phys., Vol. 23, Pg. 902, 1955 and Vol. 26, Pg. 1727, 1957.
9. Hart, R.G.; "Technological Progress in Canadian Nuclear Fuels", Reactor Core Technology Branch, Whiteshell Nuclear Research Establishment, AECL, 1963.
10. Antill, J.E., Peakall, K.A., Crick, N., and Smart, E.E.; Unpublished work at A.E.R.E., Harewell, 1957, Reference of CHEMICAL ASPECTS OF NUCLEAR REACTORS, Vol. 1 by Dawson, J.K. and Soven, R.G., Butterworths, London, 1963.
11. Wyatt, L.M.; "The Fabrication of Uranium and Its Alloys", Proc. Nucl. Eng., Series 5, Vol. 1, Pg. 39, 1956.
12. Hydro Electric Power Commission of Ontario; "CANDU 500", Ontario Hydro, Toronto, 1969.
13. Page, R.D.; "Canadian Power Reactor Fuel", AECL Nuclear Power Symposium, Lecture 7, 1974.
14. Feher, E.G.; "The Supercritical Thermodynamic Power Cycle", ASME Advances in Energy Conversion Engineering, Pg. 37, 1967.
15. Strub, R.A. and Frieder, A.; "High Pressure Indirect CO₂ Closed-cycle Gas Turbines", BNES International Symposium on Nuclear Gas Turbines, London, Pg. 51, 1970.

16. Dekhtiarev, V.L.; "Construction of a High-capacity High-efficiency Carbon Dioxide Power Plant", Elekt. Stantsil, Vol. 33, No. 5, Pg. 2, 1962.
17. Keyfitz, I.M. et al.; "1000 MWe Supercritical Pressure Nuclear Reactor Power Plant", WACP-2222P, Westinghouse Electric Co., Pittsburgh, Pa., 1967.
18. Sastry, V.; "An Analytical Investigation of Forced Convection Heat Transfer in a Circular Duct at Supercritical and Near Critical Pressures", Ph.D. Thesis, Vanderbilt University, Engineers, Mechanical, 1974.
19. Maass, O.; "Changes in the Liquid State in the Critical Temperature Region", Chem. Rev., Vol. 23, No. 1, Pg. 17, 1938.
20. Schmidt, E., Eckert, E., and Grigull, U.; "Heat Transfer of Liquid Near the Critical State", AFF Translation No. 527, Headquarters Air Material Command, Wrightfield, Dayton, Ohio, February 21, 1946.
21. Schmidt, E.; "Warme Transport Durch Naturliche Konuektion in Stoppenbei Kristishchem 24 Stand", Int. J. Heat and Mass Transfer, Vol. 1, Pgs. 92-101, 1960.
22. Petukhov, B.S., Kransnosezhkov, E.A., and Protopopov, V.S.; "An Investigation of Heat Transfer to Fluids Flowing in Pipes Under Critical Conditions", International Development in Heat Transfer, International Heat Transfer Conference, Colorado, U.S.A., Paper 67, 1961.
23. Swenson, H.S., Cariver, J.R., and Kakarala, C.R.; "Heat Transfer to Supercritical Water in Smooth Bore Tubes", J. Heat Transfer, Vol. 87, No. 4, Pg. 447, 1965.
24. Goldman, K.; "Heat Transfer to Supercritical Water at 5000 PSI Flowing at High Mass Flow Rate Through Round Tubes", International Development in Heat Transfer, International Heat Transfer Conference, Colorado, U.S.A., Paper 66, 1961.
25. Koppel, L.B. and Smith, J.M.; "Turbulent Heat Transfer in Critical Region", International Developments in Heat Transfer, International Heat Transfer Conference, Colorado, U.S.A., Paper 69, 1961.
26. Powell, W.B.; "Heat Transfer to Fluids in the Region of Critical Temperature", Jet Propulsion, Vol. 27, No. 7, Pg. 776, 1957.
27. Shitman, M.E.; "Impairment of the Heat Transmission at Supercritical Pressures", High Temperature, Vol. 1, No. 2, Pg. 237, 1963.
28. Yamagata, K., Nishikawa, K., Hasegawa, S., and Fujii, T.; "Forced Convective Heat Transfer in the Critical Region", Japan Society of Mechanical Engineers, Semi-international Symposium, September, 1967.

29. Miller, W.S., Steader, J.D., and Trebes, P.M.; "Forced-convection Heat Transfer to Liquid Hydrogen at Supercritical Pressures", Bult. Inst. Intern. Froid, Annexe, No. 2, Pg. 173, 1965.
30. Petukhov, B.S.; "Heat Transfer in a Single-phase Medium Under Supercritical Conditions", Translated from Teplofizika Vysokikh Temperature, Vol. 9, No. 4, Pg. 732, 1968.
31. Abadzic, Z. and Goldstein, R.J.; "Film Boiling and Free Convection Heat Transfer to Carbon Dioxide Near the Critical State", Int. J. Heat Transfer, Vol. 13, Pg. 1163, 1970.
32. Tanaka, H., Nistwaki, N., Hrata, M., and Tsuge, A.; "Forced Convection Heat Transfer to Fluid Near Critical Point Flowing in Circular Tube", Int. J. Heat Mass Transfer, Vol. 14, Pg. 739, 1971.
33. Knapp, K.K. and Sabersky, R.H.; "Free Convection Heat Transfer to Carbon Dioxide Near the Critical Point", Int. J. Heat Mass Transfer, Vol. 9, No. 1, Pg. 41, 1966.
34. Hauptmann, E.G.; "An Experimental Investigation of Forced Convective Heat Transfer to a Fluid in the Region of its Critical Point", Ph.D. Thesis, California Institute of Technology, 1966.
35. Kafengaus, N.L.; "On Physical Nature of Heat Transfer at Supercritical Pressure with Pseudo-boiling", Heat Transfer - Soviet Research, Vol. 1, No. 1, Pg. 88, 1969.
36. Wood, R.D. and Smith, J.M.; "Heat Transfer in the Critical Region: Experimental Investigation of Radial Temperature and Velocity Profiles", Am. Inst. Engrs. J., Vol. 10, No. 2, Pg. 10, 1964.
37. Hsu, Y.Y.; "Discussion of an Investigation of Heat Transfer of Fluids Flowing in Pipes Under Supercritical Conditions", ASME, International Development in Heat Transfer, Pg. 1-180, 1963.
38. Deissler, R.G.; "Heat Transfer and Fluid Friction for Fully Developed Water with Variable Fluid Properties", ASME Trans., J. Heat Transfer, Vol. 76, No. 1, Pg. 73, 1954.
39. Goldmann, K.; "Heat Transfer to Supercritical Water and Other Fluids with Temperature-Dependent Properties", Chem. Eng. Progr. Symp., Series 3, Vol. 50, No. 11, 1954.
40. Malhotra, A. and Hauptmann, E.G.; "Heat Transfer to a Supercritical Fluid During Turbulent, Vertical Flow in a Circular Duct", International Center for Heat and Mass Transfer, Beograd, Yugoslavia, 1976.
41. Jackson, J.D. and Feloster, J.; "Enhancement of Turbulent Heat Transfer Due to Buoyancy for Downward Flow of water in Vertical Tubes", International Center for Heat and Mass Transfer, Deograd, Yugoslavia, 1976.

42. Schnurr, N.M.; "Heat Transfer to Carbon Dioxide in the Immediate Vicinity of the Critical Point", ASME Transactions, J. Heat Transfer, Vol. 9, Pg. 16, 1969.
43. Bringer, R.P. and Smith, J.M.; "Heat Transfer in the Critical Region", AICHE J., Vol. 3, No. 1, Pg. 41, 1957.
44. Sastry, V.S. and Schnurr, N.M.; "An Analytical Investigation of Forced Convection Heat Transfer to Fluids Near the Thermodynamic Critical Point", ASME Transactions, J. Heat Transfer, Vol. 97, No. 5, Pg. 226, 1975.
45. Miropolski, L. and Shitsman, M.E.; "Heat Transfer to Water and Steam at Variable Specific Heat in Near-Critical Region", Soviet Phy.-Tech. Phys., Vol. 2, No. 10, Pg. 2196, 1957.
46. Colburn, A.P.; "A Method of Correlating Forced Convection Heat Transfer Data", AICHE Journal, Vol. 29, Pg. 174, 1933.
47. Boure, P.J., Pulling, D.J., Gill, L.E., and Denton, W.H.; "Forced Convection Heat Transfer to Turbulent CO₂ in the Supercritical Region", Int. J. Heat Mass Transfer, Vol. 13, Pg. 1339, 1968.
48. Kutateladze, S.S. and Leontiev, A.I.; TURBULENT BOUNDARY LAYER IN COMPRESSIBLE GASES, Arnold, London, 1964.
49. Kranoshchekov, E.A. and Protopopov, V.S.; "Experimental Study of Heat Exchange in Carbon Dioxide in the Supercritical Range at High Temperature Drops", High Temperature, USSR, Vol. 4, Pg. 375, 1965.
50. Kranoshchekov, E.A. and Protopov, V.S.; "A Generalized Relationship for Calculation of Heat Transfer to Carbon Dioxide at Supercritical Pressure", High Temperature, U.S.S.R., Vol. 9, Pg. 125, 1971.
51. Petukhov, B.S. and Kirillov, V.V.; "On the Question of Heat Transfer to a Turbulent Flow of Fluids in Pipes", Teploenergetika, No. 4, Pg. 63, 1958.
52. Hiroharu, K., Niichi, H., and Masaru, H.; "Studies on the Heat Transfer of Fluid at a Supercritical Pressure", Bulletin of JSME, Pg. 654, 1967.
53. Shiralkar, B.S. and Griffith, P.; "Deterioration in Heat Transfer to Fluids at Supercritical Pressure and High Heat Fluxes", ASME Transactions, J. Heat Transfer, Vol. 91, No. 2, Pg. 27, 1969.
54. Dickinson, N.L. and Welch, O.P.; "Heat Transfer to Supercritical Water", ASME Transactions, J. Heat Transfer, Vol. 80, No. 4, Pg. 746, 1958.
55. Kranoshchekov, E.A., Protopopov, V.S., Parhovhik, I.A., and Silin, V.A.; "Some Results of an Experimental Investigation of Heat Transfer to Carbon Dioxide at Supercritical Pressure and Temperature Heads up to 850°C", High Temperature, USSR, Vol. 19, No. 5, Pg. 992, 1971.

56. Petukhov, B.S., Grigorev, V.S., and Polyakov, A.F.; "Experimental Investigation of Heat Transfer in Single-Phase Near-Critical Region with Heat Input Varying Along the Length of the Pipe", Toploenergetika, Vol. 20, No. 3, Pg. 71, 1973.
57. Glushchenko, L.F. and Gandzyuk, O.F.; "Temperature Conditions at the Wall of an Annular Channel with Internal Heating at Supercritical Pressure", High Temperature, USSR, Vol. 10, No. 4, Pg. 734, 1972.
58. Protopopov, V.S. and Igamberdyev, A.T.; "Results of an Experimental Investigation of Local Heat Transfer at Supercritical Pressure in a Rectangular Channel Heated From One Side", High Temperature, USSR, Vol. 10, No. 6, Pg. 116, 1972.
59. Kellogg, H.B. and Brown, G.B.; "Seventh Quarterly Progress Report for 1000 MWE Supercritical Pressure Nuclear Reactor Plant Study", WCAP-2525, October, 1963.
60. Jackson, J.D. and Evans-Lutterodt, K.; "Impairment of Turbulent Forced Convection Heat Transfer to Supercritical Pressure CO₂ Caused by Buoyancy Forces", Research Report N.E. 2, University of Manchester, Department of Nuclear Engineering in the Faculty of Science, March, 1968.
61. Tarasova, N.V. and Leontz, V.A.I.; "Hydraulic Resistance During Flow of Water in Heated Pipes at Supercritical Pressure", High Temperature, USSR, Vol. 6, No. 4, Pg. 721, 1968.
62. Kuraeva, I.V. and Protopopov, V.S.; "Mean Friction Coefficient for Turbulent Flow of Liquid at a Supercritical Pressure in Horizontal Circular Tubes", High Temperature, USSR, Vol. 12, No. 1, Pg. 194, 1974.
63. Sastry, V.; "Thermophysical Properties of CO₂ in the Near Critical Region".
64. Vargaftik, N.B.; TABLES ON THE THERMOPHYSICAL PROPERTIES OF LIQUIDS AND GASES, Second Edition, Hemisphere Publishing Corporation, Washington, London, 1974.
65. Altunin, V.V. and Sakhabetdinov, M.A.; "The Viscosity of Liquid and Gaseous Carbon Dioxide at Temperatures of 220 - 1300°K and Pressure up to 1200 Bar", Thermal Engineering, Vol. 19, No. 8, Pg. 124, 1972.
66. Altunin, V.V. and Sakhabetdinov, M.A.; "The Thermal Conductivity of Liquid and Gaseous Carbon Dioxide in the 220 - 1300°K Temperature Range at Pressure up to 1200 Bar", Thermal Engineering, Vol. 20, No. 5, Pg. 121, 1973.
67. Brown, G., Packman, G. and Greenough, G.B.; "Fuel Elements", J. Brit. Nucl. Energy Society, Vol. 2, No. 2, Pg. 186, 1963.
68. Sutherland, W.A.; "Experimental Heat Transfer in Rod Bundles", Heat Transfer in Rod Bundles, ASME, New York, 1968.

69. Maresca, M.W. and Dwyer, D.E.; "Heat Transfer to Mercury Flowing in Line Through a Bundle of Circular Rods", ASME Trans., J. Heat Transfer, Vol. 86, No. 3, Pg. 180, 1964.
70. Friedland, A.J., Dwyer, D.E., and Bonilla, C.F.; "Heat Transfer to Mercury in Parallel Flow Through Bundles of Circular Rods", International Development in Heat Transfer, International Heat Transfer Conference, Colorado, USA, Paper 62, 1961.
71. Oldaker, I.E.; "Sheath Temperature, a G-20 Computer Program for Fuel Bundles", AECL-2269, May, 1965.
72. Rogers, J.T. and Todreas, H.E.; "Coolant Interchannel Mixing in Reactor Fuel Rod Bundles Single Phase Coolants", Heat Transfer in Rod Bundles, ASME, New York, 1968.
73. Hoffman, H.W., Wentland, J.L., and Stelzman, W.J.; "Heat Transfer with Axial Flow in Rod Clusters", Int. Development in Heat Transfer, International Heat Transfer Conference, Colorado, USA, Paper 65, 1961.
74. Hoffman, H.J., Miller, C.W., Sozei, G.L., and Sutherland, W.A.; "Heat Transfer in Seven Rod Clusters - Influence of Linear and Spacer Geometry on Sheath Fuel Performance", GEAP-5289, General Electric Co., San Jose, California, October, 1966.
75. Midvioly, W.I.; "An Investigation Into the CHP Performance of Horizontal and Vertical 37-Element Assemblies Cooled by Freon", Proceedings of the 6th Western Canada Heat Transfer Conference, May, 1976.
76. Kidd, G.J., Jr., Stelzman, W.J., and Hoffman, H.W.; "The Temperature Structure and Heat Transfer Characteristics of an Electrically Heated Model of Seven Rod Cluster Fuel Element", Heat Transfer in Rod Bundles, ASME, New York, 1968.
77. Samuels, G.; "Design and Analysis of the Experimental Gas-Cooled Reactor Fuel Assemblies", Nuclear Science and Engineering, Vol. 14, Pg. 37, 1962.
78. Kays, W.M.; CONVECTIVE AND MASS TRANSFER, McGraw-Hill, New York, 1966.
79. Pon, G.A.; "Light Water-Cooled Heavy-Water-Moderated Natural-Uranium Power Reactor", The Ninth AECL Symposium on Atomic Power, Toronto, Ontario, AECL-1807, 1963.
80. Wooten, W.R.A., Taylor, A.J., and Worley, N.E.; "Steam Cycles for Gas-Cooled Reactors", Proc. Second United Nations, International Conf. on Peaceful Uses of Atomic Energy, Geneva, Vol. 7, Paper P/273UK, 1958.
81. Fraas, A.P. and Ozisik, M.N.; HEAT EXCHANGER DESIGN, John Wiley and Sons, Inc., New York, 1965.
82. Renshaw, R.H.; "Heat Transport", AECL Nuclear Power Symposium, Lecture 6, 1971.

83. Serdual, K.J. and Green, R.E.; "Lattice Measurements with 28-Elements Natural UO_2 Fuel Assemblies, Part II: Relative Total Neutron Densities and Hyperfine Activation Distributions in a Lattice Cell", AECL-2772 Chalk River, Ontario, August 1967.

APPENDIX I. Computing Procedure

The basic approach of the computer program for heat transfer to supercritical carbon dioxide is iteration. Figure 13 shows the routine for calculating a local wall temperature when a local fluid bulk temperature, pressure, heat flux, flow rate, and geometry are given. The supercritical flow is first assumed to have constant properties. The local heat transfer coefficient and wall temperature are calculated from a correlation for constant property flow, i.e. equation (11). Then, an assumed new value of the wall temperature is increased or decreased from the calculated value in an iterative manner, and the corresponding heat transfer coefficient is, therefore, calculated from the correlation for supercritical flow; i.e. equation (19). This iteration continues until the heat flux (evaluated from the given local conditions, assumed wall temperature, and corresponding heat transfer coefficient) is equal to the given heat flux. The final value of the assumed wall temperature is the result.

Thermophysical properties of carbon dioxide near the critical point in the calculation are taken from Sastry^[63]. Thermal properties of carbon dioxide in the above critical region are taken from the data of Vargaftik^[64], and physical properties are calculated from the formulas of Altunin et al.^[65,66].

Figure 14 shows the routine for calculating pressure drop from one increment to the next along a heated pipe. An assumed pressure drop is first calculated from the correlation of constant property flow; i.e. equation (23). Then, the assumed pressure of the second increment is calculated from $P_2 = P_1 - dP$. The fluid bulk enthalpy is calculated from

the given enthalpy and input heat rate of the first increment, i.e.

$h_{b2} = h_{b1} + dh$. Based on the assumed pressure and calculated enthalpy, other fluid properties and also the wall temperature of the second increment can be evaluated. Assuming linear temperature and pressure variations between increments, a new pressure drop is calculated from the correlation for supercritical flow, i.e. equation (22). Based on the new pressure drop and known enthalpy, the properties and wall temperature of the second increment are evaluated again for the calculation of another new pressure drop. These steps are repeated until the calculated pressure drop is converged.

The procedure based on the above routines is carried out from one increment to another until the fluid bulk temperatures, wall temperatures, and pressure drop along the entire pipe are calculated. The computer program is listed in this Appendix.

```

1  C ** MAIN PROGRAM **
2      REAL P(30), TM(30), T(30,100), MD(30,100), H(30,100), CP(30,100)
3      REAL VI(30,100), K(30,100)
4      REAL L(1000), TF(1000), TP(1000), PP(1000)
5      REAL MDR, MDW, MDRX, MDWX, MDBA, MDWA
6      REAL KB, KW, KBX, KWX, KBA, KWA, MFR
7      INTEGER INC
8      I=0
9      10  I=I+1
10     READ(8,81) P(I), TM(I)
11     81  FORMAT(F10.5, F9.2)
12     IF(TM(I) .EQ. 0.0) GO TO 20
13     DO 11 J=1, 100
14     READ(8,82) T(I,J), MD(I,J), H(I,J), CP(I,J)
15     82  FORMAT(F10.2, F14.3, F13.2, F12.2)
16     IF(T(I,J) .EQ. 0.0) GO TO 10
17     MD(I,J)=1000.0/MD(I,J)
18     11  CONTINUE
19     20  I=9
20     21  I=I+1
21     READ(7,91) P(I), TM(I)
22     91  FORMAT(F9.5, F10.2)
23     IF(TM(I) .EQ. 0.0) GO TO 30
24     DO 66 J=1, 100
25     READ(7,92) T(I,J), MD(I,J), H(I,J), CP(I,J), VI(I,J), K(I,J)
26     92  FORMAT(F10.2, F14.3, F13.2, F12.2, E16.4, E15.4)
27     IF(T(I,J) .EQ. 0.0) GO TO 21
28     MD(I,J)=1000.0/MD(I,J)
29     66  CONTINUE
30     READ(5,31) D, MFR, Q, PG, TB, BTU
31     31  FORMAT(F10.6, 5F10.1)
32     READ(5,83) INC, CONT
33     83  FORMAT(I10, F10.1)
34     IF(CONT .EQ. 0.0) GO TO 24
35     WRITE(6,26)
36     26  FORMAT('-', 'THIS CALCULATION IS AT CONSTANT PRESSURE')
37     24  IF(BTU .EQ. 0.0) GO TO 77
38     WRITE(6,36)
39     36  FORMAT('-', 'GIVEN DIAMETER, MASS FLOW RATE, HEAT FLUX, PRESSURE',
40     1  ' ', BULK-TEMPERATURE, '***** BRITISH UNITS ***** ')
41     WRITE(6,17) D, MFR, Q, PG, TB, BTU
42     D=D*0.0254
43     MFR=MFR*0.45359
44     Q=Q*0.003154
45     PG=PG*1.01325/14.7
46     TB=(TB+460.0)*5.0/9.0
47     77  MFR=MFR/3600.0
48     IF((PG .GE. 75.0) .AND. (PG .LE. 100.0)) GO TO 61
49     WRITE(6,62) PG
50     62  FORMAT('-', F10.2, '      INPUT PG IS OUT OF DATA RANGE')
51     GO TO 13
52     61  IF((TB .GE. 273.15) .AND. (TB .LE. 1500.0)) GO TO 40
53     WRITE(6,63) TB
54     63  FORMAT('-', F10.2, '      INPUT TB IS OUT OF DATA RANGE')
55     GO TO 13
56     40  N=10
57     IF((TB .GT. 400.0) .OR. (PG .GT. 82.70)) N=1
58     CALL PROP(PG,TB,TM,P,T,H,MD,VI,CP,K,TMC,HB,MCB,VIB,CPB,KB,N)

```

```

59      IF(N .NE. 1) GO TO 51
60      CALL VISC(PG, TB, MDB, VIB)
61      CALL COND(PG, TB, MDB, KB)
62      51 WRITE(6,32)
63      32 FORMAT('1', 'GIVEN DIAMETER, MASS FLOW RATE, HEAT FLUX, PRESSURE',
64      1    ', BULK-TEMPERATURE, ENTHALPY, NO. OF INCREMENTS')
65      WRITE(6,17) D, MFR, Q, PG, TB, HB, INC
66      17 FORMAT(' ', 6E17.4, '118)
67      HI=HB
68      DL=D
69      A=3.1415926*D*D/4.0
70      AL=3.1415926*D*DL
71      TL=FLOAT(INC)*DL
72      VM=MFR/A
73      G=9.81
74      DS=1.0
75      M=1
76      CALL HEAT(D, DL, M, Q, AH)
77      AHB=AH/MFR
78      CALL FIND(D,MFR,AH,PG,HB,TM,P,H,T,MD,VI,CP,K,TW,FAIL,DS,M)
79      IF(FAIL .NE. 0.0) GO TO 45
80      N=10
81      IF((TW .GT. 400.0) .OR. (PG .GT. 82.7))N=1
82      CALL PROP(PG,TW,TM,P,T,H,MD,VI,CP,K,TMW,HW,MDW,VIW,CPW,KW,N)
83      IF(N .NE. 1) GO TO 33
84      CALL VISC(PG,TW,MDW,VIW)
85      CALL COND(PG,TW,MDW,KW)
86      33 CONTINUE
87      L(M)=(FLOAT(M)-0.5)*DL*1000.0
88      TF(M)=TB
89      TP(M)=TW
90      PP(M)=PG
91      IF(M .GE. INC) GO TO 98
92      M=M+1
93      HBX=HB+AHB
94      IF((HBX .GE. -95.0) .AND. (HBX .LE. 1600.0)) GO TO 18
95      WRITE(6,19) HBX
96      19 FORMAT('1', F10.2, ' HBX IS OUT OF DATA RANGE')
97      GO TO 45
98      18 CONTINUE
99      CALL HEAT(D, DL, M, Q, AHX)
100     AHBX=AHX/MFR
101     IF(CONT .EQ. 0.0) GO TO 27
102     PX=PG
103     PF=PG
104     GO TO 15
105     27 RE=VM*D/VIB
106     E=1.0/((1.82*ALOG10(RE)-1.64)**2)
107     IF(RE .GT. 100000.0) E=0.01796894
108     EV=E*((VIW/VIR)**0.22)
109     PD=EV*(VM**2)*DL*2.0/(*MDR*D)
110     PD=PD*0.00001
111     PX=PG-PD
112     TEST=0.0
113     NM=0
114     44 NM=NM+1
115     IF(NM .LE. 25) GO TO 54
116     WRITE(6,55) M

```



```

117 55 FORMAT(' ', '***** ITERATION OF PRESSURE DROP DOES NOT COVERGE *****')
118 GO TO 45
119 54 CONTINUE
120 IF((PX .GE. 75.0) .AND. (PX .LE. 100.0)) GO TO 15
121 WRITE(6,16) PX
122 16 FORMAT(' ', F10.2, ' PX IS OUT OF DATA RANGE')
123 GO TO 45
124 15 N=10
125 IF((HBX .GT. 285.0) .OR. (PX .GT. 82.7)) N=1
126 CALL PROP(PX, HBX, TM, P, H, T, MD, VI, CP, K, TMC, TRX, MCBX, VIBX, CPBX, KBX, N)
127 IF(N .NE. 1) GO TO 46
128 CALL VISC(PX, TBX, MCBX, VIBX)
129 CALL COND(PX, TBX, MCBX, KBX)
130 46 CALL FIND(D, MFR, AHX, PX, HBX, TM, P, H, T, MD, VI, CP, K, TWX, FAIL, DS, M)
131 IF(FAIL .NE. 0.0) GO TO 45
132 IF(CONT .NE. 0.0) GO TO 88
133 N=10
134 IF((TWX .GT. 400.0) .OR. (PX .GT. 82.70)) N=1
135 CALL PROP(PX, TWX, TM, P, T, H, MD, VI, CP, K, TMC, HWX, MDWX, VIWX, CPWX, KWX, N)
136 IF(N .NE. 1) GO TO 49
137 CALL VISC(PX, TWX, MDWX, VIWX)
138 CALL COND(PX, TWX, MDWX, KWX)
139 49 TRA=(TR+TBX)/2.0
140 TWA=(TW+TWX)/2.0
141 PA=(PG+PX)/2.0
142 N=10
143 IF((TBA .GT. 400.0) .OR. (PA .GT. 82.70)) N=1
144 CALL PROP(PA, TRA, TM, P, T, H, MD, VI, CP, K, TMC, HBA, MDBA, VIBA, CPBA, KBA, N)
145 IF(N .NE. 1) GO TO 65
146 CALL VISC(PA, TRA, MDBA, VIBA)
147 CALL COND(PA, TRA, MDBA, KBA)
148 65 CONTINUE
149 N=10
150 IF((TWA .GT. 400.0) .OR. (PA .GT. 82.70)) N=1
151 CALL PROP(PA, TWA, TM, P, T, H, MD, VI, CP, K, TMC, HWA, MDWA, VIWA, CPWA, KWA, N)
152 IF(N .NE. 1) GO TO 67
153 CALL VISC(PA, TWA, MDWA, VIWA)
154 CALL COND(PA, TWA, MDWA, KWA)
155 67 REA=VM*D/VIB
156 PAR=(1.0-MDWA/MDBA)*G*D*(MDRA**2)/(VM**2)
157 IF(PAR .GT. 0.0005) GO TO 72
158 FACTOR=1.0
159 GO TO 75
160 72 IF((PAR .GT. 0.0005) .AND. (PAR .LE. 0.3)) GO TO 73
161 WRITE(6,74) PAR
162 74 FORMAT(' ', F10.6, ' PAR IS TOO LARGE')
163 GO TO 45
164 73 FACTOR=2.15*(PAR**0.1)
165 75 EA=1.0/((1.82*ALOG10(REA)-1.64)**2)
166 EF=EA*((VIWA/VIBA)**0.22)
167 EF=EF*FACTOR
168 PDN=(VM**2)*((EF*DL/(2.0*MDBA*D)))+(MCB-MDBX)/(MDB*MDBX)
169 PDN=PDN*0.00001
170 PF=PG-PDN
171 CHECK=PX-PF
172 IF((TEST .GE. 0.0) .AND. (CHECK .GE. 0.0)) GO TO 53
173 WRITE(6,97) PG, PX, PA, PF, CHECK, TEST
174 97 FORMAT(' ', 'PGXPAPF', 4F10.4, 'CHECK, TEST', 2F15.6)

```

```

175      IF(ABS(CHECK) .LE. 0.1) GO TO 88
176      IF(ABS(TEST) .LE. 0.1) GO TO 88
177      PX=PG-(TEST+CHECK)
178      TEST=CHECK
179      GO TO 44
180 53     TEST=CHECK
181      DIF=ABS(PX-PF)
182      IF(DIF .LT. 0.001) GO TO 88
183      PX=PF
184      GO TO 44
185 88     PG=(PX+PF)/2.0
186      TB=TBX
187      TW=TWX
188      HB=HBX
189      VIB=VIBX
190      GO TO 33
191 98     WRITE(6,22)
192 22     FORMAT(' ', '***RESULT***----- J, L(J), TF(J), TP(J), PP(J)')
193      IF(RTU .EQ. 0.0) GO TO 78
194      WRITE(6,93)
195 93     FORMAT(' ', 'RESULTS ARE IN BRITISH UNITS')
196 78     DO 34 J=1, M
197      IF(RTU .EQ. 0.0) GO TO 79
198      L(J)=L(J)/25.4
199      TF(J)=TF(J)*9.0/5.0-460.0
200      TP(J)=TP(J)*9.0/5.0-460.0
201      PP(J)=PP(J)*14.7/1.01325
202      GO TO 39
203 79     TF(J)=TF(J)-273.15
204      TP(J)=TP(J)-273.15
205      WRITE(6,14) J, L(J), TF(J), TP(J), PP(J)
206 14     FORMAT(' ', I10, F12.2, ' ', '*****', 2F10.2, ' ', '*****', F15.2)
207 34     CONTINUE
208      ENTH=HB-HI
209      WATT=ENTH*MFR
210      WRITE(6,35) ENTH
211 35     FORMAT(' ', 'ENTHALPY CHANGE (KJ/KG)', F20.2)
212      WRITE(6,37) WATT
213 37     FORMAT(' ', 'HEAT INPUT RATE (KJ/SEC)', F20.2)
214      TP(1)=TF(1)
215      CALL SCALE(L, M, 12.0, LMIN, DL, 1)
216      CALL SCALE(TP, M, 10.0, TPMIN, DTP, 1)
217      DO 99 I=1, M
218      TF(I)=(TF(I)-TPMIN)/DTP
219 99     CONTINUE
220      CALL AXIS(0.0, 0.0, 6*HLENGTH, -6, 12.0, 0.0, LMIN, DL)
221      CALL AXIS(0.0, 0.0, 11*HTEMPERATURE, 11, 10.0, 90.0, TPMIN, DTP)
222      CALL LINE(L, TP, M, 1)
223      CALL LINE(L, TF, M, 1)
224      CALL PLOTND
225      GO TO 13
226 45     M=M-1
227      IF(M .GT. 0) GO TO 98
228      WRITE(6,25)
229 25     FORMAT(' ', 'INPUT CONDITION IS OUT OF RANGE.')
230 13     WRITE(6,23)
231 23     FORMAT('1', ' ')
232      STOP
233      END

```

```

1  C ** SUBROUTINE FOR CALCULATING LOCAL WALL TEMPERATURE **
2  SUBROUTINE FIND(D,MFR,AH,PG,HB,TM,P,H,T,MD,VI,CP,K,TW,FAIL,DS,M)
3  REAL P(30), TM(30), MD(30,100), H(30,100), CP(30,100)
4  REAL T(30,100), VI(30,100), K(30,100)
5  REAL MFR, MDB, MDW, KB, KW
6  REAL RE, PR, NUO, NUL
7  LOGICAL TRY1, TRY2, TRY3, TRY4, TRY5, TRY6
8  IF(AH .GE. 0.0) GO TO 77
9  WRITE(6,79)
10 79  FORMAT('-', '****THIS SUBROUTINE FOR THE CALCULATION OF THE',
11 1  ' HEATING PROCESS ONLY****')
12  GO TO 13
13 77  FAIL=0.0
14  DL=D
15  A=3.1415926*D*D/4.0
16  AL=3.1415926*D*DL
17  IF((PG .LE. 100.0) .AND. (PG .GE. 75.0)) GO TO 74
18  WRITE(6,34) PG
19 34  FORMAT('-', F10.3, ' PG IS OUT OF DATA RANGE.')
20  GO TO 13
21 74  IF((HB .LE. 1600.0) .AND. (HB .GE. -95.0)) GO TO 75
22  WRITE(6,36) HB
23 36  FORMAT('-', F10.3, ' HB IS OUT OF DATA RANGE.')
24  GO TO 13
25 75  N=10
26  IF((HB .GT. 285.0) .OR. (PG .GT. 82.70)) N=1
27  CALL PROP(PG,HB,TM,P,H,T,MD,VI,CP,K,TMB,TB,MDB,VIB,CPB,KB,N)
28  IF(N .EQ. 10) GO TO 66
29  CALL VISC(PG, TB, MDB, VIB)
30  CALL COND(PG, TB, MDB, KB)
31 66  RE=4.0*MFR/(3.1415926*D*VIB)
32  IF(RE .GT. 50000.0) GO TO 63
33  WRITE(6,51) RE
34 51  FORMAT('-', F10.0, ' RE IS OUT OF OPERATION RANGE')
35  GO TO 13
36 63  PR=CPB*VIB/KB
37  TRY1=.FALSE.
38  TRY2=.FALSE.
39  TRY3=.FALSE.
40  TRY4=.FALSE.
41  TRY5=.FALSE.
42  TRY6=.FALSE.
43  FF=(1.0/8.0)/(((1.82*ALOG10(RE)-1.64)**2)
44  NUO=FF*RE*PR/((12.7*SQRT(FF)*(PR**(2.0/3.0)-1.0)+1.07)
45  X=DL*(FLOAT(M)-0.5)
46  FACTOR=0.95+0.95*((D/X)**0.8)
47  COO=FACTOR*NUO*KB/D
48  TW=TB+AH/(COO*AL*DS)
49 73  IF((TW-TB) .LE. 0.0) TW=TB+0.5
50  IF((TW .LE. 1500.0) .AND. (TW .GE. 275.0)) GO TO 78
51  WRITE(6,38) TW
52 38  FORMAT('-', F10.3, ' TW IS OUT OF DATA RANGE')
53  GO TO 13
54 78  N=10
55  IF((TW .GT. 400.0) .OR. (PG .GT. 82.70)) N=1
56  CALL PROP(PG,TW,TM,P,T,H,MD,VI,CP,K,TMW,HW,MDW,VIW,CPW,KW,N)
57  IF(N .NE. 1) GO TO 88
58  CALL VISC(PG, TW, MDW, VIW)

```

```

59      CALL COND(PG, TW, MDW, KW)
60      88 RTB=TB/TMB
61      RTW=TW/TMW
62      PN=0.0
63      IF(RTB .GE. 1.2) GO TO 59
64      IF(RTW .LE. 1.0) GO TO 59
65      IF((PR .GE. 0.85) .AND. (PR .LE. 65.0)) GO TO 61
66      WRITE(6,53) PR
67      53 FORMAT(' ', F10.2, '      PR IS OUT OF OPERATION RANGE')
68      GO TO 13
69      61 IF((RTB .GT. 0.09) .AND. (RTB .LT. 1.2)) .AND.
70      1 ((RTW .GT. 0.09) .AND. (RTW .LT. 4.0)) GO TO 59
71      WRITE(6,58) RTB, RTW
72      58 FORMAT(' ', 2F10.1, '      RTB OR RTW IS OUT OPERATIONAL RANGE.')
73      GO TO 13
74      59 IF((RTW .GT. 1.0) .AND. (RTW .LE. 4.0)) PN=0.22+0.18*RTW
75      IF((RTB .GE. 1.0) .AND. (RTB .LE. 1.2)) PN=PN+(5.0*PN-2.0)*(1-RTB)
76      IF((RTB .GE. 1.2) .OR. (RTW .LE. 1.0)) PN=0.4
77      IF(PN .NE. 0.0) GO TO 57
78      WRITE(6,56) PN
79      56 FORMAT(' ', 'PN IS NOT SPECIFIED', F10.4)
80      GO TO 13
81      57 CONTINUE
82      CPA=(HW-HB)/(TW-TB)
83      RCP=CPA/CPB
84      IF((RCP .GE. 0.02) .AND. (RCP .LE. 4.0)) GO TO 41
85      WRITE(6,20) RCP
86      20 FORMAT(' ', F10.2, '      RCP IS OUT OF OPERATION RANGE')
87      GO TO 13
88      41 RMD=MDW/MDB
89      IF(RMD .GT. 0.00) GO TO 43
90      WRITE(6,22) RMD
91      22 FORMAT(' ', F10.2, '      RMD IS SMALLER THAN 0.09.')
92      GO TO 13
93      43 EP=(RMD*.3)*(RCP*PN)
94      HA=COO*ER*AL*(TW-TB)
95      DE=ABS(HA-AH)/AH
96      IF(DE .LT. 0.00005) GO TO 99
97      IF(TRY5 .OR. TRY6) GO TO 93
98      IF(TRY3 .OR. TRY4) GO TO 92
99      IF((HA-AH) .GT. 0.0) GO TO 81
100     TRY1=.TRUE.
101     IF(TRY2) GO TO 92
102     TW=TW+10.0
103     GO TO 82
104     81 TRY2=.TRUE.
105     IF(TRY1) GO TO 92
106     TW=TW-10.0
107     82 IF(.NOT. TRY1 .OR. .NOT. TRY2) GO TO 73
108     92 IF((HA-AH) .GT. 0.0) GO TO 83
109     TRY3=.TRUE.
110     IF(TRY4) GO TO 93
111     TW=TW+5.0
112     GO TO 84
113     83 TRY4=.TRUE.
114     IF(TRY3) GO TO 93
115     TW=TW-5.0
116     84 IF(.NOT. TRY3 .OR. .NOT. TRY4) GO TO 73

```

```
117      93  IF((HA-AH) .GT. 0.0) GO TO 85
118          TW=TW+1.0
119          TRY5=.TRUE.
120          GO TO 86
121      85  TW=TW-1.0
122          TRY6=.TRUE.
123      86  IF(.NOT. TRY5 .OR. .NOT. TRY6) GO TO 73
124          GO TO 99
125      13  FAIL=13.0
126          ER=1.0
127      99  DS=ER
128          RETURN
129          END
```

```

1  C ** SUBROUTINE FOR INTERPOLATING THERMOPHYSICAL PROPERTIES FROM THE TABLE *
2  C ** THE SUBROUTINE SAINT USED HERE IS AVAILABLE IN THE UBC COMPUTER LIBRARY
3      SUBROUTINE PROP(PG,HG,TM,P,H,T,MD,VI,CP,K,TMC,TC,MDC,VIC,CPC,KC,N)
4      REAL P(30), H(30,100), T(30,100), TM(30)
5      REAL MD(30,100), VI(30,100), CP(30,100), K(30,100)
6      REAL X(60), Y(60), Q(13)
7      REAL TI, MDI, VII, CPI, KI
8      REAL TF, MDF, VIF, CPF, KF
9      REAL TC, MDC, VIC, CPC, KC, TMC
10     M=4
11     IF(N .EQ. 10) M=2
12     NN=35
13     IF(N .NE. 10) NN=58
14     DO 33 I=N, 30
15     CP=PG-P(I)
16     IF(OP .EQ. 0.0) TMC=TM(I)
17     IF(OP .LT. 0.0) TMC=((PG-P(I-1))/(P(I)-P(I-1)))*(TM(I)-TM(I-1))+
18     1 TM(I-1))
19     IF(OP .LE. 0.0) GO TO 22
20 33 CONTINUE
21 22 DO 10 J=1, NN
22     X(J)=H(I,J)
23     Y(J)=T(I,J)
24 10 CONTINUE
25     TF=SAINT(MN, X, Y, HG, M, Q)
26     DO 20 J=1, NN
27     Y(J)=MD(I,J)
28 20 CONTINUE
29     MDF=SAINT(NN, X, Y, HG, M, Q)
30     DO 30 J=1, NN
31     Y(J)=CP(I,J)
32 30 CONTINUE
33     CPF=SAINT(NN, X, Y, HG, M, Q)
34     IF(OP .NE. 0.0) GO TO 81
35     TC=TF
36     MDC=MDF
37     CPC=CPF
38     IF(N .NE. 10) GO TO 88
39 81 IF(N .NE. 10) GO TO 99
40     DO 40 J=1, NN
41     Y(J)=VI(I,J)
42 40 CONTINUE
43     VIF=SAINT(NN, X, Y, HG, M, Q)
44     DO 50 J=1, NN
45     Y(J)=K(I,J)
46 50 CONTINUE
47     KF=SAINT(NN, X, Y, HG, M, Q)
48     IF(OP .NE. 0.0) GO TO 99
49     VIC=VIF
50     KC=KF
51     GO TO 73
52 99 DO 15 J=1, NN
53     X(J)=H((I-1),J)
54     Y(J)=T((I-1),J)
55 15 CONTINUE
56     TI=SAINT(NN, X, Y, HG, M, Q)
57     DO 25 J=1, NN
58     Y(J)=MD((I-1),J)

```

```

59      25 CONTINUE
60      MDI=SAINT(NN, X, Y, HG, M, Q)
61      DO 35 J=1, NN
62      Y(J)=CPI((I-1),J)
63      35 CONTINUE
64      CPI=SAINT(NN, X, Y, HG, M, Q)
65      IF(N.NE. 10) GO TO 66
66      DO 45 J=1, NN
67      Y(J)=VI((I-1),J)
68      45 CONTINUE
69      VII=SAINT(NN, X, Y, HG, M, Q)
70      DO 55 J=1, NN
71      Y(J)=K((I-1),J)
72      55 CONTINUE
73      KI=SAINT(NN, X, Y, HG, M, Q)
74      66 FACTOR=(PG-P(I-1))/(P(I)-P(I-1))
75      TC=FACTOR*(TF-TI)+TI
76      MDC=FACTOR*(MCF-MCI)+MDI
77      CPC=FACTOR*(CPF-CPI)+CPI
78      IF(N.NE. 10) GO TO 88
79      VIC=FACTOR*(VIF-VII)+VII
80      KC=FACTOR*(KF-KI)+KI
81      GO TO 73
82      88 VIC=0.0
83      KC=0.0
84      73 RETURN
85      END

```

```

1  C ** SUBROUTINE FOR CALCULATING VISCOSITY **
2      SUBROUTINE VISC(PG, TG, DG, U)
3          REAL A(5,5)
4          A(1,1)=0.24856612
5          A(1,2)=0.004894942
6          A(2,1)=-0.3733066
7          A(2,2)=1.22753488
8          A(3,1)=0.363854523
9          A(3,2)=-0.774229021
10         A(4,1)=-0.0639070755
11         A(4,2)=0.142507049
12         TC=TG/304.2
13         DC=DG/468.0
14         UT=(SQRT(TC))*(1.0E-8)*(2722.46461-1663.46068*(1.0/TC)+
15         1  466.920556*(1.0/(TC*TC)))
16         X=0.0
17         DO 71 M=1, 4
18             DO 71 N=1, 2
19                 X=X+A(M,N)*(DC**M)/(TC**(FLOAT(N-1)))
20         71 CONTINUE
21         Y=EXP(X)
22         U=Y*UT
23         RETURN
24         END

```



```

1  C ** SUBROUTINE FOR CALCUALTING THERMAL CONDUCTIVITY **
2  SUBROUTINE COND(PG, TG, DG, K)
3  REAL A(5,5)
4  REAL K
5  A(1,1)=1.18763738
6  A(1,2)=-2.73693975
7  A(1,3)=2.52042816
8  A(2,1)=-2.30778414
9  A(2,2)=4.41994872
10 A(2,3)=-0.0915667463
11 A(3,1)=2.61294395
12 A(3,2)=-4.00329344
13 A(3,3)=-1.35345324
14 A(4,1)=-1.2832559
15 A(4,2)=2.13659771
16 A(4,3)=0.376570783
17 A(5,1)=0.219542368
18 A(5,2)=-0.402133782
19 A(5,3)=0.000
20 TC=TG/304.2
21 DC=DG/468.0
22 EXK=(1.0E-6)*(57.2860124-78.1435192*(1.0/TC)+
23 1 49.1871184*(1.0/(TC*TC))-11.5094347*(1.0/(TC**3.0)))*SQRT(TC)
24 X=0.0
25 DO 71 M=1, 5
26 DO 71 N=1, 3
27 X=X+A(M,N)*(DC**M)/(TC**(FLOAT(N-1)))
28 71 CONTINUE
29 Y=EXP(X)
30 K=Y*EXK
31 RETURN
32 END

```

APPENDIX II. Typical Calculation of Ideal Overall Efficiency

1. Ideal Overall Efficiency of Dual-reheat CycleData required for calculation:

Water 1200 psia

Temperature, °F	Enthalpy, Btu/lbm
815	1389.03
567.19 (saturation)	571.85 (liquid)
245	215.00
140.6	110.59

Water 70.3 psia

Temperature, °F	Enthalpy, Btu/lbm
567.19	1315.4
302.93 (saturation)	272.74 (liquid)
245	215.00
140.6	110.59

Carbon Dioxide 85.5 Bar

Temperature, °F	Enthalpy, Btu/lbm
845	272.70
597.19	203.72
333.0	131.18
280.0	116.05
260.0	110.26

a) Steam Generation (steam produced by 1.0 lbm carbon dioxide)

All carbon dioxide in temperature range of 597.19°F to 845°F is required for producing H.P. steam (see steam generation process path as shown in Figure 43). Therefore, the enthalpy balance is

$$(1.0)(272.7 - 203.72) = x (1389.03 - 571.85) ,$$

$$x = 0.08441 \text{ bm H.P. steam .}$$

If H.P. steam were expanded isotropically from 1200 psia to 75.0 psia, the ideal final state enthalpy is 1117 Btu/lbm (from Steam Enthalpy

Versus Entropy diagram). Therefore, for a turbine efficiency of 90.0%, the actual final state enthalpy is

$$\begin{aligned} h_f &= 1389.03 - (0.9)(1389.03 - 1117) \\ &= 1144.2 \text{ Btu/lbm} . \end{aligned}$$

Enthalpy balance for heating H.P. and L.P. steam from 302.93°F to 567.19°F by carbon dioxide is

$$\begin{aligned} (203.72 - 131.18) &= 0.08441[(571.85 - 272.74) \\ &\quad + (1315.4 - 1144.2)] \\ &\quad + y(1315.4 - 272.74) , \\ y &= 0.0315 \text{ lbm L.P. steam.} \end{aligned}$$

Enthalpy of feed water which is heated by 280°F to 333°F carbon dioxide is calculated from

$$\begin{aligned} (131.18 - 116.05) &= 0.08441(272.74 - h_i) + 0.03150(272.74 - h_i) , \\ h_i &= 142.21 \text{ Btu/lbm for feed water.} \end{aligned}$$

Heat transferred to coolant loop^[12] is given by

$$1661.30 \times 10^6 \text{ watt} = 5.67 \times 10^9 \text{ Btu/hr} .$$

Therefore, mass flow rate of supercritical carbon dioxide coolant is

$$\begin{aligned} M_{\text{CO}_2} &= 5.67 \times 10^9 / (272.7 - 110.26) \\ &= 3.4905 \times 10^7 \text{ lbm/Hr.} \end{aligned}$$

H.P. steam flow rate is

$$\begin{aligned}
 M_{HP} &= 0.08441 M_{CO_2} \\
 &= 2.9463 \times 10^6 \text{ lbm/Hr.}
 \end{aligned}$$

L.P. steam flow rate is

$$\begin{aligned}
 M_{LP} &= 0.03150 M_{CO_2} \\
 &= 1.0995 \times 10^6 \text{ lbm/Hr.}
 \end{aligned}$$

Total L.P. steam flow rate which includes reheated steam is

$$\begin{aligned}
 M_{LPT} &= 2.9463 \times 10^6 + 1.0995 \times 10^6 \\
 &= 4.0458 \times 10^6 \text{ lbm/Hr.}
 \end{aligned}$$

Recuperation enthalpy balance (see Figure 44) is

$$\begin{aligned}
 (1.0995 \times 10^6 + 2.9643 \times 10^6)(142.21 - 59.71) &= M_R(1105 - 70.0) \quad , \\
 M_R &= 322500 \text{ lbm/Hr recuperating steam.}
 \end{aligned}$$

b) Ideal Overall Efficiency (calculation based on Figure)

From the flow rates at the inlets and outlets of the turbines, and their corresponding enthalpies, shaft work output can be calculated as

$$\begin{aligned}
 W_{SHAFT} &= \sum (h \cdot M)_{INLET} - \sum (h \cdot M)_{OUTLET} \\
 &= 2.9463 \times 10^6(1389.03 - 1144.2) \\
 &\quad + 4.0458 \times 10^6(1315.4 - 322500(1105) \\
 &\quad - (4.0458 \times 10^6 - 322500)(1010.0) \\
 &= 1.9263 \times 10^9 \text{ Btu/Hr.}
 \end{aligned}$$

For 100% pump efficiency, pump work for feed water circulation is

$$\begin{aligned}
W_f &= \Delta P \cdot M/\rho \\
&= [(1200 \times 144)(2.9463 \times 10^6) + (70.3 \times 144)(1.0995 \times 10^6)]/62.4 \\
&= 8.3374 \times 10^9 \text{ Ft-lbf/Hr} \\
&= 1.0714 \times 10^7 \text{ Btu/Hr.}
\end{aligned}$$

Therefore, turbine efficiency is

$$\begin{aligned}
\text{eff} &= (1.9263 \times 10^9 - 1.0714 \times 10^7)/5.67 \times 10^9 \\
&= 33.80\%.
\end{aligned}$$

For 100% pump efficiency, pump work for coolant circulation is

$$\begin{aligned}
W_c &= \Delta P \cdot M/\rho \\
&= (210 \times 144)(3.4905 \times 10^7)/31.419 \\
&= 3.3595 \times 10^{10} \text{ Ft-lbf/Hr} \\
&= 4.317 \times 10^7 \text{ Btu/Hr.}
\end{aligned}$$

Therefore, ideal overall efficiency is

$$\begin{aligned}
\text{eff} &= \frac{(1.9263 \times 10^9 - 1.0714 \times 10^7 - 4.317 \times 10^7)}{5.67 \times 10^9} \\
&= 33.02\%.
\end{aligned}$$

2. Ideal Overall Efficiency of Pickering Station

The calculation is based on the turbo-generator heat balance of Figure 50^[12], and the expansion lines shown in Figure 51^[82]. The mass flow rate at the inlet of the H.P. turbine is 5964622 lbm/Hr, and the flow rates at the outlet are 550833, 91503, 318836, 190, and 210 lbm/Hr.

There is 3050 lbm/Hr drain loss. The drain loss is expected because of high wetness of the H.P. steam. However, it is a small percentage of the total flow rate (0.05%). From the flow rates and their corresponding enthalpies, the power output of the H.P. turbine can be calculated and is

$$W_{HP} = \sum (h \cdot M)_{inlet} - \sum (h \cdot M)_{outlet}$$

$$\begin{aligned} W_{HP} &= 1201.8(5964622 - 3050) \\ &\quad - 1083.8(5550833) \\ &\quad - 319.42(91503) \\ &\quad - 1117.28(318836) \\ &\quad - 1201.8(210 + 190) \\ &= 7.6269 \times 10^8 \text{ But/Hr.} \end{aligned}$$

Similarly, the power output of the L.P. turbine stage can be calculated. The inlet flow rate is 4819224 lbm/Hr, and the outlet flow rates are (2080 - 210 - 190), 11816, 33860, 96680, 225833, 180707, 173393, and 180637 lbm/Hr. The main exhaust flow rate is calculated to be 3914738 lbm/Hr based on the "no mass loss" assumption. The enthalpy of the main exhaust steam is interpolated from the expansion line at the pressure of 1.5 in Hg (see Figure 51^[82]). The associated steam wetness and enthalpy is 10% and 1000 Btu/lbm respectively. Therefore, the output power of the L.P. turbine stage is equal to

$$W_{LP} = \sum (h \cdot M)_{inlet} - \sum (h \cdot M)_{outlet}$$

$$\begin{aligned} W_{LP} &= 1250.28(4819224) \\ &\quad - 1201.80(2080 - 210 - 190) \\ &\quad - 1068.37(11816) \end{aligned}$$

$$\begin{aligned}
& - 100.79(33860) \\
& - 120.56(96680) \\
& - 1087.06(225833) \\
& - 1116.08(180707) \\
& - 1163.65(173393) \\
& - 1210.71(180637) \\
& - 1000.00(3914738) \\
& = 1.2133 \times 10^9 \text{ Btu/Hr.}
\end{aligned}$$

The total shaft work is

$$W_{HP} + W_{LP} = 1.9760 \times 10^9 .$$

For 100% pump efficiency, the pump work for feed water circulation is

$$\begin{aligned}
W_{\text{feed}} &= \sum (\Delta P \cdot M/\rho) \\
&= (38.0 - 1.5 \times 0.491)(144)(4647277)/62.4 \\
&\quad + (700 - 38)(144)(5969862)/62.4 \\
&= 9.5197 \times 10^9 \text{ Ft-lbf/Hr} \\
&= 1.2236 \times 10^7 \text{ Btu/Hr.}
\end{aligned}$$

Therefore, the turbine cycle efficiency is

$$\begin{aligned}
\text{eff} &= \frac{1.9760 \times 10^9 - 1.2236 \times 10^7}{5.67 \times 10^9} \\
&= 34.61\%.
\end{aligned}$$

The heavy water coolant is circulated at a rate of 61300000 lbm/hr, and the pressure drop is (1443 - 1254) psia^[12]. For 100% pump efficiency, the pump work for heavy water coolant circulation is

$$\begin{aligned}
 W_{\text{COOLANT}} &= \Delta P \cdot M/\rho \\
 &= \frac{[(1443 - 1254) \times 144] \cdot (61300000)}{54.476} \\
 &= 30625 \times 10^{10} \text{ Ft-lbm/Hr} \\
 &= 3.9365 \times 10^7 \text{ Btu/Hr.}
 \end{aligned}$$

Finally, the overall efficiency is

$$\begin{aligned}
 \text{eff} &= \frac{(7.629 \times 10^8 + 1.2133 \times 10^9) - (1.2236 \times 10^7 + 3.9365 \times 10^7)}{5.67 \times 10^9} \\
 &= 33.94\%.
 \end{aligned}$$